[American Journal of Science, Vol. 316, January, 2016, P. 1–63, DOI 10.2475/01.2016.01]

American Journal of Science

JANUARY 2016

NEOPROTEROZOIC STRATIGRAPHY OF THE ZAVKHAN TERRANE OF MONGOLIA: THE BACKBONE FOR CRYOGENIAN AND EARLY EDIACARAN CHEMOSTRATIGRAPHIC RECORDS

UYANGA BOLD*, EMILY F. SMITH*, ALAN D. ROONEY*, SAMUEL A. BOWRING**, ROBERT BUCHWALDT***, FRANCIS Ő. DUDÁS**, JAHANDAR RAMEZANI**, JAMES L. CROWLEY§, DANIEL P. SCHRAG*, and FRANCIS A. MACDONALD*,†

ABSTRACT. **The Neoproterozoic Tsagaan-Olom Group is exposed in the Zavkhan Terrane of southwestern Mongolia and hosts unique geochemical, paleoclimate, and paleontological records that have become central to our understanding of this pivotal interval of Earth history. New sedimentological, stratigraphic, geochronological, and geochemical data provide context for and further develop these records. Detrital zircon provenance indicates that Neoproterozoic strata of the Zavkhan Terrane were derived from basement with age peaks between 1950 to 2100 and 2400 to 2600 Ma. At ~800 Ma, the Zavkhan Terrane transformed from an active arc and back-arc complex to a rifted ribbon continent with passive margins on both sides. Deposition was accommodated by extension, which is recorded with syn-sedimentary normal faulting and alluvial fan deposition in the Zavkhan and Khasagt formations. Passive margin sedimentation in the overlying Tsagaan-Olom Group begins with the glacigenic Maikhan-Uul Formation, which consists of two massive diamictite units separated by clast-poor graded beds of the middle member. Detrital zircon at the base of the middle member of the Maikhan-Uul Formation were dated with U-Pb chemical abrasion isotope-dilution thermal ionization mass spectrometry and constrained its age to <729.8 ± 1.4 Ma. This, along with chemostratigraphy and Re/Os geochronological constraints from the overlying Taishir Formation, supports our correlation of the Maikhan-Uul Formation with the ~717 to 660 Ma Sturtian glaciation. The Taishir Formation was deposited on a carbonate ramp in four large-scale sequence tracts that thin to the southwest. The Taishir Formation preserves a large negative $\delta^{13}C$ excursion referred to as the Taishir excursion that covaries in carbonate and organic carbon isotopes in limestone sections. A dolomitization front at the top of the Taishir Formation also results in depleted $\delta^{13}C$ values, however, these are related to local processes and do not represent a global Trezona excursion. Although $\delta^{13}C$ values in the Ol Formation are highly variable along strike, 0.70756 initial strontium isotope values in limestone of the upper Ol Formation are consistent with earliest Ediacaran values. A sandstone-filled karst surface at the top of the Shuurgat Formation that overlies the Ol Formation defines the top of the Tsagaan-Olom Group and is interpreted to mark a major unconformity. Carbon and strontium isotope values in the uppermost Shuurgat Formation are also consistent with early Ediacaran values and suggest that most of the late Ediacaran Period is missing in the Zavkhan Terrane of Mongolia. Carbon isotope profiles from sections preserved as limestone and dolostone display large differences and indicate that isotopic data from**

* Department of Earth and Planetary Science, Harvard University, 20 Oxford St., Cambridge, Massachusetts, 02138

** Department of Earth, Atmospheric, and Planetary Sciences, Massachusetts Institute of Technology, Cambridge, Massachusetts 02139

*** Department of Earth and Environment, Boston University, Boston, Massachusetts 02215

§ Department of Geosciences, Boise State University, Boise, Idaho 83725

† Corresponding author: E-mail: fmacdon@fas.harvard.edu; Tel.: (617) 496-2236; Fax: 617-495-8839

dolomites should be used with caution. With our new data and correlations, we construct composite Cryogenian and Ediacaran carbon and strontium isotope curves from limestone-dominated successions in Mongolia, and then integrate additional geochronological and geochemical data sets from around the globe.

Keywords: Neoproterozoic, Cryogenian, Ediacaran, Zavkhan Terrane, Tsagaan-Olom Group, Taishir excursion, detrital zircon geochronology, carbon isotopes, and strontium isotopes

INTRODUCTION

Neoproterozoic strata record global, low-latitude glaciations (known as Snowball Earth episodes: Kirschvink, 1992; Hoffman and others, 1998; Hoffman and Schrag, 2002), the break-up of the supercontinent Rodinia and assembly of Gondwana (Hoffman, 1991; Li and others, 2008), large perturbations to geochemical cycles (for example, Halverson and others, 2010), a putative second global oxygenation event termed the Neoproterozoic Oxygenation Event (Planavsky and others, 2010; Och and Shields-Zhou, 2012), and the diversification of eukaryotes followed by the rise of metazoans (Knoll and others, 2006; Erwin and others, 2011). Unravelling the interrelationships between these climatic, tectonic, geochemical, and biological milestones is dependent on integrating high-quality data sets from around the world.

Thick, low-grade Neoproterozoic successions are spectacularly exposed in the Tsagaan-Olom Group in the Zavkhan Terrane of Mongolia (fig. 1) (Macdonald and others, 2009a; Macdonald, 2011). The Mongolian records are important because, along with Namibia (Hoffman, 2011) and Arctic Alaska (Macdonald and others, 2009b), they represent the only carbonate-dominated Cryogenian[1] successions. Unlike the other two successions, the Tsagaan-Olom Group, particularly the Taishir Formation (Fm), is fossiliferous (Bosak and others, 2011a, 2011b, 2012; Cohen and others, submitted[2]) and composed predominantly of limestone, making it ideal for a variety of geochemical proxy studies. These paleontological and lithological features distinguish Mongolia as an ideal locality to explore Cryogenian and early Ediacaran biogeochemical cycles.

Since the conception of the Snowball Earth hypothesis, the number and duration of Neoproterozoic glacial events has been debated (Rooney and others, 2015). The lack of a robust global age model has made it difficult to integrate geochemical and paleontological data with the glacial record. Recent geochronology coupled with geochemistry has reinforced geochemical correlations and has suggested a long Sturtian glacial epoch from *ca.* 717 to 660 Ma, and a relatively short Cryogenian nonglacial interlude (Macdonald and others, 2010; Rooney and others, 2014, 2015). These geochronological constraints, directly linked to carbon and strontium isotope chemostratigraphy, provide a template to more broadly integrated global records.

Previous attempts at integrating Mongolian records into the global database have been limited not only by the lack of robust geochronology, but also by the lack of regional geological mapping and stratigraphic studies. Particularly, disagreement has centered on the number and age range of Cryogenian glacial deposits (see review in Macdonald, 2011). The earliest description of the sedimentology of the Maikhan-Uul Fm, which forms the base of the Tsagaan-Olom Group, was interpreted as evidence of two glacial advances separated by an interglacial period (Lindsay and others, 1996). This study, however, was from a single locality, Tsagaan Gol (*tr.* 'White Gorge'; here we

[1] The Cryogenian Period was redefined in 2015 by the International Commission of Stratigraphy at ~720-635 Ma.

[2] Cohen, P. A., Macdonald, F. A., Matys, E., Pruss, S. B., and Bosak, T., submitted, Cryogenian Macroscopic Organic Warty Structures (MOWS) and the Rise of Macroscopic Algae: Palaios.

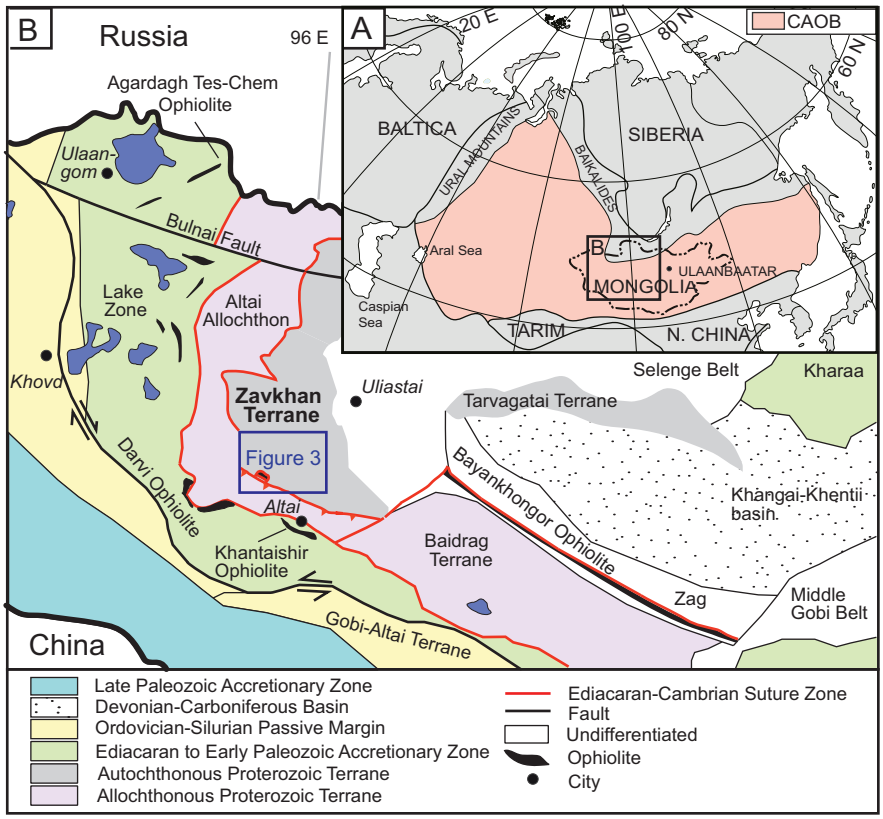

Fig. 1. Location map of the Zavkhan Terrane of Mongolia. (A) Location map showing extent of the Central Asian Orogenic Belt (CAOB) and its surrounding areas (Sengör and others, 1993). (B) Tectonic map of western Mongolia (after Badarch and others, 2002; Bucholz and others, 2014). Contacts modified from the 1:1,000,000 geological map of Mongolia (Badarch and others, 1998).

use 'gorge' in place of 'gol'), and it is unclear if these deposits represent movement in the ice-grounding line or two distinct early Cryogenian glaciations (Macdonald, 2011). Macdonald and others (2009a) discovered a large negative $\delta^{13}C$ excursion in the Taishir Fm that covaries in organic and carbonate carbon isotopes (Johnston and others, 2012), and a Marinoan age diamictite and basal Ediacaran cap dolostone in overlying strata, which defined the Cryogenian-Ediacaran boundary in Mongolia. Despite these refinements of the age model for the Tsagaan-Olom Group, it has remained uncertain whether the Maikhan-Uul Fm represents a single Sturtian glaciation or multiple Cryogenian glaciations. Moreover, it has also been unclear if the Taishir excursion is correlative with the Cryogenian Trezona excursion in Australia, Namibia, NW Canada and elsewhere (Swanson-Hysell and others, 2010; Macdonald and others, 2013), or if it represents a distinct event that has not been well-documented in records elsewhere. Here we present a comprehensive stratigraphic study of Cryogenian successions from southwest Mongolia that provides sedimentological and tectonic context to these records. We then consider the degree to which these geochemical records are affected by diagenesis and represent global conditions, refine global correlations, and then discuss how the successions of the Zavkhan Terrane inform our understanding of Cryogenian and early Ediacaran Earth history.

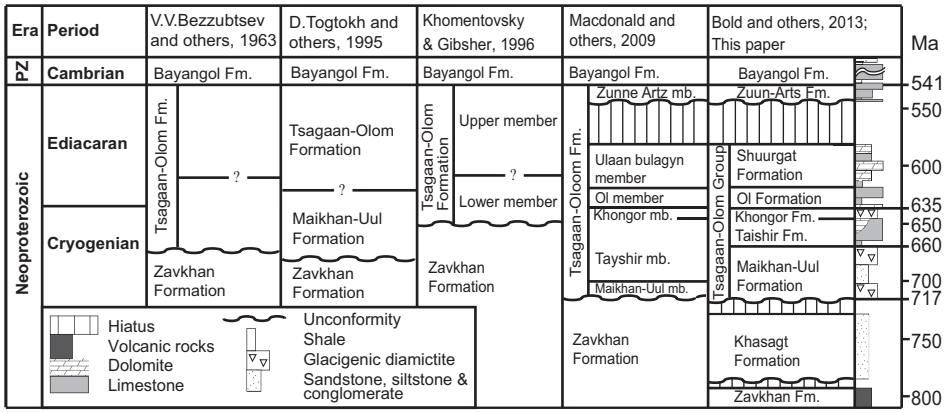

Fig. 2. Revised stratigraphy of the Tsagaan-Olom Group modified from Bold and others (2013).

GEOLOGICAL SETTING

Neoproterozoic strata are exposed in the Mongolian Altaids as crustal fragments embedded within the ~5000 km long Central Asian Orogenic Belt (CAOB) (fig. 1A). Early studies on the Mongolian Altaids divided the region into two super-units: the Neoproterozoic northern super-unit, or Mongolian continent, which was consolidated with an early Paleozoic orogeny, and an early Paleozoic southern super-unit that accreted during the late Paleozoic (Zonenshain, 1973). These were later divided into zones, blocks, and terranes (for example, Ruzhentsev and Pospelov, 1992), culminating with the separation of the Mongolian Altaids into 44 terranes (Badarch and others, 2002) (fig. 1B).

The stratigraphy of the Zavkhan Terrane (fig. 2) was first described by Bezzubtsev (1963) who named the Zavkhan, Tsagaan-Olom, and Bayangol formations (fms). After regional scale mapping (1:200,000 scale), Togtokh and others (1995) identified and named the Maikhan-Uul Fm, a unit below the Tsagaan-Olom Fm (fig. 2). The first stratigraphic descriptions in English came in 1996 with the publication of a *Geological Magazine* issue dedicated to the Neoproterozoic-Cambrian stratigraphy of southwestern Mongolia (Brasier and others, 1996a). This publication included the translation of geological maps and measured sections into English (Khomentovsky and Gibsher, 1996), a reconnaissance chemostratigraphic characterization of the Tsagaan-Olom, Bayangol, and Salaagol fms (Brasier and others, 1996b), and a detailed stratigraphic study of the Maikhan-Uul Fm at Tsagaan Gorge (Lindsay and others, 1996). More recently, this stratigraphic framework was revised by Macdonald and others (2009a) and formalized by Bold and others (2013) (fig. 2).

Although distinguished by Badarch and others (2002), the Zavkhan and Baidrag terranes are commonly grouped together and called one or the other (for example, Levashova and others, 2010), or even grouped with the Lake Zone (for example, Kröner and others, 2010). We separate the Zavkhan and Baidrag terranes because they lack a shared Neoproterozoic overlap assemblage (Badarch and others, 2002), and it appears unlikely that they were attached until at least the Cambrian. Moreover, in our distinction of terranes, we separate the Altai allochthon from the Lake Zone (also called the Ozernaya Zone, for example, Khomentovsky and Gibsher, 1996) (fig. 1B).

It is widely cited that the Zavkhan Terrane hosts Archean to Paleoproterozoic crystalline basement (for example, Yarmolyuk and others, 2008). This stems in part

from the inclusion of the Baidrag Terrane and the Dariv Range with the Zavkhan Terrane (for example, Lehmann and others, 2010). However, there is no exposed basement on the Zavkhan Terrane older than ~850 Ma (Kozakov and others, 2012). According to our study, the newly discovered Tsagaankhairkhan Fm (figs. 3 and 5), which underlies the Zavkhan Fm, is the oldest sedimentary succession on the Zavkhan Terrane. Further south, the relationship between the Tsagaankhairkhan Fm and undifferentiated Neoproterozoic units that underlie the Zavkhan Fm is unclear (fig. 3). The Zavkhan Fm (figs. 4 and 5) is overlain by siliciclastic rocks of the Khasagt Fm and glacial diamictite of the Maikhan-Uul Fm, which is the basal unit of the Tsagaan-Olom Group.

The Tsagaan-Olom Group (*tr.* 'White bridal strap') was named after the eponymous location near the Khevtee Tsakhir Range (abbreviated as KTN by Khomentovsky and Gibsher, 1996). Unfortunately, the Maikhan-Uul and Taishir fms are largely faulted out at this location, leaving just the early Ediacaran Shuurgat Fm of the Tsagaan-Olom Group exposed. Previous studies have focused on sections exposed at Bayan and Tsagaan gorges (Brasier and others, 1996; Khomentovsky and Gibsher, 1996) where ~200 m of stratigraphy in the middle of the Tsagaan-Olom Group is faulted out and poorly exposed. Recently, the Tsagaan-Olom was elevated to Group status and the informal members (Macdonald and others, 2009a) were elevated to formations (Dorjnamjaa and Enkhbaatar, 2011; Bold and others, 2013). Spelling of Formation names were changed from Russian to Mongolian and the informal Ulaanbulag fm (Macdonald and others, 2009a) was changed to Shuurgat Fm because the former name was already used for other units on regional maps (Bold and others, 2013).

The Tsagaan-Olom Group begins with the Maikhan-Uul Fm, which consists of 3 to 500 m of glacigenic diamictite and siliciclastic rocks that unconformably overlie the Khasagt and Zavkhan fms (figs. 2 and 5). The Maikhan-Uul Fm is sharply and conformably overlain by 300 to 600 m of dark-colored limestone of the Taishir Fm, which is composed of four super-sequences that are locally dolomitized towards the top. Rooney and others (2015) recently dated the base of the Taishir Fm with Re-Os on organic-rich carbonate at 659.0 ± 3.9/4.5[3] Ma (MSWD[4] = 0.67), which further supports correlation of the base of the Taishir Fm with Sturtian cap carbonates around the globe. The Taishir Fm is sharply overlain by 0 to 50 m of glacigenic diamictite of the Khongor Fm and an additional ~500 m of early Ediacaran carbonate strata of the Ol and Shuurgat fms (fig. 2).

In the late Ediacaran Period, the passive margin on the southwestern side of the Zavkhan Terrane was transformed into a foreland basin and an active margin with the arrival of the Ediacaran to Paleozoic arc terranes to the south (Macdonald and others, 2009a). Above the karstic unconformity that defines the top of the Shuurgat Fm, simple bed planar trace fossils are present within the Zuun-Arts Fm (*tr.* 'eastern Juniper') (Goldring and Jensen, 1996) as well as a large negative $\delta^{13}C$ excursion (Brasier and others, 1996; Macdonald and others, 2009a) indicating a latest Ediacaran to early Cambrian age with the Ediacaran-Cambrian boundary in the uppermost Zuun-Arts Fm (Smith and others, 2015). Consequently, the Zuun-Arts Fm (formerly the upper member of the Tsagaan-Olom Fm) was removed from the Tsagaan-Olom Group to reflect its position above a major unconformity and tectonostratigraphic affinity to the Bayangol Fm (Bold and others, 2013).

The Neoproterozoic stratigraphy of the Zavkhan Terrane was buried with ~1 km of early Cambrian foreland deposits and then deformed and weakly metamorphosed

[3] ± Internal uncertainty only/including decay constant uncertainty.
[4] Mean Square of Weighted Deviates.

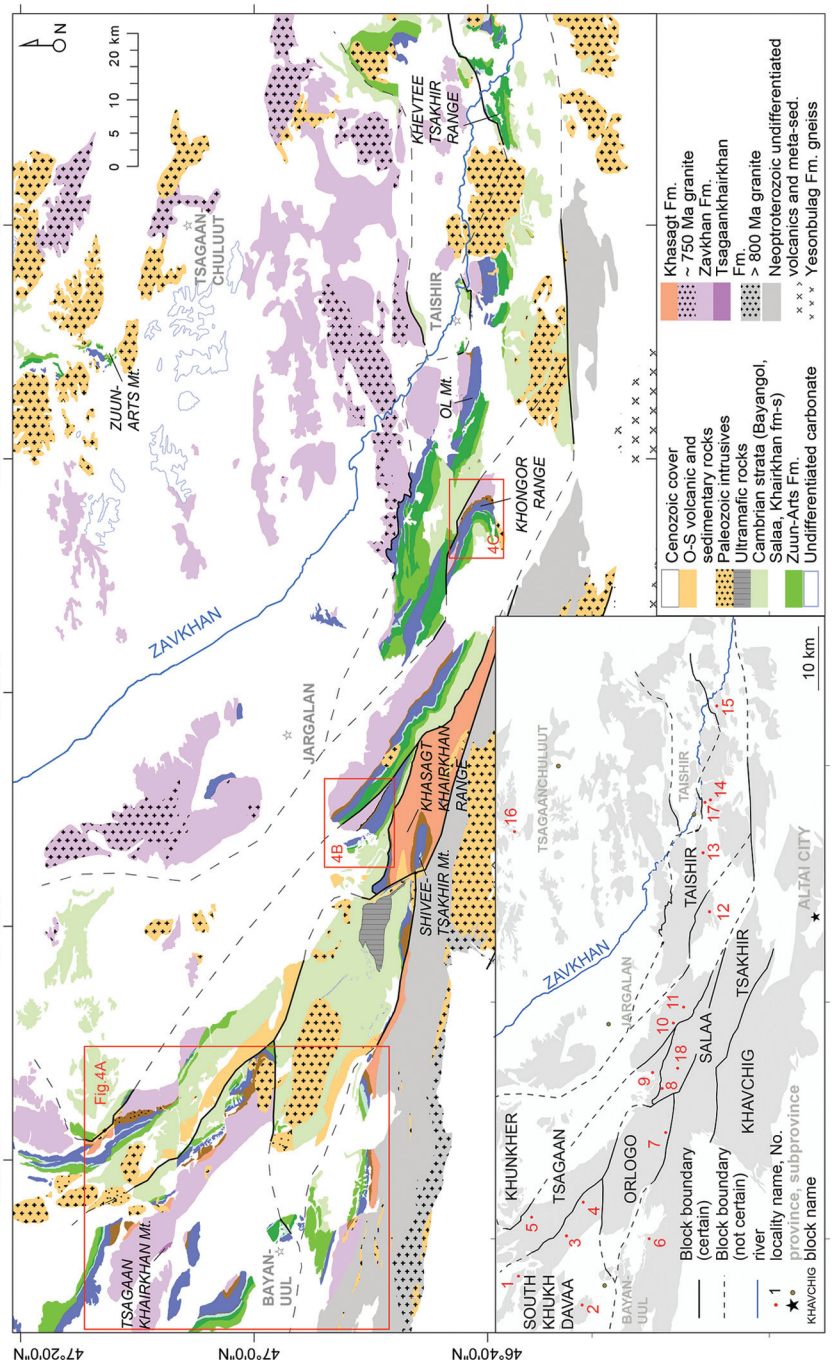

Fig. 3. Geological map of the Zavkhan Terrane (F. A. Macdonald, U. Bold, and E. F. Smith). Structural blocks are illustrated in the inset map with their corresponding names. Legend for the Tsagaan-Olom Group is in figure 4. Localities discussed in this study are numbered as follows: (1) Unkheltseg; (2) Ikh Goliin Tsakhir; (3) western Khukh Davaa; (4) southern Khukh Davaa; (5) northeastern Khukh Davaa; (6) Tsakhir Range; (7) Orlogo Gorge; (8) Salaa Gorge; (9) Tsagaan-Gorge; (10) Uliastai Gorge; (11) Khunkher Gorge; (12) Khongor Range; (13) Ol Mountain; (14) eastern Taishir; (15) Khevtee Tsakhir Range (KTN); (16) Zuun-Arts locality; (17) western Taishir; and (18) Shivee Tsakhir.

during multiple Paleozoic orogenic events in the CAOB (fig. 1A). After late Ediacaran to Ordovician accretion of arc terranes to the south (Macdonald and others, 2009a; Jian and others, 2014), the late Ordovician to Silurian record of Mongolia is marked by sinistral transtension (fig. 3), extensional magmatism and basin formation (Kröner and others, 2010; Gibson and others, 2013). During this time, the Zavkhan Terrane is interpreted to have been part of a composite ribbon continent that was located between North China and Siberia (Wilhem and others, 2012). From the Devonian to early Permian, the Zavkhan Terrane was oroclinally buckled during the convergence between North China, Tarim, and Siberia (Lehmann and others, 2010; Edel and others, 2014). Locally, in the Zavkhan Terrane, this late Paleozoic collision is manifested in dextral strike-slip wrench structures (fig. 1B) and widespread Permian plutonism (Jahn and others, 2009).

STRATIGRAPHY

Here we briefly describe the Zavkhan and Khasagt fms. Then we describe measured stratigraphic sections of the Tsagaan-Olom Group in more detail. The Tsagaan-Olom Group is exposed on the Zavkhan Terrane in eight structural blocks, referred to here as the Taishir, Salaa, Tsakhir, Khavchig, Tsagaan, Orlogo, Khunkher, and South Khukh Davaa blocks, each of which are bound by major faults (fig. 3) and characterized by distinct stratigraphy.

Zavkhan and Khasagt Formations

The Zavkhan Fm consists of >1 km of volcanic and volcanoclastic rocks dominated by rhyolite with subsidiary dacitic and basaltic flows that are exposed in the Zavkhan Terrane for >400 km along strike (fig. 3). Rhyolites of the Zavkhan Fm are red to green in color and form massive domes and thin-bedded ignimbrites and lithic tuffs. On the South Khukh Davaa block (fig. 4A), the Zavkhan Fm begins with >1 km of boulder clast conglomerate with interbedded rhyolite flows that structurally overlie the Tsagaankhairkhan Fm (fig. 5). Although the contact is locally faulted, the lower few tens of meters of this conglomerate unit are dominated by redeposited clasts of the Tsagaankhairkhan Fm dolostone, which suggests a stratigraphic relationship between the two. Up-section, conglomerate is interbedded with medium-bedded sandstone and the clasts become dominated by sedimentary quartzite of an unknown source that is not exposed on the Zavkhan Terrane. Hence, it is inferred that these clasts preserve an inverted footwall stratigraphy from a syn-sedimentary fault, providing a window into units underlying the Zavkhan and Tsagaankhairkhan fms. This conglomerate unit is topped by >500 m of thin-bedded rhyolite flows and felsic tuffs, which are overlain by massive rhyolite domes that are >1 km thick.

On the Taishir, South Khukh Davaa, Tsakhir and Salaa blocks (fig. 4B), the Zavkhan Fm is unconformably overlain by conglomerate and sandstone of the Khasagt Fm (named after the Khasagt Khairkhan Range where these rocks are the ridge-former and best exposed). On the Taishir, South Khukh Davaa, and Tsakhir blocks, the Khasagt Fm consists of 0 to 200 m of red to green, medium-bedded sandstone and siltstone with common large-scale trough cross-stratification, channelization, and minor basalt flows (fig. 5). Thickness of the Khasagt Fm increases abruptly across the fault that marks the western margin of the Salaa block. There the Khasagt Fm is composed of >1 km of red to green graded beds of siltstone, sandstone and conglomerate (fig. 5).

Tsagaan-Olom Group

Measured stratigraphic sections of the Maikhan-Uul, Taishir, Khongor, Ol and Shuurgat fms of the Tsagaan-Olom Group are reported in this paper with locations marked on figures 3 and 4. The stratotype sections are assigned and presented in Bold

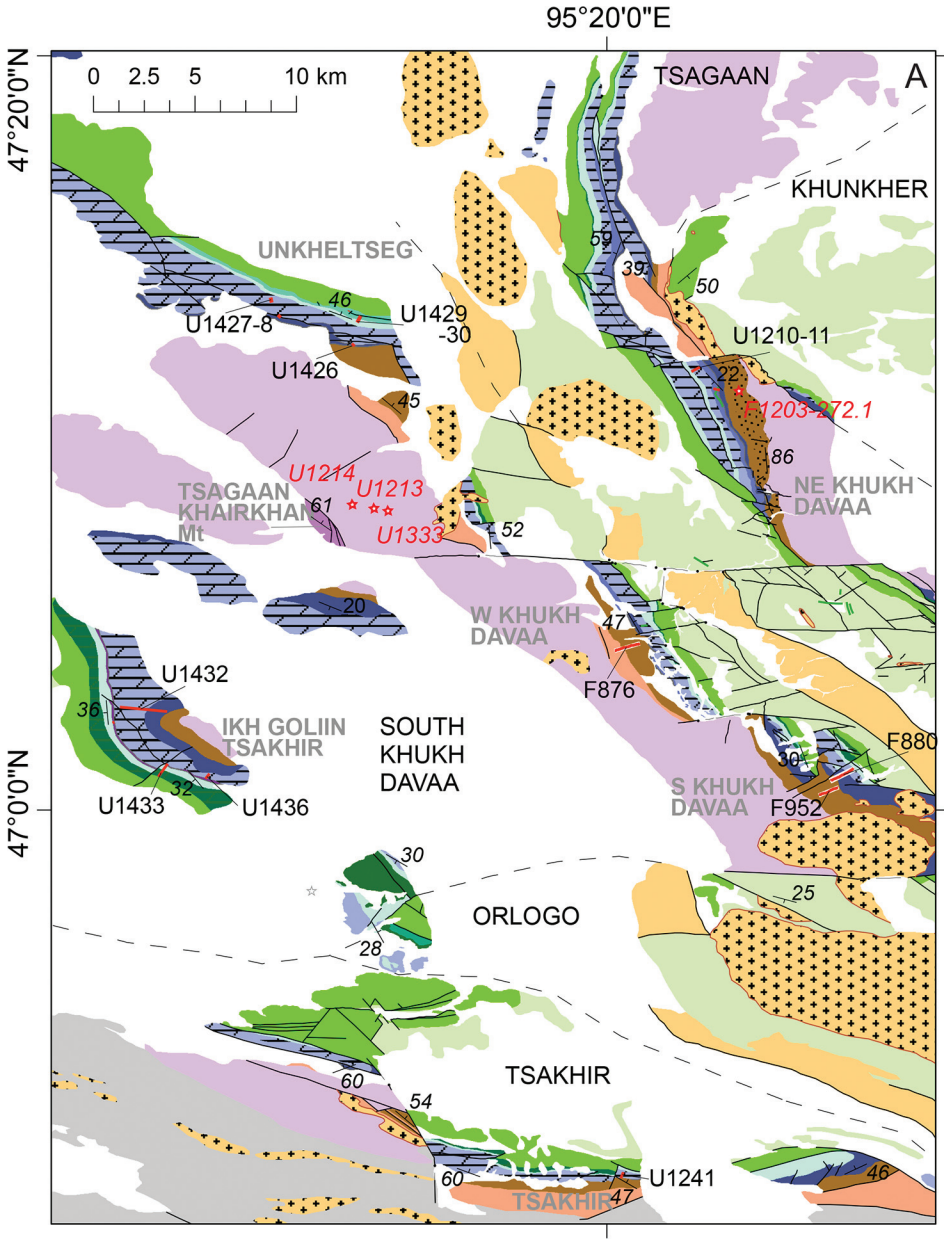

Fig. 4. Detailed geological maps with samples and sections labeled. (A) Western Zavkhan Terrane, Tsakhir, Orlogo, southern Khukh Davaa, Tsagaan and Khunkher blocks. (B) Salaa, Tsagaan, and Khunkher blocks. (C) Khunkher block. Measured stratigraphic sections included in this study are shown in red with corresponding labels. Key for units except the Tsagaan-Olom Group is the same as in figure 3. Color schemes used in figure 3 (1. Maikhan-Uul Formation; 2. Taishir Formation; 3. Khongor Formation; 4. Ol Formation; 5. Shuurgat Formation) are shown along with detailed color schemes used in figure 4 for members of each formation of the Tsagaan-Olom Group. Location names are labeled in dark gray. Structural blocks are labeled in black in all capitalized letters. Inferred structural block boundaries are illustrated with dashed line.

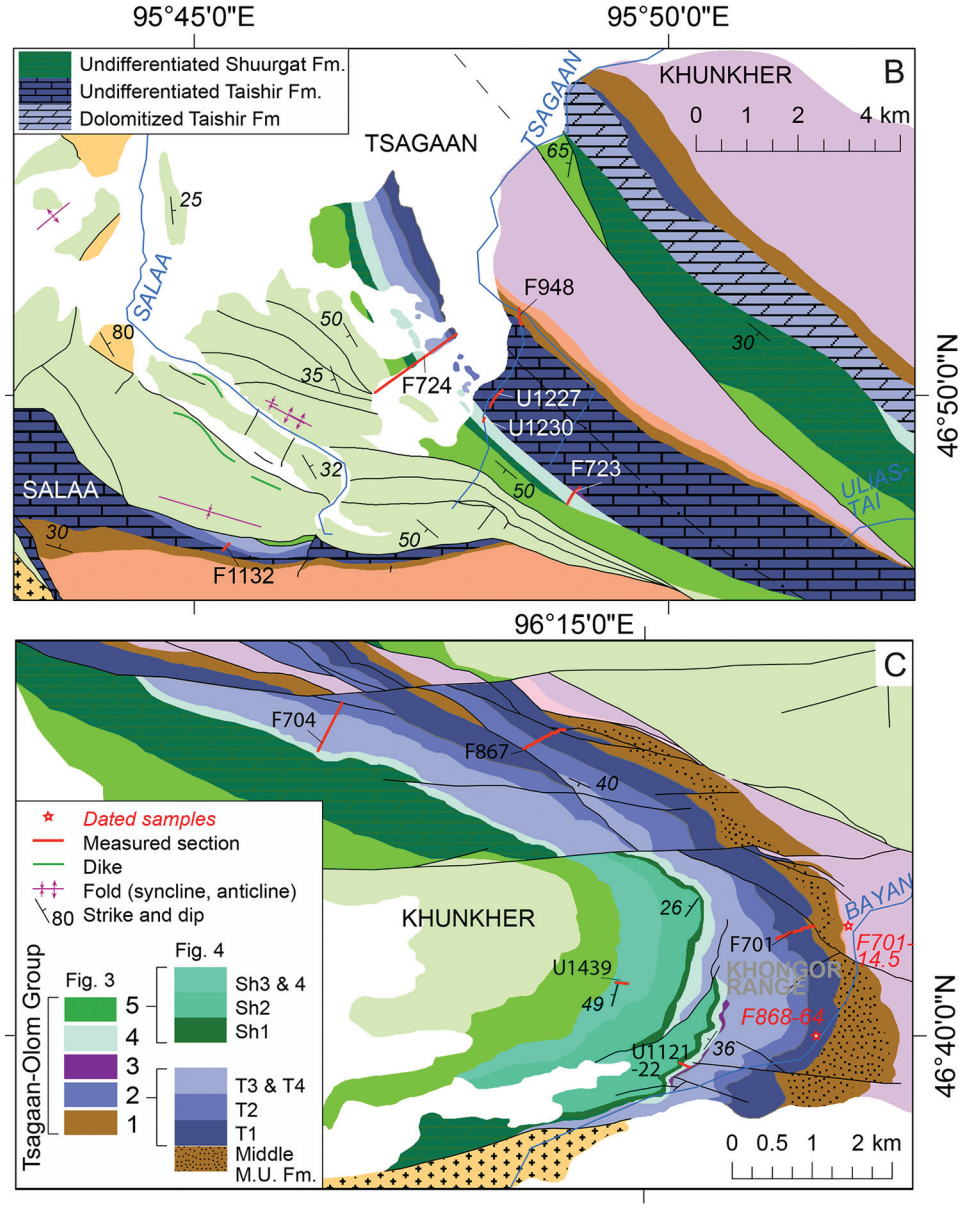

Fig. 4 (continued).

and others (2013). Carbonate and siliciclastic lithofacies are defined in table 1. We have further distinguished facies assemblages in table 2 for glacigenic facies of the Maikhan-Uul and Khongor fms and for carbonate facies of the Taishir, Ol, and Shuurgat fms.

Maikhan-Uul Formation.—The Maikhan-Uul Fm (*tr.* 'tent mountain') rests on the Khasagt Fm at Tsagaan Gorge, Salaa Gorge, Shivee Tsakhir, and Khukh Davaa, the Zavkhan Fm near Khunkher Gorge, Khongor Range and west of Taishir (fig. 6) and on

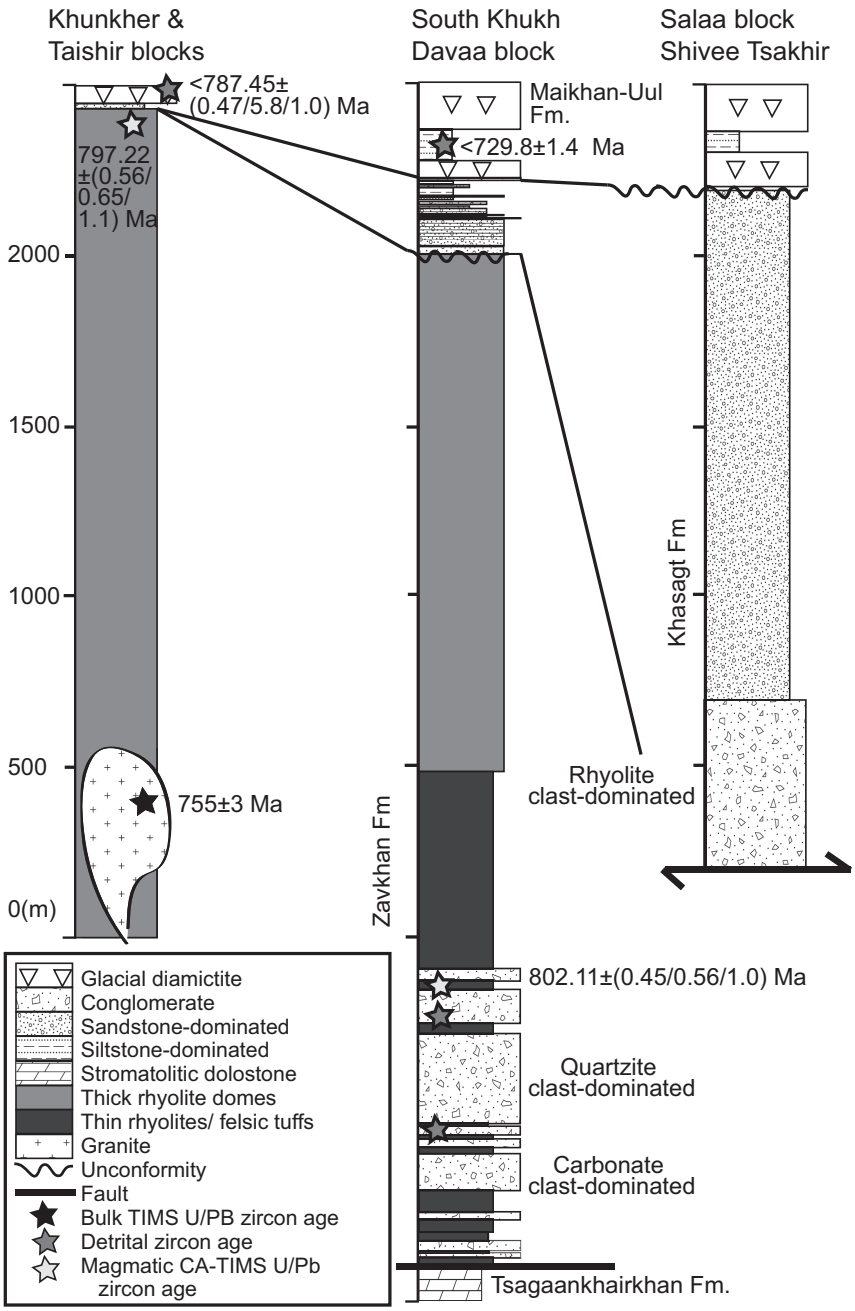

Fig. 5. Stratigraphy of the Zavkhan and Khasagt formations with age constraints discussed in the geochronology section. Bulk TIMS U-Pb zircon age is from Yarmolyuk and others (2008).

~850 Ma gneiss to the north in the Zavkhanmandal zone (Kozakov and others, 2012). The Maikhan-Uul Fm progressively thickens to the west-southwest (fig. 6), but also displays considerable variability along strike. For mapping purposes, the Maikhan-Uul

TABLE 1

Carbonate and siliciclastic lithofacies used in this paper with descriptions of lithology, bedding, grains, and sedimentary structures that distinguish these facies

Lithofacies	Bedding	Grains	Sedimentary Structures
		Carbonate Facies	
Micrite	Flat thin beds	Mud	Grading
Calcisilitite	Flat to nodular	Mud to silt	Ripple cross-lamination and grading
Grainstone (includes wackestone and packestone)	Thin to thickly bedded	Peloids, ooids, and chips of microbialite	Trough cross-bedding and normal grading
Microbialaminite	Crinkly laminated	Boundstone with cement and organic mats	Microbial bounding of grains, cements, dolomitized tops
Breccia	Massive	Carbonate clasts with ubiquitous cement	Teepee structures, void-filling cement and dolomitization
Heterolithic interbeds	Thin to thickly bedded	Angular to sub-rounded clasts and grains	Imbrication and normal grading
		Siliciclastic Facies	
Massive diamictite	Massive to thickly bedded	Shale to sandstone matrix with common boulder- to gravel-sized clasts of underlying units	Shear fabrics, soft-sedimentary folding, concretions, scours
Stratified diamictite	Fine laminated to medium bedded	Shale to sandstone matrix with rare lonestones	Normally graded with lamination penetrating clasts
Conglomerate	Massive to medium bedded	Clasts of carbonate, quartzite, and volcanic rocks	Weakly graded with imbrication
Sandstone	Thin to massive	Fine- to coarse grained volcaniclastic (quartz, feldspar, lithic fragments)	Both normally graded and cross-bedded facies
Siltstone	Thin to medium, commonly graded between shale and fine-sandstone	Volcaniclastic (quartz, feldspar, lithic fragments)	Grading from shale to fine sandstone, ripple cross-lamination
Shale	Thin	Green to black colored	Suspension lamination

Fm is separated into informal lower, middle, and upper members. Generally, the lower and upper members are composed of diamictite with clear evidence of a glacial origin including lamination-penetrating dropstones (fig. 7A) and striated (fig. 7B) and faceted clasts (Lindsay and others, 1996; Macdonald, 2011) that are separated by a middle, diamictite-free siliciclastic unit.

In the Maikhan-Uul Fm, we distinguish stratified diamictite from massive diamictite and use other sedimentary features to identify glacitectonic deformation such as soft-sedimentary folding and shear fabrics (table 1). Massive diamictite is distinguished from conglomerate in that diamictite facies are matrix-supported and poorly sorted. In both the upper and lower members of the Maikhan-Uul Fm, the diamictite matrix is composed of shale to sandstone that varies in color from black to green to brown to red

Table 2

Carbonate and glacial facies assemblages used in this paper with descriptions of lithofacies associations and depositional environments

Assemblage	Lithofacies Associations	Depositional environments
Carbonate Facies Assemblage		
Inner ramp	Micrite, calcisiltite, grainstone, microbialaminite, intraclast breccia in m-scale parasequences.	Periodically restricted and sub-aerially exposed intertidal platform with early dolomitization capping parasequences
Mid-ramp	Medium-bedded micrite, calcisilitite, grainstone and heterolithic interbeds.	Near or below wave-base with ooid-grainstone shoals and frequent storm-derived grain- and debris flows
Outer ramp	Flat, graded, thin beds of micrite, calcisilitite, grainstone, and conglomerate interpreted as debris flow with minor slump folding.	Below wave base with gravity deposits on lower ramp to basin
Glacial Facies Assemblage		
Subglacial-ice contact	Massive to weakly bedded diamictite with glacio-tectonic deformation, minor sandstone.	Lodgment till and till in a proximal ice-contact fan deposited below an ice sheet grounded to a marine margin
Sub-ice shelf or glacio-laucustrine	Graded beds of shale to sandstone.	Turbidites and shale deposited below an ice shelf or distal to the grounding line without evidence of significant ice-breakup
Proglacial	Pebbly cross-stratified sandstone, and both massive and stratified diamictite	Marine ice contact fan to glacio-fluvial environments

(fig. 6). Clasts are commonly sub-rounded and faceted and consist predominantly of felsic volcanic rocks from the underlying Zavkhan Fm, siliciclastic rocks from the Khasagt Fm, minor dolostone clasts from the Tsagaankhairkhan Fm, granite, and meta-sediments and meta-volcanics of unknown origin. Clast-size varies from granule to boulder (Macdonald, 2011). Below we describe the stratigraphy from northeast to southwest in 11 measured stratigraphic sections (fig. 6) of the Maikhan-Uul Fm.

In the Khukh Davaa region (stratigraphic sections F1203 and F1204, fig. 6) of the Tsagaan block, the Maikhan-Uul Fm is 250 to 370 m thick. The lower member rests on an erosional unconformity and consists predominantly of red-green colored, massive diamictite. The contact between the massive diamictite of the lower member and the green shale and siltstone at the base of the middle member is marked by a ~20 cm thick bed of concretionary limestone. The middle member coarsens upwards to massive sandstone, which is in turn succeeded by a second succession of recessive, thinly bedded shale and siltstone. Rare lonestones and lamination-penetrating drop-stones are present in the upper ~20 m of the middle member. The middle member culminates with massive, channelized sandstone bodies that are <10 m wide with ~4 m of local relief on incising margins. These sandstone bodies are succeeded by massive diamictite of the upper member. Striated clasts and carbonate concretions are common. At western Khukh Davaa, the upper member consists of interbedded siltstone, sandstone, conglomerate, and diamictite. Mudcracks are present near the top of the upper member (fig. 7E).

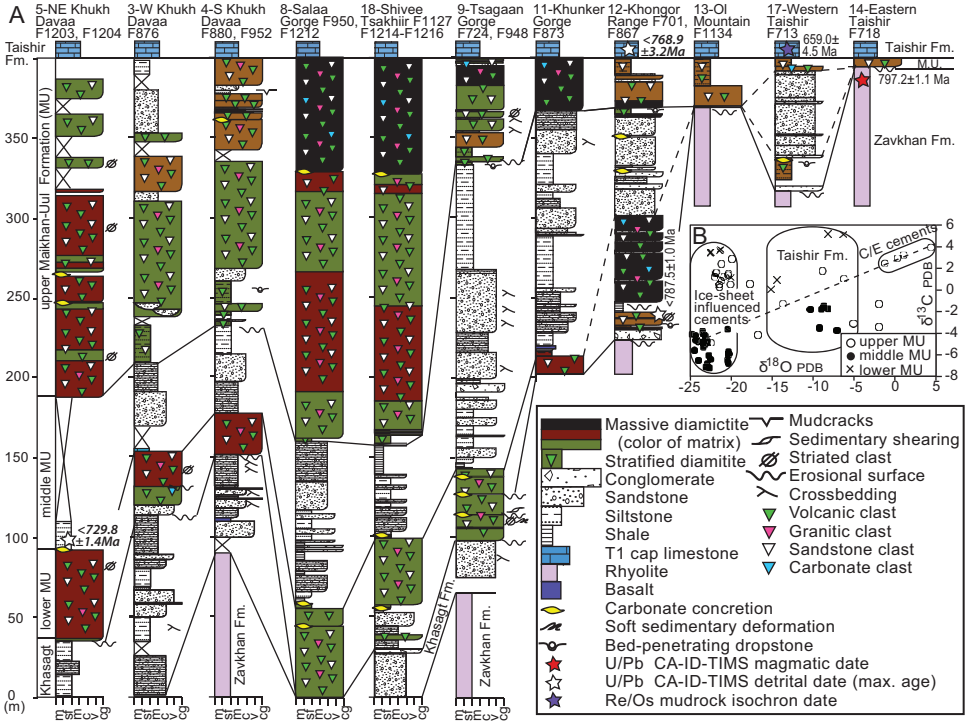

Fig. 6. (A) Stratigraphy of the Maikhan-Uul Formation. Location of sections is shown in figure 3. MU - Maikhan-Uul, m - mudstone, sf - siltstone to fine-grained sandstone, ms - medium-grained sandstone, c - coarse-grained sandstone, cg - conglomerate. (B) Carbon-oxygen isotope cross-plot of cements in the Maikhan-Uul Formation. C/E – clathrate- or evaporation-influenced cement. Dashed line is a mixing line between ice-sheet influenced cements and clathrate- or evaporation-influenced cements. Values of carbon and oxygen isotopes from the Taishir Formation, which includes both cements and micritic groundmass, are also outlined to show range of values from cements that could have precipitated at a later stage.

To the southeast on the Salaa block, in Salaa Gorge (stratigraphic sections F950 and F1212, fig. 6) and at Shivee Tsakhir (stratigraphic sections F1127 and F1214-1216, fig. 6) (fig. 3), the lower member of the Maikhan-Uul Fm consists predominantly of massive, green wackestone matrix diamictite with minor siliciclastic strata and common concretionary carbonate. Similar to northeastern and western Khukh Davaa, the lower member is sharply overlain by green shale and siltstone with the contact marked by a <20 cm thick concretionary limestone bed. The middle member of the Maikhan-Uul Fm is composed of graded beds of sandstone, siltstone and shale. Lonestones have only been observed in the uppermost ~5 m of the middle member, directly below an erosive contact with the upper member that is marked by a concretionary limestone. At both Salaa Gorge and Shivee Tsakhir the upper member is composed of green and red colored massive diamictites composing the lower ~150 m and a >50 m massive diamictite with a black colored wackestone matrix forming the uppermost unit. This upper black diamictite unit is separated from the underlying red and green diamictites by a laterally continuous, ~50 cm thick concretionary carbonate bed.

On the Tsagaan block, in Tsagaan Gorge (stratigraphic sections F724 and F948, fig. 6), where the Maikhan-Uul Fm measures >275 m, again two diamictites are separated by a thick sequence of flat bedded, shale, siltstone and sandstone (Lindsay and others, 1996). There the lower member consists of at least five massive diamictite

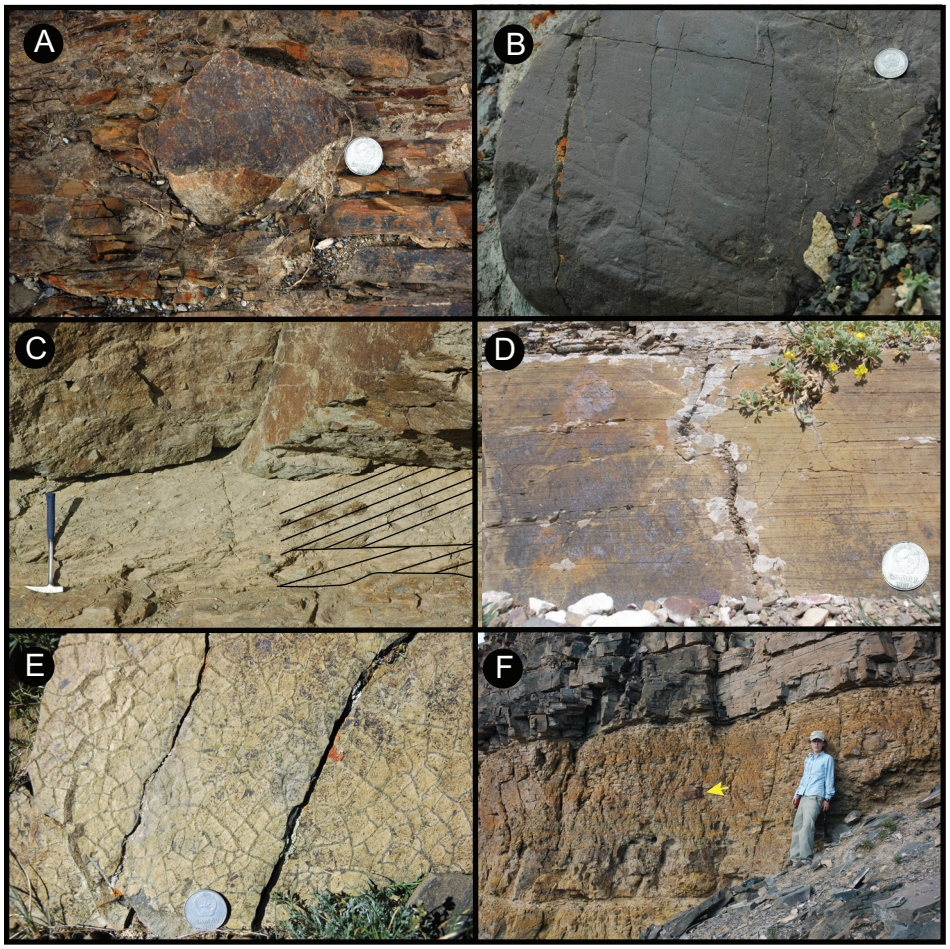

Fig. 7. Sedimentary features of the Maikhan-Uul Formation. Mongolian coin is 2.25 cm in diameter. (A) Bed-penetrating dropstone in lower member of the Maikhan-Uul Formation at Khongor Range. (B) Striated clast from lower member of the Maikhan-Uul Formation at Khukh Davaa. (C) Top to the right (southwest) shear fabric and concretionary carbonate horizon from the lower member of the Maikhan-Uul Formation at Tsagaan Gorge. Fabric is traced on right side of image. (D) Brown weathered, green when fresh, mm-laminated and varve-like shale, siltstone and sandstone of middle member of the Maikhan-Uul Formation exposed in Tsagaan Gorge. (E) Mud-cracks in the upper member of the Maikhan-Uul Formation at South Khukh Davaa. (F) Orange when weathered, stratified rain-out deposit at the top of the upper member of the Maikhan-Uul Formation at western Taishir, sharply overlain by the Taishir Fm. Arrow points to boulder lonestone.

units separated by carbonate concretions, erosive surfaces, boulder pavements, shear fabrics (fig. 7C) and evidence of soft sedimentary deformation. Striated and faceted bullet-shaped clasts are common. The top of the lower member is marked by 20 cm of stratified diamictite and succeeded by shale, and then ~50 m of siltstone dominated graded beds with 1 to 5 m intervals of graded sandstone. The middle member coarsens up from a lower package of graded siltstone to massively bedded very coarse sandstone with weakly developed ~50 cm scale tabular cross-beds. This very coarse sandstone is succeeded by green, mm-laminated, varve-like shale and siltstone (fig. 7D). Cobble lonestones are present in the upper 50 cm of the middle member. The upper member begins with a massive diamictite unit above an erosive base that is marked with a

concretionary carbonate. In total, the upper member at Tsagaan Gorge consists of massive diamictite separated by <50 cm thick sandstone beds and weakly stratified diamicite. Clasts of felsic volcanic rocks, carbonate, and siliciclastic rocks are present with several siltstone clasts that preserve soft-sedimentary folding. The contact between the Maikhan-Uul Fm and the overlying laminated limestone of the Taishir Fm is not exposed.

Farther east, in the Khongor Range (stratigraphic section F701, fig. 6) of the Taishir block, the Maikhan-Uul Fm is composed of three distinct massive diamictite intervals separated by siliciclastic strata. The lower diamictite-rich interval begins with a massive, clast-dominated conglomerate, dominated by Zavkhan Fm clasts. This is succeeded by an interval of interbedded massive and stratified diamictite that contains both bed-penetrating dropstones (fig. 7A) and striated clasts (fig. 7B). The lower unit is succeeded by graded siltstone and shale beds and then black shale to wackestone matrix, massive diamictite. This second diamictite-rich interval contains clasts of the Zavkhan Fm, the Tsagaankhairkhan Fm dolostone, sandstone and siltstone of the Khasagt Fm, and granite. It is succeeded by siltstone and sandstone with rare cobble lonestones and at least two ~20 cm thick bands of concretionary carbonate. The uppermost diamictite-rich interval exposed at Khongor Range has an erosive base and contains both massive and stratified diamictite facies with bed-penetrating dropstones and striated clasts, and minor sandstone beds. A ~10 cm thick layer of red clay separates the Maikhan-Uul Fm from the overlying Taishir Fm.

East of the Khongor Range, the Maikhan-Uul Fm rests unconformably on the Zavkhan Fm, with the contact commonly mantled with a boulder pavement. At the easternmost exposures on the Taishir block (stratigraphic section F718, fig. 6), the Maikhan-Uul Fm is only ~7 m thick and composed predominantly of a massive cobble to boulder clast diamictite, whereas just 1 km to the west (stratigraphic section F713, fig. 6) it thickens to ~82 m with two diamictite-rich intervals separated by ~57 m of massive, medium to very coarse-grained sandstone (fig. 6). The lower diamictite-rich interval consists of stratified diamictite with bed-penetrating dropstones. Clast composition is dominated by felsic volcanic rocks, presumably from the Zavkhan Fm. Beds of the overlying middle member of the Maikhan-Uul Fm are commonly graded in cm thick beds, but massive, poorly-sorted, several meter-thick beds with cross-beds and outsized gravel to cobble clasts are also present. The upper diamictite-rich interval begins with massive diamictite with clasts of sandstone and volcanic rocks and culminates with stratified diamictite and a ~10 cm thick clay bed that is sharply overlain with laminated limestone of the Taishir Fm (fig. 7F).

Taishir Formation.—The Taishir Fm consists of 300 to 600 m of carbonate that is comprised of four members (T1, T2, T3 and T4), which record four super-sequences (fig. 8). Carbonate lithofacies are defined (table 1) and used in the lithostratigraphic descriptions. In the discussion section, carbonate lithofacies are grouped into facies assemblages (table 2) to interpret evolving depositional environments and distinguish stratigraphic sequences. Sequences described are composed of nested parasequence sets within larger systems tracts (Sarg, 1988).

At all localities, the base of the lower member (T1) rests sharply on the Maikhan-Uul Fm with a 1 to 10 cm thick claystone layer at the contact (fig. 9A). In the Taishir region, the T1 cap carbonate is composed of ~0.1 to 0.5 m graded beds of grainstone and calcisiltite (fig. 9A) within background sedimentation of mm-pinstripe laminated micritic limestone (fig. 9B). The T1 cap carbonate is tan when weathered, dark gray when fresh. It is succeeded by 10 to 100 m of pink when weathered and recessive shale, limestone micrite, calcisiltite with minor nodular chert, and carbonate clast breccias interpreted as debris flows. T1 culminates with black lime-grainstone that also contains

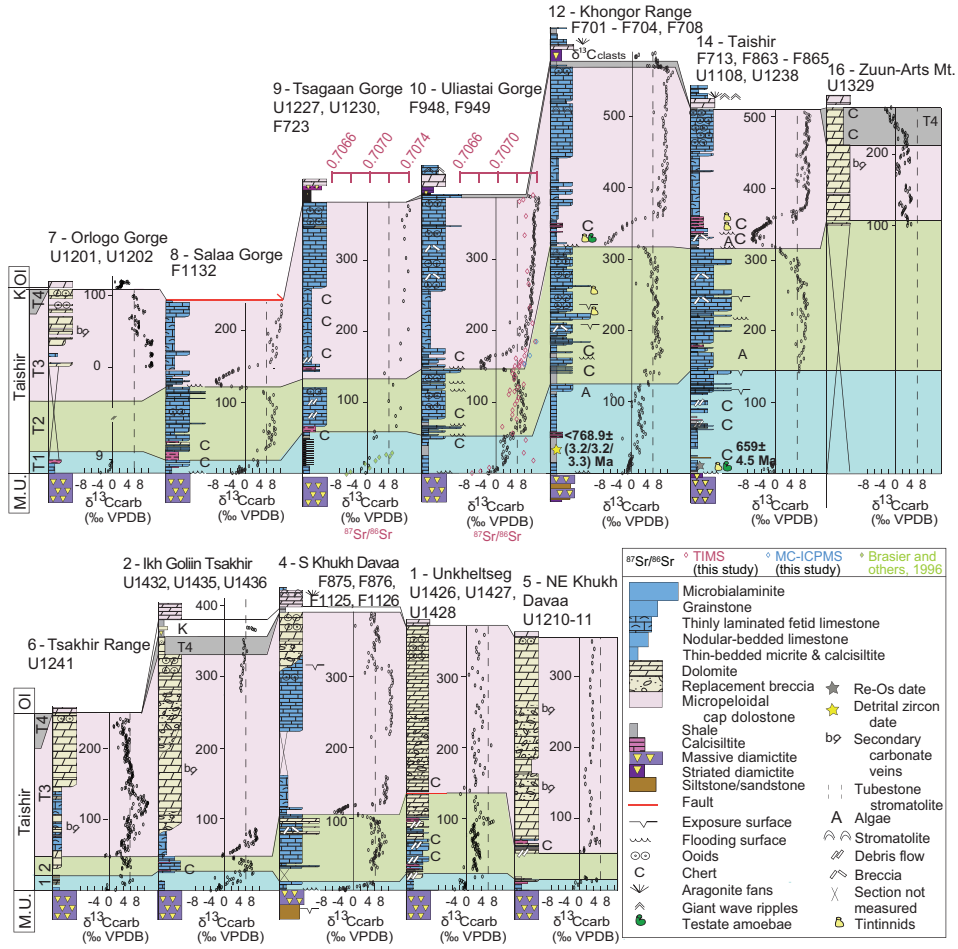

Fig. 8. Stratigraphy of the Taishir and Khongor formations. Location of sections is depicted in inset outline map. Key for the localities labeled in inset map is the same as in figure 3. Dashed line is drawn to highlight +6‰ $\delta^{13}C$ values. Microfossils, testate amoebae (Bosak and others, 2011a), tintinnids (Bosak and others, 2011b), and algae (Cohen and others, 2015) are shown stratigraphically. $^{206}Pb/^{238}U$ CA-ID-TIMS detrital age on tuffaceous sandstone from Member T1 of the Taishir Fm is shown with the corresponding maximum age. $\delta^{13}C$ values plotted in Tsagaan Gorge section are from Brasier and others (1996).

nodular chert. To the south and west, T1 thins to <10 m and is composed entirely of mm-laminated micritic limestone (fig. 9B).

The second sequence (T2), thins to the south and west and begins with 1 to 10 m of limestone calcisiltite and thin-bedded micrite with abundant chert nodules, followed by 50 to 200 m of blue when weathered carbonate in 1 to 10 m thick carbonate parasequences (fig. 9C). The parasequences typically begin with flat- to nodular-bedded calcisiltite and micrite (table 1), succeeded by grainstone and capped either by microbialite or brecciated exposure surfaces. The tops of these parasequences are also commonly partially dolomitized (fig. 9D). Giant ooids, <1 cm in diameter, are common in T2 (fig. 4C).

T2 is sharply overlain by an abrupt, recessive flooding surface (fig. 9E), marking the base of T3. The third Member, T3, begins with 10 to 50 m of thin-bedded limestone micrite with interbeds of debris flows with numerous black chert beds and nodules.

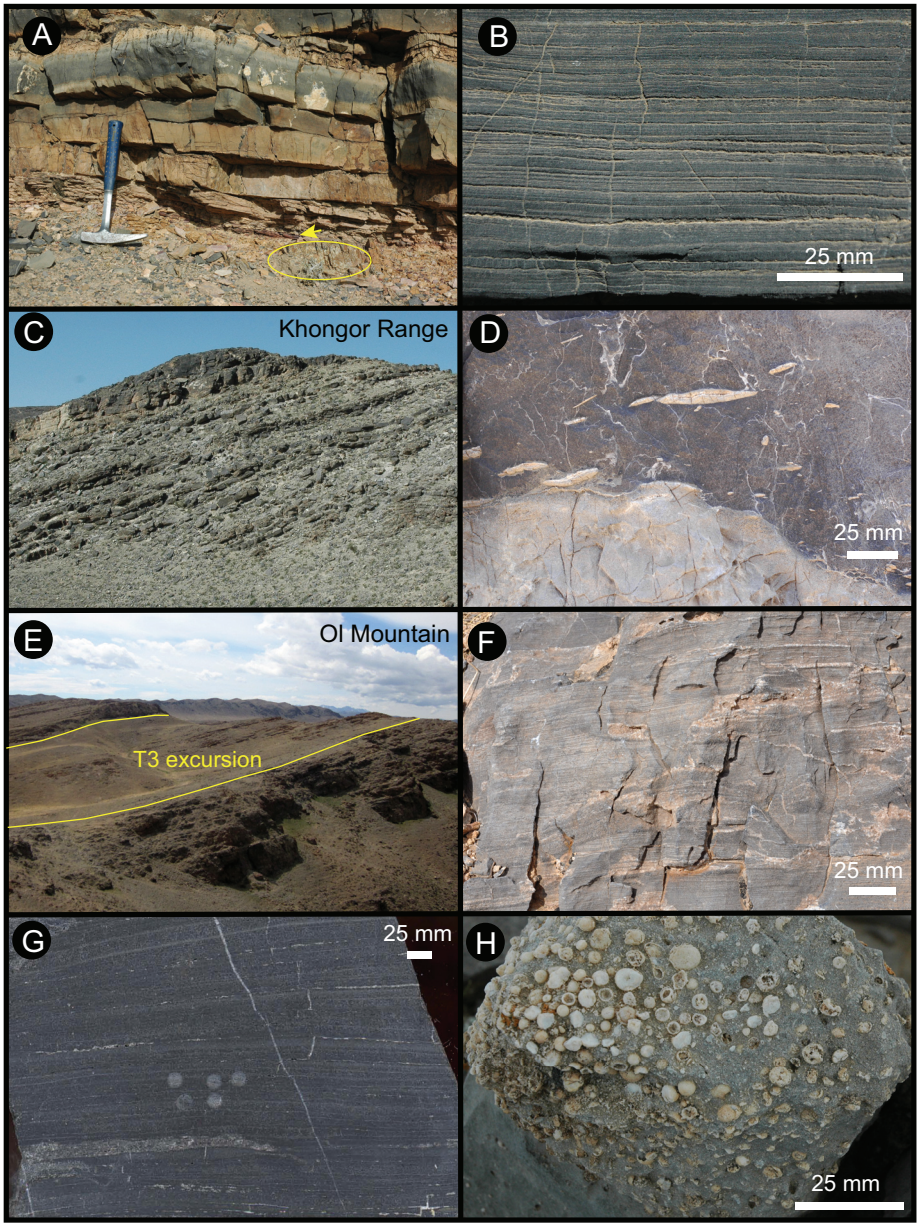

Fig. 9. Sedimentary textures in the Taishir Formation. (A) Basal contact of Taishir Formation at western Taishir. Rhyolite clast in uppermost Maikhan-Uul Formation is circled. Arrow points to red claystone layer that separates the Maikhan-Uul and Taishir formations. At this locality, the basal Taishir Formation consists of ~0.1 m of graded beds of grainstone and calcisiltite in a background of mm-pinstripe laminated micrite. (B) Pinstripe lamination of the basal T1 cap limestone at Shivee Tsakhir. (C) Resistant ledges marking meter-scale parasequences in T2 at Khongor Range. Field of view is ~20 m. (D) Partially dolomitized top of parasequence in T2 at Khukh Davaa. Dolomitized parasequence cap is cut by a scour surfaced and filled with a lime-grainstone with chips of the underlying dolomitized unit. (E) Recessive calcisiltite and shale interval marking the onset of T3 and the Taishir excursion at Ol Mountain. Field of view is ~35 m. Note how bedding becomes thinner above the recessive interval. (F) Dolomitized T3 of the Taishir Formation exposed in the Unkheltseg Mountain (U1427). (G) Polished slab showing micro-grading and mm-scale bands of remineralization in sulfidic calcisiltite of T3 at Salaa Gorge. Pits are micro-drill holes used to extract carbonate powder for geochemical analyses. (H) Partially dolomitized giant ooids from top of T3 near Ol Mountain.

These beds are succeeded by massive weathering, mm-laminated, dark, fetid thin-bedded limestone micrite with common contortions interpreted as slump folds. The lamination is highlighted by mm-scale lighter bands of calcite (fig. 9G), presumably created through remineralization and the *in situ* production of carbonate alkalinity. These massive black mudstone facies were originally interpreted as deepwater microbialaminites (Macdonald and others, 2009a; Johnston and others, 2012) due to their superficial similarity to massive microbialaminites in the Rasthof Fm (Pruss and others, 2010). However, petrographic examination has revealed micro-grading without strong microbial fabrics (fig. 9G). Consequently, we have reinterpreted these facies as allodapic micritic carbonate deposited below storm wave base and distal to massive grain flows and debris flows. Although microbes may have been involved in remineralization and the creation of the thin bands of light-colored calcite and crinkly lamination, these microbes did not necessarily form mats. This massive unit of black carbonate mudstone is succeeded by thickly bedded grainstone with giant ooids. Unlike other units that generally thin to the south and west, the thickness of T3 is relatively consistent across the platform.

Exposure in the Khongor Range (stratigraphic sections F701-704 and F708, fig. 8) is similar to what is exposed in the Taishir Region. Here, T1 culminates with lime-grainstone. T2 begins with shale and calcisiltite, followed by m-scale carbonate parasequences defined by interbeds of thin-bedded limestone micrite and calcisiltite and blue when weathered, dark gray when fresh grainstone. T2 is ~20 m thicker than T2 at the Taishir locality and chert nodules are common in the lower portion, whereas <1 cm ooids become common towards the top. The base of T3 is also well-exposed and succeeded by thick fetid limestone. Top of T3 is defined by massively bedded lime-grainstone with <1 cm ooids at the top. Importantly, this unit is overlain by <10 m of thin-bedded limestone micrite and black shale (T4), which is sharply overlain by the Khongor Fm diamictite.

The Taishir Fm exposure in Uliastai Gorge (stratigraphic sections F948 and F949) of the Khunkher block is comparable and similar to exposures in Tsagaan Gorge (stratigraphic sections U1227, U1230 and F723) of Tsagaan block (fig. 8). T1 is thinner but T2 is thicker than Khunkher block section. The direct contact of the Maikhan-Uul Fm and the T1 cap carbonate is not exposed in Tsagaan Gorge although the Maikhan-Uul Fm is well-exposed and preserved. In addition, T1 recessive interval is composed of dominantly black shale with interbeds of thinly-bedded and dark colored carbonate and thin-bedded micrite and nodular-bedded limestone with lenticular chert nodules. T2 is composed of massively bedded lime-grainstone with abundant intraclast breccia and lenticular chert nodules with redeposited clasts and coated grains that become more common up-section. However, in Uliastai Gorge, T2 is dominated by ooid lime-grainstone. The lower T3 that hosts the Taishir excursion is not well-exposed in Tsagaan Gorge compared to Uliastai Gorge but the rest of the T3 including fetid and massively weathered limestone mudstone and ooid lime-grainstone is similarly well-exposed. Although not complete, the Member T4 is preserved in Uliastai Gorge and consists of ~2 m of microbialiminite, which is overlain by <2 m of shale.

In Salaa Gorge (stratigraphic section F1132, fig. 8) of the Salaa block, T1 becomes even thinner and is entirely composed of mm-laminated micritic limestone with a few meters of pink calcisiltite on top. At the top of the pink calcisiltite unit, gray when fresh dolostone bed with occasional chert nodules is present and is succeeded by patchily exposed, dark gray when fresh lime-grainstone. The overall thickness of T2 is greater than elsewhere. The T2 flooding surface begins with shale and is succeeded by lime-grainstone with minor interbeds of <10 m thick thin-bedded limestone micrite with black chert nodules. The base of T3 and the overlying fetid, thin-bedded

limestone micrite and calcisiltite are well-exposed at Salaa Gorge and starts out with interbeds of thin-bedded micrite, nodular-bedded limestone, and grainstone followed by dark gray when fresh, fetid limestone mudstone with an interbed of lime-grainstone. The uppermost part of T3, usually characterized by ooid lime-grainstone, is faulted out at this locality.

In Orlogo Gorge (stratigraphic sections U1201 and U1202, fig. 8) of the Orlogo block, the Taishir Fm is patchily preserved compared to elsewhere with some units that are not exposed in the transition between the members. Thin (mm)-laminated micritic limestone of the T1 cap carbonate is overlain by recessive, poorly exposed, pink when weathered calcisiltite. The upper portion of T1, the whole of T2, and the lower portion of T3 were not measured at this locality due to poor exposure. However, T3 starting from the upper part of the fetid, massively weathered, thin-bedded limestone micrite to the Ol Fm carbonate was measured. The upper portion of T3 is dolomitized at this locality and transitions from limestone to partially dolomitized limestone to dolostone are well-preserved. The dolomitized strata of T3 are composed of brown- to yellow-colored ooid dolostone grainstone that is sugary and vuggy with abundant secondary calcite veins. More than a meter of non-exposure separates the Taishir Fm and the overlying Ol Fm, which could be correlated to either T4 or the Khongor Fm.

Similar facies of the Taishir Fm are exposed at the NE Khukh Davaa (stratigraphic sections U1210 and U1211) and Unkheltseg (stratigraphic sections U1426, U1427 and U1428) localities although most of the carbonates are dolomitized (fig. 8). T1 is only 10 to 13 m thick at both localities and composed of thinly laminated micritic limestone at the base that is succeeded by a recessive unit composed of fine- to medium-bedded, gray limestone and pink calcisiltite. Interbeds of black shale are common at Unkheltseg Mountain where the overlying ~80 m thick interval of T2 is characterized by carbonate parasequences that are composed of dolomite allochems marked by intraclast breccia with bedded and nodular chert. Although the parasequences are mostly dolostone, the lower ~50 m of this sequence are dominated by limestone, and the transition from limestone to dolostone is characterized by alternations of limestone and dolomite breccia up to the shale and calcisiltite at the base of the T3. The recessive unit is composed of pink calcisiltite and brown to gray, thinly-laminated, dark gray limestone with occasional intraclast breccia and chert nodules succeeded by lime-grainstone. The rest of the T3 is heavily dolomitized and composed of recrystallized, sugary, and vuggy dolo-grainstone.

In the South Khukh Davaa block (stratigraphic sections F875, F876, F1125 and F1126; fig. 8), the contact between the Maikhan-Uul and the basal Taishir Fm is well-preserved and exposed. However, the T1 cap carbonate becomes very thin and is composed solely of mm-laminated black limestone. It is overlain by lime-grainstone and a ~20 m interval that is not exposed. The base of T2 is characterized by thick limestone microbialite and thin-bedded limestone micrite. It is succeeded by thick lime-grainstone with several interbeds of microbialite towards the top. The base of T3 is well-exposed at this locality and is composed of thin-bedded limestone micrite. Aside from a thick non-exposed interval, the upper portion of T3 is well-exposed with a transition from limestone to dolostone towards the top. Above the non-exposed interval, the upper part of the T3 continues for ~170 m with the upper ~85 m dolomitized. The dolostone is characterized by sugary and vuggy dolo-grainstone with abundant ooids. Due to silicification, the ooids stand out in relief.

At Ikh Goliin Tsakhir Mountain (stratigraphic sections U1432, U1434 and U1436, fig. 8) of the South Khukh Davaa block, the contact between the Maikhan-Uul and Taishir fms is well-exposed, and T1 and T2 are thin. T1 is composed of mostly mm-laminated micritic limestone, which is succeeded by a recessive unit with fine (<10 cm) interbeds of limestone. A massively-bedded limestone caps the recessive unit. The

base of T2 is well-exposed and characterized by a recessive unit, which is composed of interbeds of red and pink shale, calcisiltite and weakly-laminated, light brown when weathered limestone. This light brown limestone is succeeded by medium- to thick-bedded, black gray limestone with bedded to lenticular chert beds, followed by massively weathering, black limestone with occasional beds of intraclast breccia. The lower recessive portion of T3 is composed of <10 cm bedded, massively weathered orange to brown limestone micrite. It is overlain by fetid thin-bedded limestone micrite and an additional ~250 m of dolomitized T3. The dolomitized strata are intensely veined and brecciated. Similar to Unkheltseg, both texture retentive and destructive dolostone are present. The brecciated interval is succeeded by coarsely recrystallized, vuggy and sugary dolostone with silicified ooids. Above the ooid dolo-grainstone, dolomitized T4 is present (fig. 8) and characterized by a ~25 m thick, weakly-laminated, blue-gray, recrystallized dolostone that is overlain by the Khongor diamictite.

In the Tsakhir Range (stratigraphic section U1241, fig. 8) of the Tsakhir block, the Taishir Fm is relatively thin. At this locality, the contact of the Maikhan-Uul and Taishir fms is well-exposed. Mm-laminated micritic limestone of the T1 cap carbonate is overlain by a poorly exposed recessive unit characterized by subcrop of pink calcisiltite and thinly-bedded black limestone. The upper portions of T1 through the base of T3 are not exposed but subcrop measures to <50 m. The overlying fetid thin-bedded limestone micrite of the T3 is present but partially dolomitized. Similar to the other localities, the Taishir Fm is preserved as dolostone that is heavily veined and brecciated. Both texture retentive and destructive dolostone are present and are capped by sugary and vuggy, recrystallized ooid dolostone grainstone. In the Tsakhir Range the Ol Fm directly overlies the Taishir Fm.

At Zuun-Arts Mountain (stratigraphic section U1329, fig. 8), due to abundant Permian intrusions nearby, T1 and T2 are poorly exposed. Laterally, they crop out and are composed of limestone. However, in section U1329, only the upper T3 and its transition to Ol Fm are captured. Here, the whole T3 is composed of recrystallized, sugary, and vuggy dolo-grainstone. It is succeeded by medium-bedded, light blue gray when weathered, black blue gray when fresh, and recrystallized dolostone that is attributed to T4.

Khongor Formation.—The Khongor Fm is composed of carbonate clasts in weakly stratified shale, siltstone, or calcisiltite matrix. Clasts range from gravel to boulder in size and are typically sub-angular to sub-rounded (figs. 8 and 10A). The Khongor Fm is thickest and best exposed and preserved in three localities: the eastern tributary of Tsagaan Gorge (stratigraphic section F723), Khongor Range (stratigraphic sections F708 and F949) and Ikh Goliin Tsakhir Mountain (stratigraphic section U1433) (fig. 8). However, like the Maikhan-Uul Fm, there are significant facies changes due to channelization.

In the eastern tributary of Tsagaan Gorge (figs. 8 and 10A), the Khongor Fm diamictite is ~25 m thick and is composed of pebble- to boulder-sized clasts of blue-gray limestone from the underlying Taishir Fm in a dark gray wackestone matrix that becomes lighter colored upwards with increasing carbonate content. A glacial origin is demonstrated by the presence of spectacular striated clasts (Macdonald and others, 2009a), and cobble dropstones (fig. 10C) that penetrate and deform the bedded, shale matrix. Just 6 km west, the diamictite is nearly absent with only 2 m of recessive siltstone preserved.

The Khongor Fm in the Khongor Range (stratigraphic section F708, fig. 8) consists of ~16 m of sub-rounded limestone pebbles and cobbles in weakly stratified, gray shale to wackestone matrix. Elsewhere, on the thrust blocks to the northeast, the Khongor Fm is either thin or absent. Although most clasts in the exposure of the

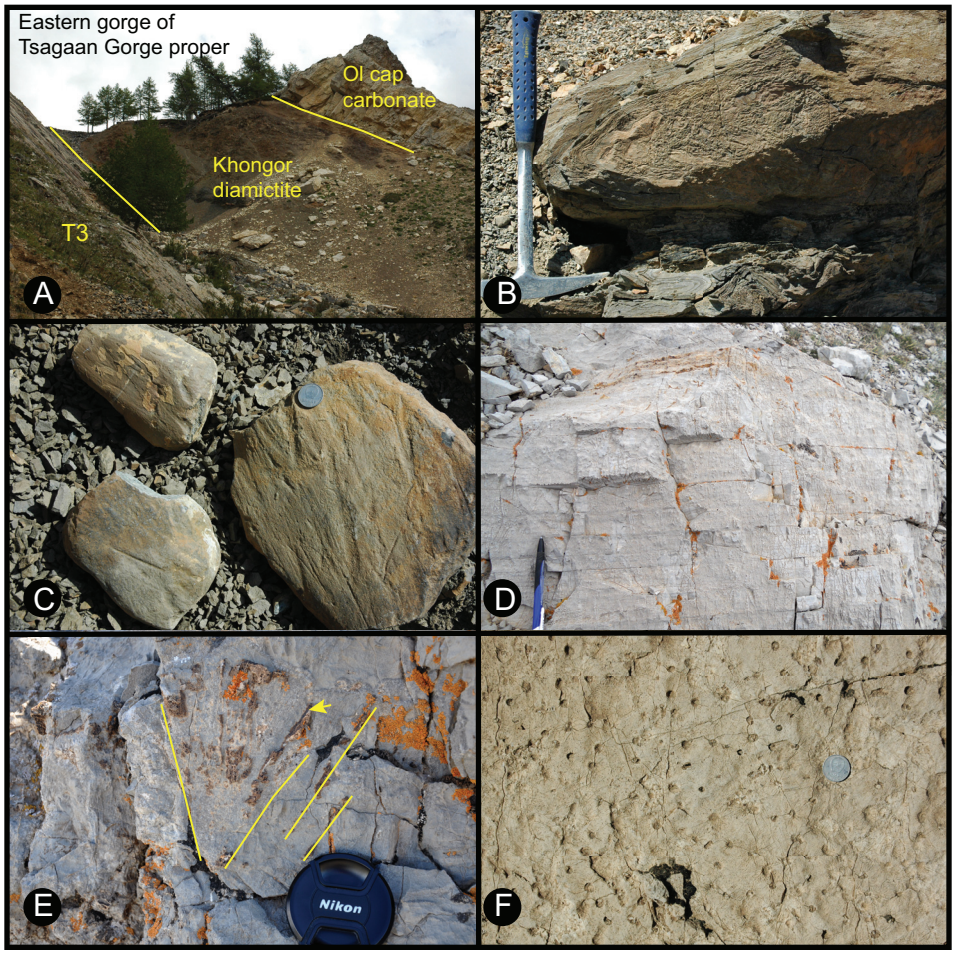

Fig. 10. Sedimentary textures in the Khongor and Ol formations. Mongolian coin is 2.25 cm in diameter. (A) Khongor diamictite and Ol cap dolostone exposure at Tsagaan Gorge tributary (eastern gorge of Tsagaan gorge proper). Tree in foreground is growing off of the basal contact with T3. Section is 22 m thick. Ol cap dolostone is in top right of frame. (B) Limestone clast with soft-sedimentary, glacitectonic folding from Khongor diamictite. (C) Striated clasts of the Khongor Formation as preserved in the eastern tributary of Tsagaan Gorge. (D) Finely laminated, pale white colored Ol cap dolostone. Photo is taken in South Khukh Davaa block (U1216). Pen is 14 cm in length. (E) Silicified aragonite fan growth in the Ol Formation carbonate (U1217). (F) Plan view of tubestone stromatolites in Ol cap dolostone taken from near Taishir.

Khongor Fm at the eponymous location can be identified as sourced from the Taishir Fm, clasts of carbonate mudstone with intense soft sediment deformation (fig. 10B) were not recognized from exposures of the underlying Taishir Fm. Concentrations of boulder clasts ('boulder nests') are present in the Khongor Range exposures (Macdonald, 2011).

The Ikh Goliin Tsakhir (stratigraphic section U1435, fig. 8) is the third locality where the Khongor Fm is preserved as a thick diamictite (fig. 11A). At this locality, the basal part of the Khongor Fm is not well-exposed but is characterized by subcrops of shale and siltstone with pebble-sized carbonate clasts. Interestingly, there is <5 m thick, brown weathered, black to gray fresh, coarsely recrystallized dolostone preserved

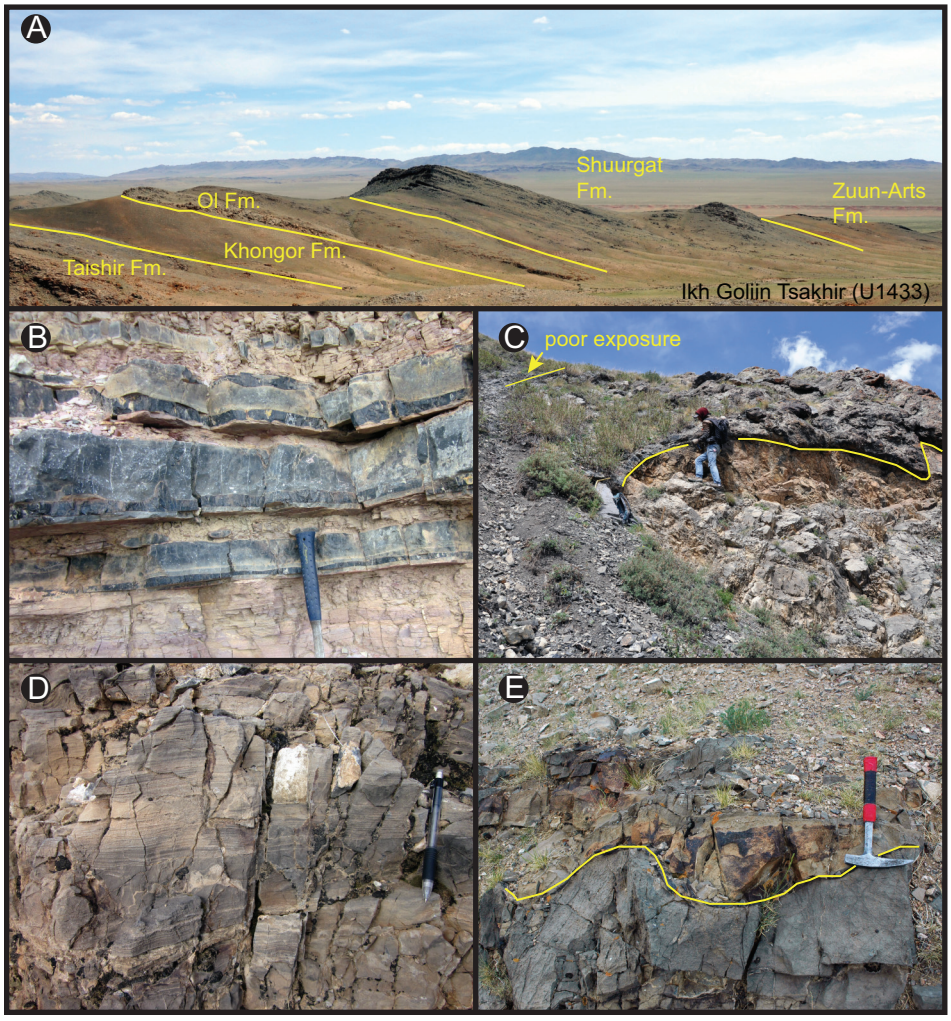

Fig. 11. The Shuurgat Formation. (A) Complete section of the upper Tsagaan-Olom Group, T3 to the base of Zuun-Arts Formation. Photo is taken in the Ikh Goliin Tsakhir Mountain of the southern Khukh Davaa block. View to the west. (B) Sh1 Member of the Shuurgat Formation characterized by interbedded black limestone, bedded chert and pink calcisiltite. (C) An extensively silicified exposure surface at the top of the Sh2 in Khunkher Gorge (F872 and U1437). Person in scale is 1.8 m tall. (D) Laminated dolo-micrite of Sh2 of the Shuurgat Formation at Ol Mountain (U1337). Quartz-sand filled karst surface present at the top of the Shuurgat Formation in northeastern Khukh Davaa Region of Tsagaan block (F1206).

a few meters above the poorly exposed base of the Khongor Fm. It is succeeded by dark green to gray wackestone matrix diamictite with gravel to cobble clasts. This dolostone could either represent a large clast or could be part of T4.

At the South Khukh Davaa block (stratigraphic section F875, fig. 8), the Khongor Fm is also present, albeit poorly exposed. Here the Khongor Fm is 7 m in thickness, including 2 m of unit that is not exposed at the base and overlying subcrops of rounded clasts in a green wackestone matrix.

Ol Formation.—The Ol Fm sharply overlies the Khongor diamictite and marks the beginning of the Ediacaran Period on the Zavkhan Terrane (Macdonald and others, 2009a). The sequence begins with <40 m of buff-colored, finely-laminated micropeloi-

dal dolostone (fig. 10D), which locally contains tubestone stromatolites (fig. 10F) and giant wave ripples (Macdonald and others, 2009a; Macdonald, 2011; Bold and others, 2013). At some localities, the cap dolostone is succeeded by aragonite crystal fans that are pseudomorphed by dolomite and sometimes silicified (pseudomorphed aragonite crystal fans) (fig. 10E) present both as individual blades growing upwards into the sediment, similar to the Hayhook Member in the Mackenzie Mountains of Canada (Aitken, 1991), and as crystal fan shrubs that are over 10 cm across, as is seen in northern Namibia (Hoffman and Halverson, 2008). Elsewhere, this limestone is dolomitized to a chocolate brown colored dolostone that co-occurs with disseminated barite, barite breccia (dolomitized pseudomorphed barite breccias, recognized visually by crystal habit), and locally barite fans (Hoffman and others, 2011). For mapping purposes, the first transgressive sequence above the finely laminated micropeloidal dolostone is included in the Ol Fm.

At the Zuun-Arts locality (stratigraphic section U1329, fig. 12), the Ol cap dolostone is ~6 m thick. It is succeeded by ~28 m of light brown when fresh, chocolate brown when weathered, finely-bedded dolostone.

At Ol Mountain (stratigraphic section U1337, fig. 12) of the Taishir block, the cap dolostone is ~7 m thick and is succeeded by thinly-bedded, chocolate brown colored dolostone with <50 cm tall wave ripples and disseminated barite. The start of the overlying transgressive sequence is poorly exposed. At Ol Mountain, the top of the Ol Fm consists of ~22 m of massively bedded, dark gray dolostone.

In the Khongor Range (stratigraphic sections F708 and F949, fig. 12) of the Taishir block, the Ol Fm is very well-exposed and preserved, and it overlies one of the thickest sequences of the Khongor Fm diamictite. There the base of the Ol Fm, the cap dolostone, is ~8 m thick and consists of buff-colored micropeloidal dolostone. It is succeeded by blue-gray nodular-bedded limestone and thinly-bedded, dark gray lime-micrite interbedded with shale and calcisiltite. This succession contains abundant chert nodules and is capped by massively bedded lime-grainstone (fig. 12).

In Khunkher Gorge (stratigraphic sections F872 and U1437, fig. 12), the basal Ol cap dolostone is ~11 m thick and overlies a ~2 m poorly exposed interval above the ooid lime-grainstone of the T3 Member of the Taishir Fm. The cap dolostone is overlain by a recessive unit and is composed of interbeds of blue dolostone grainstone and calcisiltite. It is succeeded by a recessive unit composed of mostly thin-bedded mircrite and nodular-bedded limestone, interbedded with thin beds of calcisiltite. The uppermost unit of the Ol Fm, which is often massively bedded blue limestone is faulted out and juxtaposed against the second member of the Shuurgat Fm.

In the western tributary of Tsagaan Gorge (stratigraphic sections F724 and U1235, fig. 12), the basal contact of the Ol Fm with the underlying Khongor Fm is well-exposed. Although the basal exposure is poor in the main Tsagaan Gorge, the mm-laminated, micropeloidal dolostone of the Ol Fm is well-exposed and is ~11 m thick. It is succeeded by light blue dolostone. The overlying recessive unit is not exposed for ~4 m. At this locality, the uppermost Ol Fm is composed of blue dolostone with black chert nodules. The contact between the upper Ol Fm and the overlying Shuurgat Fm is poorly exposed.

At the northeastern Khukh Davaa locality (stratigraphic section F1206, fig. 12) of the Tsagaan block and in Shuurgat Range of the Taishir block, the Ol Fm is not well-exposed. A series of faults are mapped both below and above the different units of the Ol Fm. At Unkheltseg and Ikh Goliin Tsakhir localities of the South Khukh Davaa block, the Ol Fm is better exposed and appears thicker. At the Unkheltseg locality, a meter of non-exposure is present below the base of the Ol Fm. The buff-colored, finely-laminated micropeloidal dolostone is ~23 m thick and is overlain by massively-bedded, dark blue to gray dolostone. It is succeeded by finely-laminated, chocolate

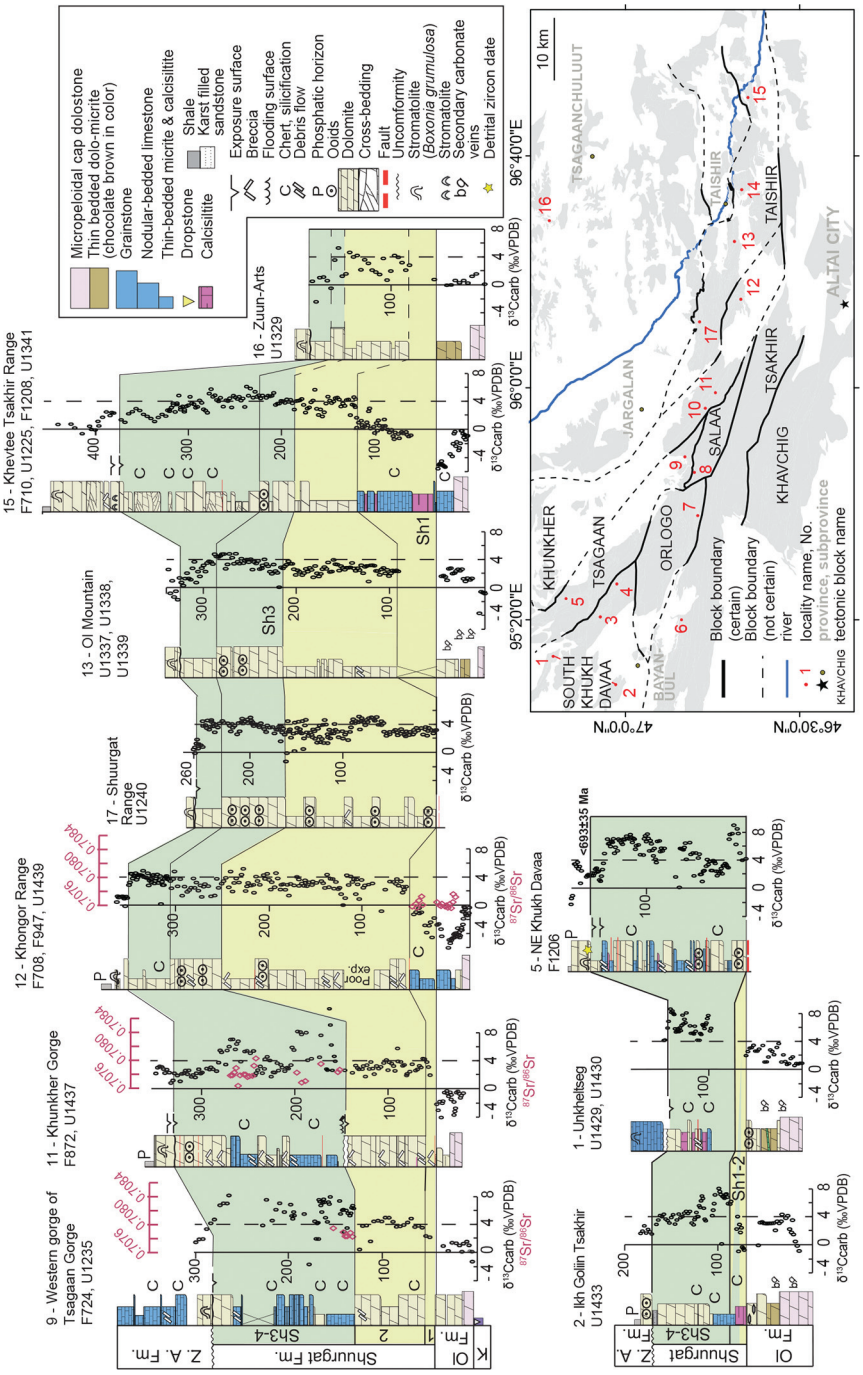

Fig. 12. Stratigraphy of the Ol and Shuurgat formations. Location of sections is depicted in inset outline map. Key for the localities labeled in inset map is the same as in figure 3. Dashed line is drawn to highlight +4‰ $\delta^{13}C_{carb}$ values. $^{87}Sr/^{86}Sr$ values are co-plotted with $\delta^{13}C$ where measured.

brown colored dolostone. The overlying recessive unit is poorly exposed, but all of the interbeds that crop out are massively-bedded dolostone, which culminates with beds of ooid dolo-grainstone. Due to silicification, ooids become prominent and are lithologically indistinguishable from silicified giant ooids at the top of T3.

At Ikh Goliin Tsakhir (stratigraphic sections U1433 and U1435, fig. 12), the contact with the underlying Khongor Fm is well exposed. The buff-colored, finely-laminated micropeloidal cap dolostone is comparatively thicker than elsewhere. It is succeeded by ~15 m thick, chocolate brown, finely-bedded dolostone. There is no recessive unit present at this locality. Instead, finely laminated micropeloidal dolostone is overlain by dark gray when fresh, poorly-bedded dolo-grainstone. Above, the exposure becomes poor but where it crops out the dolostone unit is composed of nodular-bedded dolostone with lenses of green siltstone and shale. The micropeloidal dolostone as well as the overlying dolostone contains veins of pseudomorphed calcite and barite. Recessive interbeds of black limestone and pink calcisiltite of the basal Shuurgat Fm overlie the Ol Fm.

Shuurgat Formation.—The Shuurgat Fm (Bold and others, 2013) is composed of 100 to 500 m of carbonate that comformably overlies the Ol Fm. The Shuurgat Fm is best exposed at Khongor, Shuurgat, Ol Mountain and in the Khevtee Tsakhir Range. For mapping purposes, we have divided the Shuurgat Fm into four members (Sh1, Sh2, Sh3, and Sh4). Broadly, Sh1 is dominated by recessive calcisiltite that shoal upwards into massively weathering dolostones of Sh2. Although these dolomites are massive on the outcrop scale, where primary fabrics are preserved, Sh2 consists predominantly of finely-laminated micrite, with rare ooid grainstone beds, but dolomitization was fabric destructive, leaving a zebra dolostone texture (Vandeginste and others, 2005). Sh1 and Sh2 exhibit large lateral facies changes and vary in thickness from ~20 to 200 m. Sh2 is capped by a karstic erosional surface that is best developed at Khunkher Gorge (fig. 11C). The overlying members Sh3 and Sh4 consist of blue colored limestone and dolostone with well-developed parasequences and common chert nodules and beds. Dolomitization is fabric retentive and more common to the northeast. The top contact of the Shuurgat Fm is defined by quartz sandstone-filled grikes (fig. 11E) along a karstic unconformity, locally with several meters of relief. Below we describe 10 measured sections of the Shuurgat Fm from representative structural blocks.

At Zuun-Arts (stratigraphic section U1329, fig. 12), the Shuurgat Fm is comparatively thin. The recessive Member Sh1 is poorly-exposed. It is overlain by thinly-bedded, dolo-micrite and nodular-bedded dolostone of Sh2 and dolo-grainstone of Sh3. Sh4 is composed of light blue-gray when fresh, medium-bedded micritic dolostone, which is capped by the uncomformity that defines the top of the Shuurgat Fm.

In Khevtee Tsakhir Range (stratigraphic sections F1208, U1225, and U1341, fig. 12) of the Taishir block, all four members are well-defined and exposed. Member Sh1 is composed of interbeds of purple when weathered calcisiltite and dark gray nodular-bedded limestone. The basal ~60 m is dominated by calcisiltite, which is overlain by nodular-bedded limestone with abundant chert nodules and beds. The upper ~30 m is carbonate-dominated with minor interbeds of calcisiltite and shale. Local folding is apparent at the top of Sh1 with fold axes trending ENE-WSW. The overlying Sh2 is characterized by thinly-bedded dolo-micrite that is variably brecciated. It is succeeded by Sh3 that is recrystallized, sugary and vuggy dolo-grainstone with occasional ooid shoals. Sh4 is ~150 m thick (fig. 12) and is composed of crossbedded nodular bedded dolostone and dolo-grainstone in ~5 meter-scale parasequences that are variably silicified with abundant chert beds and nodules. Multiple karst surfaces are present at the top of Sh4 and are defined by <0.5 m local relief filled with carbonate breccia. The

uppermost karst surface is overlain by dolo-grainstone with both domal and columnar stromatolites of the Zuun-Arts Fm.

At Ol Mountain (stratigraphic sections U1337, U1338, and U1339, fig. 12) of the Taishir block, the Shuurgat Fm begins with non-exposed interval above the massively bedded dolostone of the upper Ol Fm. Abundant black chert, red calcisiltite, and pink siltstone of Sh1 are present in the scree. These strata are succeeded by thinly laminated dolostone of Sh2 that is variably brecciated with massively bedded dark gray dolostone in the middle. Sh3 begins with brown to gray, sugary dolo-grainstone with ooids that are variably silicified. It is overlain by Sh4 that is composed of medium-bedded, light-gray when weathered nodular-bedded limestone with silicified vugs towards the top. Here the karsted surface at the top of the Shuurgat Fm is not well-exposed.

In the Shuurgat Range (stratigraphic section U1240, fig. 12) of the Taishir block, Sh1 is faulted and the rest of the Shuurgat Fm is very-well exposed. Hence, exposed Sh2 is ~160 m thick and composed of alternations of thinly laminated dolo-micrite (fig. 11D) that is variably brecciated and occasional massive, dark gray ooid dolo-grainstone. Succeeding Sh3 is composed of light blue-gray silicified ooid dolo-grainstone and is lithologically similar to that exposed at Ol Mountain. Sh4 at this locality is composed of variably silicified nodular-bedded dolostone.

The Khongor Range (stratigraphic sections F708 and U1439, fig. 12) of the Khunkher block is another locality where the Shuurgat Fm is well exposed and thick. Member Sh1 is composed of pink calcisiltite with interbedded black limestone and bedded chert (fig. 11B). Sh2 is thickest in the Khongor Range and is composed of primarily thinly laminated dolo-micrite that is variably brecciated and occasional massive-bedded ooid dolo-grainstone. Sh3 is thinner consisting of thinly-bedded, light-gray, variably silificied ooid dolo-grainstone and is succeeded by variably silicified, fine- to medium-bedded, light gray dolo-grainstone that is assigned to Member Sh4.

In Khunkher Gorge of Khunkher block as well as in Tsagaan and South Khukh Davaa blocks, carbonate facies of Sh3 change dramatically from east to west and are composed of thinly laminated micrite and nodular-bedded limestone with abundant chert nodules and lenses (fig. 12). At these localities, Sh4 is also dominated by limestone and it is especially prevalent in Khunkher and western tributary of Tsagaan gorges with interbeds of calcisiltite and a few meters thick dolostone. Due to the carbonate facies similarity between Sh3 and Sh4 in these localities, on figure 12, we group these together as Sh3-4 but acknowledge that in other localities, Member Sh3 is easily identifiable as thickly bedded blue-gray dolo-grainstone with ooid shoals.

In Khunkher Gorge (stratigraphic sections F872 and U1437, fig. 12), the basal member of the Shuurgat Fm is not exposed. Member Sh2 is faulted against the upper part of the Ol Fm and is composed of massively recrystallized thinly-laminated dolo-micrite and nodular bedded dolostone that are variably brecciated. A sandstone-filled karst with a meter of relief is present at the top of Sh2 (fig. 11C). It is succeeded by Sh3 and Sh4 that are composed of fine- to medium-bedded lime-micrite with black chert, calcisiltite and shale with thin interbeds of intraclast breccia. There is a ~40 m-thick dolo-micrite and nodular bedded dolostone present in the middle of this limestone dominated succession, and the uppermost ~65 m are also composed of dolostone that is characterized by recrystallized, massive-bedded dolo-grainstone with minor ooid shoals developed at the top. Above the unconformity at the top of the Shuurgat Fm, dolo-grainstone with columnar stromatolites is present with multiple small-scale exposure surfaces that are defined by local relief and secondary silicification.

In the western tributary of Tsagaan Gorge (stratigraphic sections F724 and U1235, fig. 12), the whole Shuurgat Fm is patchily exposed. The basal Sh1 recessive unit is poorly exposed and abundant black chert, black limestone and pink when weathered calcisiltite are present in the scree. It is overlain by fine- to medium-bedded dolostone and massive-bedded dolo-grainstone that are variably brecciated of Sh2. Facies-wise, Sh3 is similar to the exposure at Khunkher Gorge and is limestone dominated. The limestone dominated strata of Sh3 and Sh4 at this locality starts out with thin-bedded micritic limestone that is capped by dolo-micrite. The transition from limestone to dolostone is poorly exposed here. Similarly to the Khunkher Gorge, this dolostone succession is succeeded by thin-bedded lime-micrite and nodular-bedded limestone. This limestone dominated strata of Sh4 is capped by massively-recrystallized dolo-grainstone. The uncomformity with the basal Zuun-Arts Fm at the top of the Sh4 is well-exposed at this locality and is defined by a white colored, poorly sorted sandstone that fills a karast surface.

At northeastern Khukh Davaa, Unkheltseg and Ikh Goliin Tsakhir localities, the whole Shuurgat Fm thins dramatically. In NE Khukh Davaa region (stratigraphic section F1206, fig. 12) of the Tsagaan block, Sh1 and 2 are faulted against the upper Ol Fm and parts of Sh3 and Sh4 are preserved as limestone. It is composed of ooid dolo-grainstone at the base that is succeeded by carbonate succession dominated by thin-bedded micritic limestone. The rest of the carbonate succession exposed at this locality is distinct by its ~30 m thick parasequences composed of alternating beds of thin-bedded micritic limestone, nodular-bedded calcisiltite and grainstone with occasional conglomerates interpreted as debris flows, pink when weathered calcisiltite and dolo-grainstone. Chert nodules and lenses are abundant throughout this succession. At the Unkheltseg locality (stratigraphic sections U1429 and U1430, fig. 12), the base of the Shuurgat Fm is not-exposed, and the overlying strata consists of recessive interbeds of <40 cm micritic nodular-bedded limestone, lime-grainstone, and pink when weathered calcisiltite with abundant chert nodules that are sometimes bedded to lenticular. These are succeeded by massively bedded, light gray when weathered lime-grainstone with occasional 2 by 1 cm chert nodules and are capped by a significant karst surface filled with quartz arenite. Above this uncomformity, the basal unit of the Zuun-Arts Fm is present and composed of massively bedded lime-grainstone with stromatolites.

At Ikh Goliin Tsakhir locality (stratigraphic section U1433, fig. 12) (fig. 11A), the base of the Shuurgat Fm, Sh1, is well-exposed but thin, which is composed of massive-bedded, black to gray dolo-micrite and purple calcisiltite with interbeds of limestone with intraclast breccia. The succeeding carbonate succession of Sh3 and Sh4 are ~85 m thick. The lower ~20 m are composed of thin-bedded micritic limestone with interbeds of purple calcisiltite, which is capped by massive-weathering, thin- to medium-bedded and light blue gray dolo-micrite. The uppermost ~6 m succession of Sh4 at this locality is characterized by primarily orange green when weathered siltstone with <2 m thick interbeds of brown gray when fresh dolo-grainstone. The base of the Zuun-Arts Fm that is usually represented by dolo-grainstone with stromatolite that is overlain by phosphatic shale is not present here. Instead, 6 m thick ooid dolo-grainstone is present below the phosphatic shale of the basal Zuun-Arts Fm.

U-Pb GEOCHRONOLOGY

Zircons were separated from samples of rhyolite, sandstone and a quartzite clast from the Zavkhan Fm and were subjected to U-Pb analyses by the isotope-dilution thermal ionization mass spectrometry (ID-TIMS) and *in situ* laser-ablation inductively coupled plasma mass spectrometry (LA-ICPMS) techniques in order to infer provenance for the Zavkhan Terrane basement and to constrain the age of the Zavkhan Fm volcanism. Zircons were also analyzed from a rhyolite and two tuffaceous sandstones

TABLE 3

Summary of magmatic and detrital samples dated

Sample No.	Member/Formation name	Location	Latitude	Longitude	Elevation, m
U1213	Zavkhan Fm	South Khukh Davaa	47°8.020'N	95°13.667'E	2180
F718	Zavkhan Fm	Taishir	46°41.241'N	96°34.567'E	1725
F701-14.5	Maikhan-Uul Fm	Khongor Range	46°40.801'N	96°16.524'E	2020
U1214	Zavkhan Fm	South Khukh Davaa	47°7.8370'N	95°13.105'E	2175
U1333	Zavkhan Fm	South Khukh Davaa	47°7.887'N	95°13.732'E	2245
F1203-272.1	Maikhan-Uul Fm	Tsagaan Block	47°11.280'N	95°23.580'E	1900
F868-64	Taishir Fm	Khongor Range	46°39.990'N	96°16.250'E	2018
F1206-146.1	Shuurgat Fm	Tsagaan Block	47°5.433'N	95°28.721'E	2070

(U-Pb ID-TIMS methods) from the Maikhan-Uul and Taishir fms, as well as sandstone from the Shuurgat Fm (LA-ICPMS methods), in order to establish a chronostratigraphy for the Tsagaan-Olom Group. Analyzed samples are listed in table 3 and the analytical methods are described in the Appendix (http://earth.geology.yale.edu/~ajs/SupplementaryData/2016/Bold). Complete U and Pb isotopic data are given in tables A1 and A2 (http://earth.geology.yale.edu/~ajs/SupplementaryData/2016/Bold) and plotted in figures 5, 13 and 14. The results are discussed in stratigraphic order below.

Geochronology Results

Sample U1213: Rhyolite in the lower Zavkhan Formation.—A 27.5 meter-thick green rhyolite flow bound by beds of conglomerate (figs. 4A and 5) was sampled on the South Khukh Davaa block (table 3). Thirty six zircon grains were dated by LA-ICPMS (table A1, http://earth.geology.yale.edu/~ajs/SupplementaryData/2016/Bold) from which five euhedral zircons were selected and pre-treated with the chemical abrasion method and analyzed (CA-ID-TIMS), yielding a statistically coherent cluster of data (fig. 13A) with a weighted mean $^{206}Pb/^{238}U$ date of 802.11 ± 0.45/0.56/1.0 Ma (see Appendix for date uncertainty notation, http://earth.geology.yale.edu/~ajs/SupplementaryData/2016/Bold) and a MSWD of 0.7. The latter serves as the best estimate for the age of rhyolite eruption.

Sample U1214: Sandstone in the lower Zavkhan Formation.—A dark purple, bedded sandstone was sampled in the conglomerate unit of the lower Zavkhan Fm in South Khukh Davaa block (table 3). Sample U1214 was taken from ~250 m below sample U1213 (see above). 162 detrital zircon grains (cores and magmatic rims) were dated by LA-ICPMS [figs. 4A, 14A, A3 and table A1 (http://earth.geology.yale.edu/~ajs/SupplementaryData/2016/Bold)]. Prominent peaks in the age spectra occur at 800 Ma, 2050 Ma, and 2500 Ma. Several (Archean) grains were analyzed, with the oldest having a $^{207}Pb/^{206}Pb$ date of 3699 ± 22 Ma.

Sample U1333: Quartzite clast in the conglomerate unit of the Zavkhan Formation.—A brown quartzite clast was sampled from within the conglomerate unit of the Zavkhan Fm in South Khukh Davaa block, to the NE of the Tsagaankhairkhan Mountain (table 3). 122 zircon grains were dated by LA-ICPMS [figs. 4A, 14A, A2 and table A1 (http://earth.geology.yale.edu/~ajs/SupplementaryData/2016/Bold)]. The dominant peaks are at 2000 to 2350 Ma and 2450 to 2550 Ma, in addition to several Archean age grains with the oldest having a $^{207}Pb/^{206}Pb$ date of 3366 ± 40 Ma.

Sample F718: Rhyolite from the top of the Zavkhan Formation.—A massive, ~5 meter-thick, green rhyolite was sampled at the top of the Zavkhan Fm near the town of Taishir

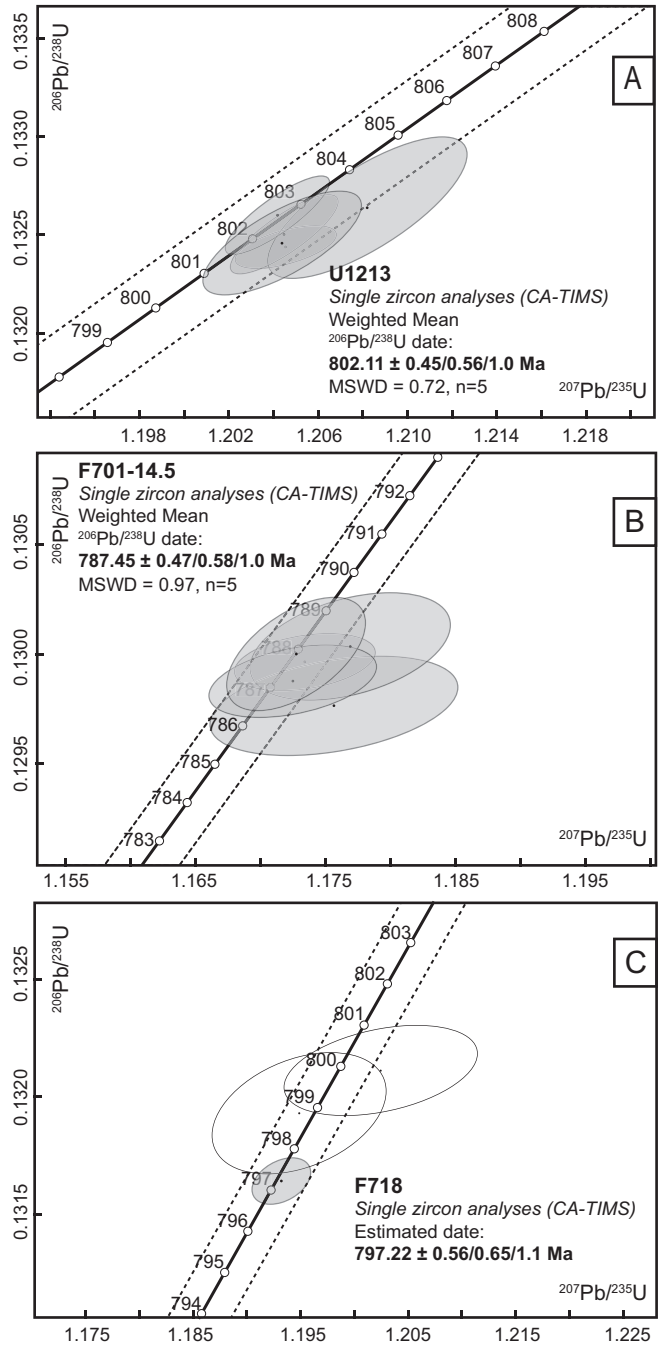

Fig. 13. Concordia diagrams of zircon $^{206}Pb/^{238}U$ CA-ID-TIMS dates. (A) U1213 – rhyolite from the Zavkhan Formation. (B) F701-14.5 – rhyolite olistolith near base of the Maikhan-Uul Formation. (C) F718 – rhyolite from the top of the Zavkhan Formation.

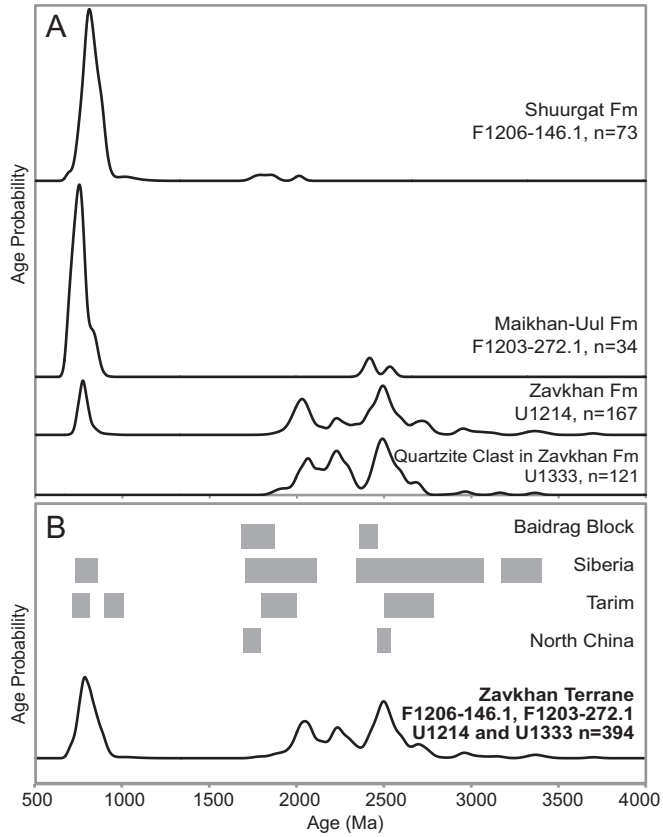

Fig. 14. Normalized probability plots. (A) Normalized probability plots of U-Pb dates obtained by LA-ICPMS from zircon from samples U1333, U1214, F1203-272.1, and F1206-146.1. (B) Dominant age peaks present in detrital zircon spectra of Precambrian rocks of Siberia, North China, Tarim, and Zavkhan Terrane. Dates used in normalized probability plot of the Zavkhan Terrane are the composite of the detrital zircon spectra in A. Dates used in the plots of Siberia, North China and Tarim are from Rojas-Agramonte and others (2011), Sun and others (2012) and Zhang and others (2013).

(table 3) and yielded only few quality zircons suitable for analysis. Three grains were analyzed by the CA-ID-TIMS method, producing scattered $^{206}Pb/^{238}U$ dates that range from 799.9 ± 1.1 Ma to 797.22 ± 0.56 Ma [figs. 5, 13C and table A2 (http://earth.geology.yale.edu/~ajs/SupplementaryData/2016/Bold)]. Because no statistically meaningful weighted mean date can be calculated, the youngest analysis is interpreted as a maximum age for the eruption/deposition of rhyolite.

Sample F701-14.5: Rhyolite olistolith (?) near base of the Maikhan-Uul Formation.—A green rhyolite was sampled 14.5 m above the base of the Maikhan-Uul Fm in the Khongor Range, along the southernmost part of the Bayan Gorge (table 3). It was from ~1 m thick rhyolitic welded tuff with eutaxitic texture and was originally interpreted as a bed as it extends laterally for <10 m, but cannot be followed further and disappears in non-exposure. Hence we interpreted it as a Zavkhan Fm rhyolite olistolith that forms a part of the Maikhan-Uul diamictite. Five overlapping zircon CA-ID-TIMS analyses yield a weighted mean $^{206}Pb/^{238}U$ date of 787.45 ± 0.47/0.58/1.0 Ma (MSWD = 0.97) [figs. 4C, 5 and 13B and table A2 (http://earth.geology.yale.edu/~ajs/SupplementaryData/2016/Bold)] that is interpreted as a maximum depositional age for the basal Maikhan-Uul Fm.

Sample F1203-272.1: Tuffaceous sandstone in the middle Maikhan-Uul Formation.—A green tuffaceous sandstone was sampled at the base of the middle Maikan-Uul Fm, directly above the lower massive diamictite of the Maikhan-Uul Fm, in exposures in the northeastern limb of the Khukh Davaa Range in Tsagaan block (table 3). Thirty four euhedral zircon grains were analyzed with LA-ICPMS [figs. 4A, 14A, A4 and table A1 (http://earth.geology.yale.edu/~ajs/SupplementaryData/2016/Bold)], yielding a dominant age peak at 700 to 850 Ma, and three older grains with $^{207}Pb/^{206}Pb$ dates ranging from 2534 ± 55 Ma to 2406 ± 66 Ma. Five additional zircons analyzed by CA-ID-TIMS produced significantly scattered $^{206}Pb/^{238}U$ dates ranging from 792.3 ± 2.1 Ma to 729.8 ± 1.4 Ma [fig. 5 and table A2 (http://earth.geology.yale.edu/~ajs/SupplementaryData/2016/Bold)], with the latter providing a maxium depositional age for the middle Maikhan-Uul Fm.

Sample F868-64: Tuffaceous sandstone in the lower Taishir Formation.—A green tuffaceous sandstone was sampled in the lower Taishir Fm in the Khongor Range (table 3). Six CA-ID-TIMS zircon analyses yielded widely scatterd $^{206}Pb/^{238}U$ dates that range from 1741.4 ± 5.8 Ma to 768.9 ± 3.2 Ma [fig. 4C and table A2 (http://earth.geology.yale.edu/~ajs/SupplementaryData/2016/Bold)]. Judging from stratigraphic superposition, all analyzed zircons were detrital and significantly older than the expected depositional age.

Sample F1206-146.1: Sandstone in karst-fill at the top of the Shuurgat Formation.—A brown sandstone was sampled from the karst-fill at the top of the Shuurgat Fm in the northeastern Khukh Davaa of Tsagaan block (table 3). One hundred zircon grains of similar morphology (mostly long and prismatic) were mounted and 71 grains were analyzed with the LA-ICPMS method [figs. 12, 14A, A5 and table A1 (http://earth.geology.yale.edu/~ajs/SupplementaryData/2016/Bold)]. Data indicate a prominent age peak is at 750 to 900 Ma, with the remaining 10 percent of the grains extending in age up to 2000 Ma. The youngest single analysis from this sample yielded a $^{206}Pb/^{238}U$ date of 693 ± 35 Ma, which is interpreted as a maximum depositional age for the upper Shuurgat Fm.

GEOCHEMISTRY

In addition to sampling volcanic and siliciclastic rocks of the Tsagaan-Olom Group for chronostratigraphic constraints, carbonates were sampled for $\delta^{13}C$, $\delta^{18}O$, and $^{87}Sr/^{86}Sr$ analyses. See Appendix (http://earth.geology.yale.edu/~ajs/SupplementaryData/2016/Bold) for methods used.

Carbonate Carbon and Oxygen Isotope Results

Reconnaissance-scale carbon and oxygen isotopes from the Tsagaan-Olom Group were previously reported by Brasier and others (1990) and Shields and others (1997, 2002), and higher resolution single sections by Macdonald and others (2009a) and Johnston and others (2012). However, in relation to our detailed mapping and stratigraphic work, we report carbonate $\delta^{13}C$ and $\delta^{18}O$ measurements of 3581 samples from multiple parallel vertical sections of the Taishir, Khongor, Ol, and Shuurgat fms (table A3, http://earth.geology.yale.edu/~ajs/SupplementaryData/2016/Bold) from each locality (figs. 3 and 4).

Carbon and oxygen isotope analyses were performed on cements from the Maikhan-Uul Fm to determine the origin of the cements and the isotopic composition of the fluids that these cements precipitated from. Carbon isotope values vary from −7 to +5 permil and $\delta^{18}O$ values vary from −25 to +5 permil with the majority being extremely depleted (fig. 6).

Carbon isotope values in the black laminated limestone of the basal Taishir Fm are moderately negative with values increasing up-section through the highstand of T1 to +4 permil (fig. 8). $\delta^{13}C$ values increase abruptly at the base of T2 to +8 permil and

return to +4 permil at the top of T2. These values plummet abruptly at the transgression at the base of Member T3 reaching a low of −7.5 permil. From this nadir (the Taishir excursion), $\delta^{13}C$ values increase smoothly to +10 permil where they remain for the majority of Member T3 before declining again in T4 to +4 permil near the top of the Taishir Fm. Where undolomitized, these trends can be reproduced for over 100 km across the Zavkhan Terrane through large facies changes and differences in thicknesses of the members (fig. 8).

Different carbonate lithologies, however, do affect the $\delta^{13}C$ values of the Taishir Fm. The $\delta^{13}C$ values vary by as much as 8 permil within the upper Taishir Fm between limestone and dolostone strata. For instance, where the dolomitization front cuts down in sections on the South Khukh Davaa, northern Tsagaan, Orlogo, western Taishir and Tsakhir blocks, $\delta^{13}C$ values of the uppermost dolomitized succession of the Taishir Fm are less enriched at ~+2 to +3.5 permil whereas in undolomitized sections, equivalent horizons yield values of between +10 to +12 permil (fig. 8). Specifically, in both the Orlogo Gorge (U1202) and South Khukh Davaa (F875, F876, F1125 and F1126) localities, the $\delta^{13}C$ values of the dolomitized upper T3 decrease from +10 to +12 permil down to ~+6 permil (fig. 8).

In the Taishir Fm, carbonate $\delta^{13}C$ and $\delta^{18}O$ do not covary (table A3, http://earth.geology.yale.edu/~ajs/SupplementaryData/2016/Bold). In members T1, T2, and the lower half of T3, $\delta^{18}O$ varies between −20 and −3 permil, in the upper ~150 m of the Member T3, $\delta^{18}O$ values get markedly more enriched and vary between −10 and 0 permil.

Carbon isotope values of limestone clasts in the Khongor Fm range from +1 to +8 permil (fig. 8). The clasts with $\delta^{13}C$ values at +1 permil also contain soft sedimentary folding and are not recognizable Taishir lithologies, suggesting that they were from a bed deposited above the Member T3 that was eroded by the Khongor diamictite. There is a <4.5 m thick, bedded dolo-grainstone clast that is ~10 m in length and not traceable along strike present in the basal part of the Khongor Fm at the Ikh Goliin Tsakhir (U1433 and U1435, fig. 8) locality as well. Interestingly, there is no apparent soft sedimentary folding in this clast, and the lithology may be correlated with T3 ooid-grainstone although the weathering color is brown gray and it is coarsely recrystallized. $\delta^{13}C$ values of this bedded dolostone clast range between +6.5 permil to +9.2 permil within individual beds, and the $\delta^{18}O$ values range between −3 permil to −4.9 permil (table A3, http://earth.geology.yale.edu/~ajs/SupplementaryData/2016/Bold).

Overlying the Khongor Fm, in the localities where the Taishir Fm carbonates are preserved as limestone, $\delta^{13}C$ profiles through the Ol Fm form a sigmoidal pattern that reaches a nadir of −6 permil (Macdonald and others, 2009a) (fig. 12), similar to basal Ediacaran cap dolostones elsewhere (Hoffman and others, 2007). The $\delta^{13}C$ profiles of the Ol Fm successions that overlie the dolomitized Taishir carbonates show large lateral variations (fig. 12). At the Ikh Goliin Tsakhir, NE Khukh Davaa and Unkheltseg localities, the $\delta^{13}C$ values of the Ol Fm become enriched. Rather than recording negative values, the Ol Fm reaches values as high as ~+4 permil. In the western tributary of Tsagaan Gorge (F724) and at Zuun-Arts (U1329), the $\delta^{13}C$ values reach +2 permil. However, the Ol Fm in the Tsagaan Gorge is underlain by undolomitized Taishir succession.

In the Ol Fm, carbonate $\delta^{13}C$ and $\delta^{18}O$ do not covary (table A3, http://earth.geology.yale.edu/~ajs/SupplementaryData/2016/Bold). In the Tsagaan Gorge, where the underlying Taishir Fm is undolomitized, $\delta^{18}O$ varies between −12 and −2 permil. However, in the Khongor Range, it varies dramatically between −27 and −5 permil. In the Ol Fm sections that overly the dolomitized Taishir Fm carbonates, at the Ikh Goliin Tsakhir and Unkheltseg localities, carbonate $\delta^{13}C$ and $\delta^{18}O$ also do not

covary. In general, the $\delta^{18}O$ varies between −7.8 and −1 permil (table A3, http://earth.geology.yale.edu/~ajs/SupplementaryData/2016/Bold).

Carbon isotope values in limestone of Member Sh1 of the Shuurgat Fm gradually increase up-section from −4 permil to −0.3 permil (F708, fig. 12). In the variably brecciated, thin-bedded dolo-micrite, nodular-bedded calcisiltite, and grainstone of Sh2, $\delta^{13}C$ values hover between +2 and +4 permil. There are no sections of Sh2 preserved as limestone that can be used to assess the degree to which dolomitization has altered the $\delta^{13}C$ values of this interval. In members Sh3 and Sh4, $\delta^{13}C$ values vary between sections preserved as limestone and those that have been dolomitized. In Khunkher Gorge, the western gorge of Tsagaan Gorge, NE Khukh Davaa, Unkheltseg and Ikh Goliin Tsakhir localities, where Sh3 and Sh4 are either dominated by limestone or partially preserved as limestone (described herein as Sh3-4), $\delta^{13}C$ values increase abruptly to +8 permil, decline back to +2 to +4 permil and increase again to +8 permil before returning back to ~+ 2 permil at the top of the Shuurgat Fm. However, in Shuurgat Range, Ol Mountain, Khevtee Tsakhir Range and Zuun-Arts locality, where Sh3 and Sh4 are dominated by dolostone, these features of the $\delta^{13}C$ profile are not as well defined and positive peaks are subdued to ≤+6 permil (fig. 12).

In the Shuurgat Fm, carbonate $\delta^{13}C$ and $\delta^{18}O$ do not covary (table A3, http://earth.geology.yale.edu/~ajs/SupplementaryData/2016/Bold). In Sh1, $\delta^{18}O$ varies between −15 and −7 permil. In members Sh2 and Sh3, $\delta^{18}O$ values become heavier and vary between −16 and +1.5 permil. In Sh4, $\delta^{18}O$ values stay enriched between −10 and 1.5 permil.

Strontium Isotope Results

Strontium isotopes were measured in both Cryogenian and Ediacaran strata on the Zavkhan Terrane to construct a high-resolution Cryogenian curve and to test if deposition of the Shuurgat Fm was restricted to early Ediacaran or extended throughout the Ediacaran. Samples with high Sr concentration and low clay content (0.4–16.5% with an average at 5%, table A4, http://earth.geology.yale.edu/~ajs/SupplementaryData/2016/Bold) were targeted and diagenetic alteration was screened using carbonate content and a cross-plot of $^{87}Sr/^{86}Sr$ vs. Sr concentration (Halverson and others, 2007) for each sample. Values discussed here are selected by a cutoff value of Sr concentration of <500 ppm (fig. A1). $^{87}Sr/^{86}Sr$ values considered diagenetically altered are included in table A4 (http://earth.geology.yale.edu/~ajs/SupplementaryData/2016/Bold) but are not shown in the plots.

Sr concentration in the analyzed Taishir Fm limestone was >500 ppm (table A4, http://earth.geology.yale.edu/~ajs/SupplementaryData/2016/Bold) and all analyses were used. The $^{87}Sr/^{86}Sr$ values in finely laminated T1 cap carbonate start at 0.70673 and increase abruptly through T1 until the transition with T2 transgression. Values drop gradually to 0.70704 and eventually increase slightly to as much as 0.70726 through the rest of T2. Values increase again in the lower portion of T3 to 0.70736 where they plateau for the rest of T3 and T4.

Strontium concentration in both the Ol and Shuurgat Fm limestones was between a minimum of 61 and as high as 2250 ppm (table A4, http://earth.geology.yale.edu/~ajs/SupplementaryData/2016/Bold). Of the 52 samples analyzed, six samples were considered diagenetically altered because they yielded Sr concentrations <121 ppm. The $^{87}Sr/^{86}Sr$ values of the recessive limestone succession of the Ol Fm (U1121, table A4, http://earth.geology.yale.edu/~ajs/SupplementaryData/2016/Bold) start enriched at 0.70756 and increase slightly to 0.70765 through the rest of the Ol Fm limestone. At the start of the transgressive sequence of the basal Shuurgat Fm [U1122, table A4 (http://earth.geology.yale.edu/~ajs/SupplementaryData/2016/Bold)], Sh1, the $^{87}Sr/^{86}Sr$ values become more radiogenic to as high as 0.70773 and decrease

gradually to 0.70757 (fig. 12). All of the measured samples in Sh3 and Sh4 of the Shuurgat Fm (U1235, F872 and U1437) yielded $^{87}Sr/^{86}Sr$ values of <0.70795. In Khunkher Gorge, the values ranged between 0.70765 and 0.70785. Seven samples from stratigraphically equivalent succession (section U1235, fig. 12) in the western tributary of Tsagaan Gorge yielded similar values and ranged between 0.70783 and 0.70795.

DISCUSSION

Depositional Environments

Tectonic setting of the Zavkhan Formation.—The Zavkhan Fm has been previously suggested to record magmatism in either a rift-related setting (for example, Ilyin, 1990) or on an active continental arc (for example, Kuzmichev and others, 2001). The former interpretation stems from the bimodal volcanic rock assemblage and the overlying passive margin deposits. The interpretation that the Zavkhan Fm formed as an active continental arc is supported by major and trace elemental analysis (for example, Levashova and others, 2010), and by correlation with Sarkhoi Volcanics of the Tuva-Mongolia Zone (for example, Kuzmichev and Larionov, 2011). This is further supported by zircon trace element geochemistry (Yang and others, 2012) with low Nb/Hf and high Th/Nb ratios [sample U1213 in table A1 (http://earth.geology.yale.edu/~ajs/SupplementaryData/2016/Bold)], which are based on studies that showed depleted Nb content in magmatic arc magmas (for example, Pearce and Peate, 1995). However, the presence of km-scale fan conglomerate sequences in the lower Zavkhan Fm succeeded by thick, fault confined exposures of continentally-derived sediments of the Khasagt Fm (figs. 3 and 5), culminating in extensive marine deposition throughout the Cryogenian to early Ediacaran Tsagaan-Olom Group is consistent with deposition on a rifted passive margin. Hence, it appears that the Zavkhan Terrane transformed from an active arc and back-arc complex to a rifted ribbon continent with passive margins on both sides, which is typically achieved through the subduction of a ridge (Stampfli and Borel, 2002), analogous to the rifting of Baja, California.

Glacial facies associations in the Maikhan-Uul Formation.—Broadly, the Maikhan-Uul Fm consists of two diamictites separated by clast poor siliciclastic strata that prograde southwestward (Macdonald, 2011) (figs. 6, 15A, 15B, 15C, and 16A). The lower portions of both diamictite members are interpreted to have been deposited in a sub-glacial environment as lodgement tills in contact with the ice sheet. Features indicative of ice-grounding are particularly common in the lower member, including sedimentary shear fabrics (fig. 7C) and blocks with soft-sedimentary folding (Boulton and others, 2001), bullet shaped clasts (Boulton, 1978; Lindsay and others, 1996), and carbonate concretions along reactivation surfaces at the base of individual diamictite units (Lindsay, 1989; Fairchild and Spiro, 1990; Macdonald, 2011).

The middle member has previously been interpreted to represent an interglacial period separating two distinct glacial events (Lindsay and others, 1996); however, the dearth of laminated diamictite with dropstones characteristic of ice rafted debris in between the lower and upper member is inconsistent with the interpretation of a full, global scale-deglaciation (Macdonald, 2011). Instead, the contact above the lower member is sharp, succeeded by graded beds of sandstone and shale. West of the Khongor Range, these beds coarsen up to coarse-grained sediment gravity flow facies. These facies are interpreted to reflect local retreat of the ice grounding line without whole-scale deglaciation, and deposition beneath an ice shelf (compare, Domack and Hoffman, 2011) or in a proglacial lake (Benn and others, 2015). Unfortunately, sub-ice shelf facies models are in their infancy and are limited to ice cores retrieved below the Larson ice shelf and Ross Sea (Domack and others, 1998; Domack and others, 1999). At these localities, deposition beneath an ice shelf is marked by turbidite and shale

deposition and the lack of diamictite facies. Another possibility is that these facies reflect the development of a waterbelt, as predicted in the Jormungand hypothesis (Abbot and others, 2011) or movement of the ice-line during increased seasonality in the late stages of glaciation (Benn and others, 2015).

At Tsagaan and South Khukh Davaa blocks, dropstones occur in the uppermost meter of the middle Maikhan-Uul Fm, followed by glacial erosion surfaces, concretionary carbonates, and soft sedimentary folding, and provide additional evidence for a second advance of the ice grounding line. In the upper member, these features become less common upward and are succeeded by massive to weakly-bedded, graded diamictite interbedded with graded and channelized beds of cross-stratified sandstone. This facies assemblage (table 2) is interpreted to represent deposition in an ice contact fan in a sub- to pro-glacial environment (Powell, 1990; Domack and Hoffman, 2011).

In South Khukh Davaa block, the upper diamictite culminates with sandstone and siltstone with abundant mudcracks (Macdonald, 2011) (fig. 7E) demonstrating subaerial exposure in a proglacial setting. Finally, the base of the Taishir Fm represents a global deglaciation, flooding of the margin and open water deposition based on its carbonate facies and geochemical signature. Thus, the stratigraphic succession of the Maikhan-Uul Fm is interpreted to reflect retreat of the ice-grounding line in the middle member, either due to tectonic subsidence or local thinning of a cold based ice sheet (Davis and others, 2006), and a readvance of the grounding line in the upper member (Macdonald, 2011), potentially by a wet-based glacier during deglaciation. Without further geochronological constraints it is difficult to determine the timescale of the ice-line advance and retreat. Moreover, the complexity of ice advance and retreat documented in the most recent glaciation (Ridge and others, 2012) suggests that we may not have sufficient geochronological resolution (10 Ka – 100 Ka) to sort out advance and retreat in the Cryogenian. Nonetheless, the presence of exposure surfaces in the upper member implies either that, locally, deglaciation and glacio-isostatic rebound occurred before the global glacioeustatic transgression, or that there was a local regression due to ice gravity effects (Creveling and others, 2012).

Concretionary carbonates are present in all of our glacial facies associations. Carbonate is a very minor clast constituent in the diamictites. The matrix and clasts of the Maikhan-Uul Fm are dominated by volcaniclastic material, and consequently, the generation of carbonate alkalinity in subglacial porewater must have been the product of the reaction of CO_2 with the weathered rock. In this setting, precipitation occurs due to relegation processes with pressure melting occurring on the up flow side of protuberances and refreezing on their lee side (Aharon, 1988). Carbonate coatings of shear surfaces and clasts have been previously reported at several other localities and have also been interpreted to have formed through pressure dissolution and reprecipitation (Deynoux, 1985; Fairchild and Spiro, 1990). Subglacial carbonates from section F1216 sampled from the base of the lower Maikhan-Uul at Shivee Tsakhir region, and F1204 sampled from the lower portion of the upper member of the Maikhan-Uul Fm at Khukh Davaa tend to have extremely depleted $\delta^{18}O$ values (mostly between -22 and $-20‰$) and relatively positive $\delta^{13}C$ (0 to $+4‰$; fig. 6). The oxygen isotopic composition of subglacial rocks is largely dependent on that of local glacier ice (Aharon, 1988; Fairchild and Spiro, 1990) and thus, these data suggest that the isotopic value of the subglacial ice in the Maikhan-Uul Fm ranged from -22 to -20 permil. These values are between the $\delta^{18}O$ value of subglacial carbonates in Quebec and Switzerland (Fairchild and Spiro, 1990) and we suggest they in part preserve a primary signature because they are far more depleted than any values of bulk rock or cements from both underlying and overlying strata.

Carbonate precipitates also occur at the base of the middle member of the Maikhan-Uul Fm, directly above the massive diamictite of the lower member. These beds are all limestone, but aragonite pseudomorphs are present in some samples suggesting an original aragonitic mineralogy and authigenic precipitation at or near the sediment-water interface. Carbonates in sections F1203, F1214 and F1212 have depleted $\delta^{13}C$ values (ranging from −1 to −7.5‰) and depleted $\delta^{18}O$ values (with F1203 and F1214 largely between −25 and −20‰ and F1212 more enriched at −10 to −8‰; fig. 6). The wide range of both carbon and oxygen isotope values in these rocks are difficult to explain in a marine setting during a glacio-eustatic transgression and are more consistent with glacial lacustrine values. Like the $\delta^{18}O$ of the subglacial carbonates, the $\delta^{18}O$ values from F1203 and F1214 can be interpreted to reflect the isotopic value of the ice. While the carbonates from sections F1205 and F1214 are composed of limestone, F1212 samples are dolomite, and thus may have also been affected by post-depositional fluids, as most of the carbonates in the overlying Tsagaan-Olom Group have $\delta^{18}O$ values around −10 permil. Alkalinity to generate carbonate was likely driven by anaerobic remineralization of organic matter that formed during the lift off of the ice sheet, generating negative $\delta^{13}C$ values. Thus, proglacial carbonates formed below the water column that was not in communication with seawater, but it is unclear if this was below an ice-shelf or within a proglacial lake.

Proglacial carbonate concretions in sandstones of the upper member display a spread of $\delta^{13}C$ and $\delta^{18}O$ values between glacial melt water values and extremely enriched values (fig. 6), which may reflect a mixture of glacial water and some other reservoir. Within proglacial lakes, evaporation can lead to enrichment in oxygen isotope values and the isotopic value of carbonates can reflect a mixture between an evaporitic and ice end-members (Fairchild and Spiro, 1990). Alternatively, $\delta^{18}O$ enriched cements within Neoproterozoic glacial deposits have been interpreted to reflect methanogenesis (Kennedy and others, 2008).

Diamictite-free facies within Sturtian glacial deposits have previously been interpreted to represent an open water, interglacial period, not only in the Maikhan-Uul Fm of Mongolia (Lindsay and others, 1996), but also in the Ghubrah Fm of Oman (Allen and Etienne, 2008), the Sturt of Australia (Le Heron and others, 2011; Le Heron, 2012), the Chuos of Namibia (Le Heron and others, 2013), and the Kingston Peak Fm of Death Valley, California (Le Heron and others, 2014; Le Heron and Busfield, 2015). The presence of diamictite-free facies has been used alternatively to argue that the Sturtian glaciation is globally diachronous and does not represent Snowball conditions (Allen and Etienne, 2008) or that there is an interglacial period within the Sturtian glacial epoch (Le Heron and others, 2014). Instead, our data suggest that these facies reflect either deposition beneath an ice shelf (Domack and others, 1998; Domack and others, 1999), the opening of a waterbelt (Abbot and others, 2011) or movement of the ice-line during increased seasonality in the late stages of glaciation or late stages of glaciation with increased seasonality (Benn and others, 2015), but not a full global deglaciation (Macdonald, 2011). Moreover, all of these successions lack age constraints within the diamictites, and consequently these successions may largely record deglaciation rather than the tenure of the glaciation.

Carbonate facies assemblages in the Taishir Formation.—The facies patterns of the Taishir Fm are interpreted to represent deposition on an open carbonate ramp (Ahr, 1973) that forms a basin tapering wedge composed of four large-scale stratigraphic sequences that gradually thin to the west-southwest over 100 km with no sharp facies changes (figs. 15D, 16B, and 16C). Previous authors have separated carbonate ramps into homoclinal and distally steepened ramps (Read, 1982; Burchette and Wright, 1992), distinguished by a change in slope in the ramp, which results in mass wasting and slump folding in more distal localities. Slump folds are extremely rare, and no

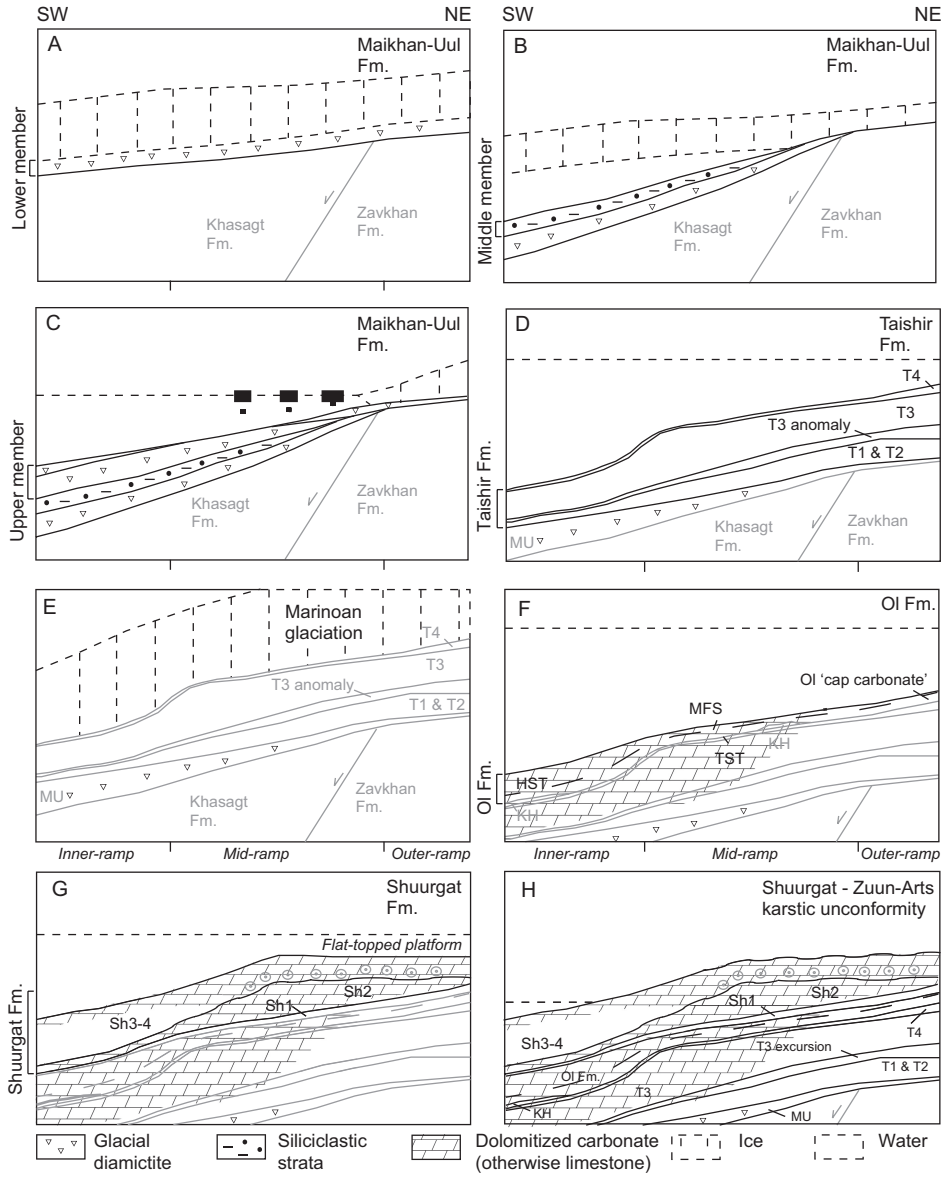

Fig. 15. Depositional model for the Tsagaan-Olom Group formations. Orientation of transect in present coordinates. (A) Lower member of the Maikhan-Uul Formation. (B) Middle siliciclastic member of the Maikhan-Uul Formation. (C) Upper member of the Maikhan-Uul Formation. In general, the Maikhan-Uul Formation thickens to the southwest in the Zavkhan Terrane. (D) Taishir Formation. Both T1 and T2 thin to the southwest. (E) Marinoan glaciation. Mantling of grounded ice throughout the Marinoan glaciation is preferred. (F) Ol Formation. Khongor (KH) diamictite formed as a rainout deposit during deglaciation filling ice-cut channels. Fluid event responsible for dolomitizing upper Taishir and Ol Formation limestone took place before the deposition of Sh1 of the Shuurgat Formation. (G) Shuurgat Formation. Flat-topped platform formed during Sh2 to Sh3 as a result of progradation of the margin during Ol to Sh2 and consequently, the sharp facies change in Sh3-4 is observed as well as the well-development of carbonate parasequences in Sh4. (H) Exposure of the platform after the deposition of the Shuurgat Formation responsible for eroding and karsting the carbonates of the upper Tsagaan-Olom Group.

evidence has been found for a major break in depositional style in members T1 to T4 up to the faults that bound the Zavkhan Terrane. Consequently, the homoclinal carbonate ramp is preferred as a facies model.

Homoclinal ramps have relatively uniform slopes of less than 1° and within these facies models have distinguished inner-ramp, mid-ramp, outer-ramp, and basinal facies assemblages (table 2), although true basinal facies have proven difficult to identify (Burchette and Wright, 1992). Inner-ramp sediments are deposited above fair weather wave base (FWWB) and are dominated by sand shoals, shoreface deposits, and back-barrier peritidal to intertidal deposits. Periodically restricted and sub-aerially exposed peritidal to intertidal environments can readily preserve m-scale parasequences capped by exposure surfaces that are prone to early dolomitization. Our inner-ramp facies assemblage consists of nodular-bedded carbonate, grainstone, microbialaminite, and intraclast breccia packaged in well-developed m-scale parasequences (table 2).

Mid-ramp sediments form between FWWB and storm wave base (SWB) and are influenced by frequent storm reworking. Ooid-grainstone shoals and grain flows are also common in this environment, as is seen in the Jurassic Smackover Fm on the US Gulf Coast, which hosts a ~100 m thick build-up of ooid and pellet grainstone and oncolitic packstone (for example, Ahr, 1973). Our mid-ramp facies assemblage includes thin-bedded micritic limestone with heterolithic interbeds, nodular-bedded calcisiltite and grainstone with common graded beds and thick ooid shoals (table 2). Mid-ramp facies is distinguished from inner-ramp facies by the lack of exposure-capped parasequences and a predominance of graded beds in the former.

Outer-ramp environments extend from storm wave base to the basin plain (Burchette and Wright, 1992). Sediments in these environments show little evidence for storm reworking but do include minor distal turbidites and slump folding. Our outer-ramp facies consist of shale, micrite, and calcisiltite with minor graded beds of grainstone. The outer-ramp is distinguished from the mid-ramp facies assemblage by the lack of evidence of wave base and the lack of thick beds of redeposited grain flows. Here, the basinal environments are included with our outer-ramp facies assemblage because of the inability to confidently distinguish between the two.

T1 consists predominantly of thin-bedded micritic limestone and shale, interpreted to represent deposition in an outer-ramp environment (figs. 8 and 15D). The lower 10 to 20 m of T1 is succeeded by calcisiltite without grainstone flows and is interpreted to represent the maximum flooding surface (MFS) of sequence 1. Upsection, graded beds of carbonate with chert nodules and carbonate clast breccias, interpreted as debris flows, become more common within the background calcisiltite sedimentation, consistent with high-stand (HST) shedding and a transition to a mid-ramp environment. The succession becomes more carbonate rich and resistant upwards, culminating with a silicified bed of black limestone that marks the top of the T1 HST.

The sequence T2 transgressive sequence tract (TST) begins with thin-bedded micritic limestone and interbedded graded beds of limestone that are commonly recessive. Defining the large-scale MFS is complicated by the presence of multiple smaller scale sequences in sequence T2. The lower 10 to 50 m of T2 oscillates between outer- and mid-ramp environments before shoaling up to an inner-ramp facies assemblage marked by well-developed exposure-capped parasequences (fig. 8, composite sections 8, 10, 12 and 14). The top parasequence is not obviously different from the underlying parasequences and is succeeded by a sharp flooding surface that marks the top of T2.

The basal TST of T3 is a sharp flooding surface of thin-bedded micritic limestone (fig. 9B) that corresponds with the onset of the Taishir excursion (fig. 8). Within the

TST, graded carbonate grainstone beds and carbonate clast breccias are common within the background micritic carbonate sedimentation and are interpreted as sediment gravity flows deposited in a mid- to outer-ramp environment. Black chert beds and nodules are particularly common within the T3 TST. The MFS is marked by the disappearance of graded beds and is succeeded by ~100 m of massively bedded, thinly laminated, fetid limestone mudstone. Above, massive to graded grainstone beds become more common in the T3 HST, marking the reappearance of mid-ramp environments. The total thickness of T3 is between 200 and 300 m across the basin. Overall, thickness variations within T3 suggest a topographic high formed during the deposition of T3 (figs. 15D and 16C).

Although T4 is not well-exposed or well-preserved throughout the basin, the thin-bedded micritic limestone overlain by black shale (fig. 8, composite section 12) marks another MFS at the base of T4. Hence it is interpreted to document a return to an outer-mid-ramp environment in the basin.

Here the lack of siliciclastic input to the Taishir Fm suggests that it is consistent with deposition on an isolated platform, but that the facies assemblages of the Taishir Fm are more akin to that of a homoclinal carbonate ramp. Traditionally, facies models for isolated platforms and carbonate ramps have been separated, with models of isolated platforms influenced heavily by the Bahama Banks and distinguished by high relief margins and abundant slope failure (for example, Read, 1982). The development of a homoclinal carbonate ramp on an isolated platform may reflect the fact that the margin was very mature, having subsided for ~150 Ma after rifting at ~800 Ma.

The facies architecture of T1 and T2 was heavily influenced by progradation of the margin during deposition of the Maikhan-Uul Fm. The Maikhan-Uul Fm thickens to the southwest (figs. 6 and 16A), controlling the inverse thickening of T1 and T2 to the northeast (figs. 8 and 16B). Additionally, drowning of the margin, both in lower T1 and in lower T3, would have favored the development of ramp morphology (Read, 1982). However, the systematic stacking of the measured sections (figs. 15D and 16C) suggests that during the progradation of T3, the ramp morphology started its initial step towards development of an outer rim.

Glacial facies associations in the Khongor Formation.—The Khongor diamictite is not as well developed as the glacial diamictite in the Maikhan-Uul Fm, potentially due, in part, to the difference in accommodation later in the subsidence history, and also to the shorter duration of the Marinoan glaciation. Thus, the interpretation of its depositional environments is necessarily limited. With the exception of the Khongor Range, eastern tributary of Tsagaan Gorge and Unkheltseg localities, the Khongor diamictite is not preserved, implying that the Zavkhan Terrane was either exposed or mantled by grounded ice throughout the Marinoan glaciation (fig. 15E). The presence of striated limestone clasts (fig. 10B) and clasts with intense soft-sedimentary folding (Macdonald, 2011) suggests that grounded ice was at least nearby if not present on the whole of the margin. The distribution of diamictite is similar to that of the Marinoan Ghaub Fm in Namibia where irregular preservation of diamictite on the platform has been interpreted to represent either moraines or channel fills (Hoffman, 2011). Where the Khongor diamictite is preserved, there is no evidence for incision into the underlying Taishir Fm. In fact, in the Khongor Range at the type locality of the Khongor diamictite, more of T4 is preserved than in at other localities. Moreover, the presence of boulder nests (Macdonald, 2011) and weak lamination in otherwise massive diamictite facies is also more consistent with the interpretation of the Khongor diamictite as a moraine deposited during ice retreat rather than a channel fill deposit or a wedge of lodgement till. Thus, the most of the Marinoan glaciation and some of the preglacial time are suggested to have been lost at the top contact of the Taishir Fm due to sub-glacial erosion and that the

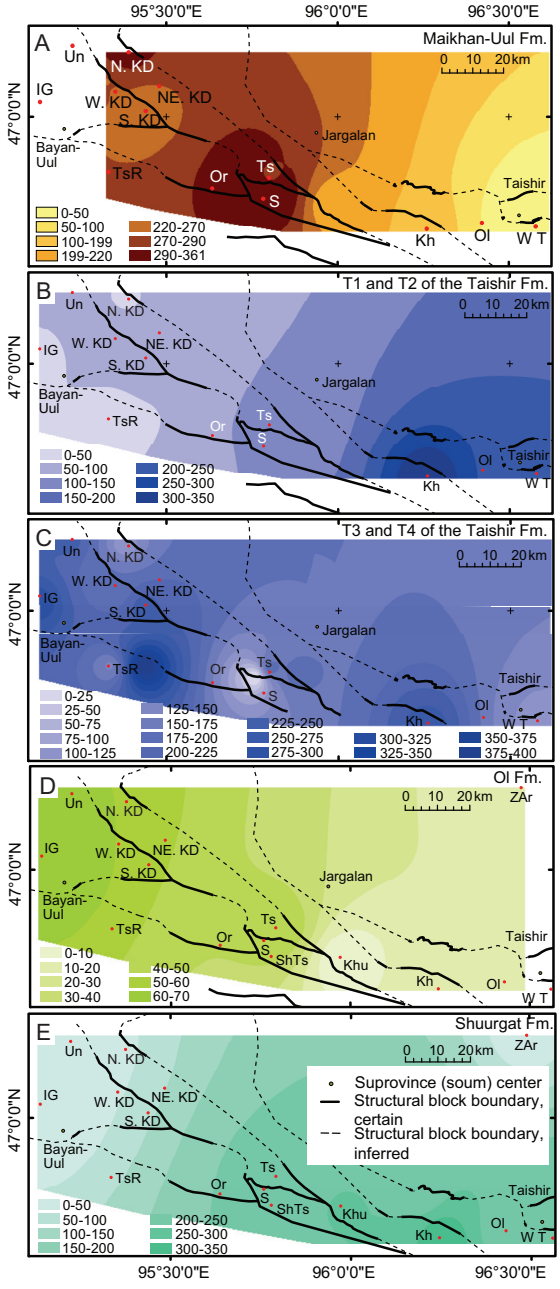

Fig. 16. Isopach map of the Tsagaan-Olom Group formations. Tectonic block boundaries are traced. Solid lines = certain faults. Dashed lines = inferred faults. Labels on maps are as follows: South Khukh Davaa block = Un – Unkheltseg, IG – Ikh Goliin Tsakhir, S. KD – southern Khukh Davaa, W. KD – western Khukh Davaa; Tsakhir block = TsR – Tsakhir Range; Orlogo block = Or – Orlogo Gorge; Salaa block = S – Salaa Gorge, ShTs – Shivee Tsakhir; ZAr – Zuun-Arts; Khunkher block = Kh – Khongor Range, Khu – Khunkher Gorge; Taishir block = W.T – western Taishir, E.T – eastern Taishir, Ol – Ol Mountain; Tsagaan block = N. KD – northern Khukh Davaa, NE. KD – northeastern Khukh Davaa, Ts – Tsagaan Gorge. Each map is color coded according to thickness (m). The extent of our study area is within the structural block boundaries. (A) Maikhan-Uul Formation. (B) T1 and T2 of the Taishir Formation. (C) T3 and T4 of the Taishir Formation. (D) Ol Formation. (E) Shuurgat Formation.

three localities in which the Khongor Fm is well-developed record only the termination of the Marinoan glaciation.

Carbonate facies assemblages in the Ol Formation.—The TST begins with the cap dolostone of the basal Ol Fm, which is exposed throughout the basin with thickness ranging from 10 to 35 m. The MFS of the Ol Fm is marked by thin-bedded micritic limestone interbedded with shale and nodular-bedded calcisiltite. This sequence is carbonate-dominated in the mid-inner-ramp environment in the eastern part of the exposure area, namely in the Taishir, Ol, and Khongor localities and becomes thinner (fig. 16D), more siliciclastic-dominated at the western and southwestern exposures, especially in South Khukh Davaa block and is not present to the north at Zuun-Arts (fig. 12). Up-section, the Ol Fm HST sequence is >10 m thick (with the exception of the Zunn-Arts section) and defined by medium to massively bedded limestone, which is locally dolomitized. At Taishir, Ol, Khongor, Khunkher, and Tsagaan Gorge localities, the thickness of the HST averages ~15 m, and the carbonate facies are dominated by massively bedded lime-grainstone. In Khukh Davaa, on the other hand, the sequence becomes as thick as 70 m, and ooids are developed at the top of the sequence.

The fact that thickness and facies change do not vary in the Ol Fm across the Zavkhan Terrane is still suggestive of ramp morphology. Due to an early stage of rim build-up during T3, the thickness of the Ol Fm as a whole increases to the southwest (fig. 16D) and at locations, namely in Ikh Goliin Tsakhir, Unkheltseg and NE Khukh Davaa regions, the HST sequence of the Ol Fm becomes thicker with ooids forming at the top, which can be seen as thickened in inner-mid-ramp environment in figure 15F.

Carbonate facies assemblages in the Shuurgat Formation.—In general, the Shuurgat Fm carbonates form two large-scale stratigraphic sequences dominated by TST and HST, separated by an uncomformity (figs. 11C and 12). Facies changes and thickness variations with general thinning towards the west-southwest are developed throughout the basin (figs. 12, 15G, and 16E). Although the depositional environment for these carbonates is interpreted as a carbonate ramp (Read, 1982), stratigraphic patterns suggest a proto-rim formed during the deposition of Sh2 that may have been responsible for the distribution of early dolomitization and the carbonate facies change observed within Sh3 and Sh4 between outer-mid-ramp and mid-inner-ramp depositional environment (for example, Dunham and Olson, 1980) (fig. 12, section F872). Due to an absence of slump folding and mass wasting representative of slope facies, and the lack of thick stromatolitic build-ups marking a reef, it is problematic to invoke a depositional environment with a true rimmed margin, so instead a flat-topped platform is envisioned.

Member Sh1 is preserved as limestone and composed of gray weathering, grainstone interbedded with pink calcisiltite with chert lenses and nodules, interpreted to represent deposition in a mid- to outer-ramp depositional environment (figs. 11B, 12, and 15G). Sh1 represents the TST of a sequence 1. Up-section, the succession becomes more carbonate rich and dominated by bedded lime-grainstone with thin interbeds of calcisiltite. The transition to Sh2 has been difficult to document due to poor exposure and minor faulting and folding at the top of Sh1.

Overall, both Sh1 and Sh2 thin dramatically to the west and southwest on the margin. Sh2 carbonate strata are dominated by dolo-micrite, nodular-bedded dolostone, and minor ooid grainstone shoals that are variably brecciated and are attributed to later dolomitization. Hence, both members are interpreted to largely represent deposition in a mid- to upper-ramp environment in the HST of sequence 1.

Above the unconformity at the top of Sh2, on the Khunkher, Tsagaan and South Khukh Davaa blocks, limestone-dominated carbonate facies of Sh3 and Sh4 are composed of thin-bedded micritic limestone and nodular-bedded calcisiltite that are

interpreted to represent the TST and HST on the mid- to upper-foreslope (fig. 15G). On the platform, the TST to HST above Sh2 is represented by dolo-grainstone with ooid shoals. The overlying Sh3-4 displays well-developed parasequences, which are the product of small-scale base-level changes that become well-defined on the flat-topped platform margin. Progradation of the margin during Ol to Sh2 time, followed by exposure at the top of Sh2 is suggested to have led to transformation of the margin from a carbonate ramp to a flat-topped platform, resulting in the sharp facies changes and well-developed parasequences seen in Sh3 and Sh4. In general, the combined thickness of Sh3 and Sh4 varies from place to place due in part to the development of a platform margin geometry, concomitant facies change, and to the uncomformity (fig. 15H) at the top contact of the Shuurgat Fm.

Geochronology

Maximum depositional age within the clastic sediments.—Five clastic samples are discussed and the detrital age spectra of four of these (fig. 14) are used to infer provenance of the Zavkhan Terrane basement. The youngest LA-ICPMS dates from the sandstone and the quartzite clast in the conglomerate unit of the Zavkhan Fm are 743 ± 28 Ma ($^{206}Pb/^{238}Pb$) and 1887 ± 78 Ma ($^{207}Pb/^{206}Pb$) respectively, which are broadly taken as maximum depositional ages. However, the CA-ID-TIMS date of 802.11 ± 0.45/0.56/1.0 from a rhyolite flow directly above the sandstone bed demonstrates the limitations of LA-ICPMS ages from individual grains (Condon and Bowring, 2011). CA-ID-TIMS dates from tuffaceous sandstones from the Maikhan-Uul and Taishir fms suggest a detrital population and that the maximum depositional ages are 729.8 ± 1.4 and 768.9 ± 3.2 Ma, respectively. Finally, sandstone from the karsted surface at the top of the Shuurgat Fm yielded a youngest LA-ICPMS date of 692.8 ± 34.7 Ma, which is broadly taken as the maximum age of the sandstone.

Detrital zircon provenance.—The Zavkhan and Baidrag terranes are often lumped into one composite Precambrian terrane (for example, Levashova and others, 2010). However, the Baidrag Terrane lacks overlap assemblages equivalent with the Zavkhan Fm volcanics and the Tsagaan-Olom Group and hosts Ediacaran metamorphism and magmatism that is absent in the Zavkhan Terrane (Kozakov and others, 2012). Consequently, these terranes were possibly separated until at least the Cambrian and may have separate Proterozoic tectonic and detrital zircon provenance histories. Ruzhentsev and Burashnikov (1996) suggested that the two terranes were part of a rifted portion of western Gondwana. This inference was supported by a paleomagnetic study that yielded a paleolatitude of 47^{+16}_{-12}°N on Zavkhan Fm rhyolites, consistent with paleomagnetic data from India, South China, Tarim or Australia (Levashova and others, 2010). Rojas-Agramonte and others (2011) proposed that the terranes originated from Tarim due to a detrital and xenocrystic age peaks from Mongolian and Tarim samples that are not present in those from China or Siberia. However, these data are from Paleozoic samples that formed after many of these basement terranes had accreted with each other and with additional juvenile arc terranes. Alternatively, using the multigrain bulk TIMS date of 755 ± 3 Ma from an alkali granite that intrudes the Zavkhan Fm volcanics (Yarmolyuk and others, 2008), Wilhem and others (2012) proposed that the Zavkhan and Baidrag terranes experienced the Baikalian Orogeny (Kuzmichev and others, 2001) and were part of a single, ribbon microcontinent that was periodically associated with Siberia. These interpretations suffered from a lack of detailed geological work and from lumping results from the Zavkhan and Baidrag terranes together. We provide evidence that Precambrian basement ages, metamorphic ages, and overlap assemblages of the Zavkhan Terrane that are distinct from those in the Baidrag Terrane, offering strong evidence that these were two separate terranes during the Neoproterozoic.

Recent detrital spectra compilations from Paleozoic strata of Siberia (Rojas-Agramonte and others, 2011 and references therein), display dominant pre-1000 Ma age peaks at 1700 to 2500, 2350 to 3100, and 3250 to 3400 Ma. For Tarim, the spectra peaks are at 900 to 1100, 1700 to 1900, and 2450 to 2700 Ma (Zhang and others, 2013). North China has a broad spectrum that spans 1650 to 2600 Ma with distinct peaks at 1847 Ma and 2500 Ma (Sun and others, 2012) (fig. 14B). Our samples from Neoproterozoic strata on the Zavkhan Terrane (fig. 14A) have peaks at 1950 to 2100 and 2400 to 2600 Ma that form a broader hump between 1800 and 2800 Ma. These age peaks resemble those from Siberia, Tarim, and North China, but are not a perfect match with any of the proposed source terranes. Another prominent peak in the age spectra from Mongolia is present between 780 to 810 Ma, which is interpreted to have been sourced from the Zavkhan Fm. Hence it is suggested that the detrital population of the Zavkhan Terrane is locally derived from the underlying basement and that it may have its own distinctive characteristics.

Age of the Zavkhan Formation volcanics.—The first reported age constraint on the Zavkhan Fm was reported by Burashnikov (1990) with $^{207}Pb/^{206}Pb$ TIMS bulk zircon dates of 850 ± 2 and 750 ± 3 Ma (Badarch and others, 2002). Levashova and others (2010) dated rhyolites in the upper Zavkhan Fm near Tsagaan Gorge at 773.5 ± 3.6 Ma and in the lower part of the section near Bayan Gorge of 803.4 ± 8.0 Ma, both with LA-ICPMS $^{206}Pb/^{238}U$ on zircon. The entire Zavkhan Fm is further constrained in this study with CA-ID-TIMS dates at 802.11 ± 0.45, 797.22 ± 0.56, and 787.45 ± 0.47 Ma. The latter age is obtained from rhyolite that is interpreted to be an olistolith of the Zavkhan Fm that is from a flow that is younger than what is preserved in the uppermost-Zavkhan Fm at the Taishir locality. This interpretation is supported by the discontinuous exposure of the *ca.* 787 Ma rhyolite, the maximum depositional age of middle Maikhan-Uul Fm of 729.8 ± 1.4 Ma from detrital grains, and the erosional uncomformity at the base of the erosional unconformity at the base of the Maikhan-Uul Fm.

Age of the Maikhan-Uul Formation.—Maximum depositional age constraints for the Sturtian glaciation on the Zavkhan Terrane are provided by our 787.45 ± 0.47/0.58/1.0 Ma date on a rhyolite olistolith near the base of the Maikhan-Uul Fm, and our 729.8 ± 1.4 Ma date on a detrital grain in the tuffaceous sandstone in the middle Maikhan-Uul Fm (figs. 5 and 13D). Globally, the duration of the Sturtian glaciation is bracketed within a ~57 Ma window. The 717.4 ± 0.2 Ma date on the Mount Harper Volcanic Complex and the 716.5 ± 0.2 Ma date on the Rapitan Group (both $^{206}Pb/^{238}U$ CA-ID-TIMS single grain zircon dates) in northwestern Canada (Macdonald and others, 2010) and 715.9 ± 2.8 Ma and 716.1 ± 3.4 Ma dates (SIMS weighted mean $^{206}Pb/^{238}U$ zircon date) on a tuffaceous siltstone in the Gongdong Fm in South China (Lan and others, 2014) constrain the onset of the Sturtian glaciation. The 663 ± 4 Ma $^{206}Pb/^{238}U$ TIMS date on combined multi-grain separates of zircon from the Datangpo Fm in South China (Zhou and others, 2004), 659.7 ± 5.3 Ma $^{206}Pb/^{238}U$ SHRIMP date on the Wilyerpa Fm in Australia (although these were reported in an abstract without data) (Fanning and Link, 2008), a Re-Os date of 662.4 ± (3.9/4.6) Ma on the Sturtian-age Twitya cap carbonate in NW Canada (Rooney and others, 2014) and 659.0 ± (3.9/4.5) Ma Re-Os date on the basal Taishir Fm (Rooney and others, 2015) constrain the end of the Sturtian glaciation. The 687.4 ± 1.3 Ma and 685.5 ± 0.4 Ma dates from Idaho (Condon and Bowring, 2011; Keeley and others, 2013) and 711.5 ± 0.3 Ma from Oman (Bowring and others, 2007) (both $^{206}Pb/^{238}U$ CA-ID-TIMS single grain zircon dates) are interpreted to represent syn-glacial depositional ages. Because the middle member of the Maikhan-Uul Fm is interpreted to record local stepback of the ice grounding line during a larger glacial epoch, and not full-scale

deglaciation, we correlate the whole of the Maikhan-Uul Fm to the *ca.* 717 to 660 Ma Sturtian glacial epoch (fig. 17).

Chemostratigraphy

Carbon isotopes.—Limestone successions of the Taishir Fm preserve the post-Sturtian Rasthof $\delta^{13}C$ excursion in the basal T1 TST and the mid-Cryogenian Taishir excursion in the basal T3 TST. In general, within the Taishir Fm, carbonate $\delta^{13}C$ values are more negative in TSTs and more positive in HSTs (fig. 8). The oceanic $\delta^{13}C$ signal preserved in carbonate rocks can be obscured by noise from detrital carbon (Swart, 2008; Johnston and others, 2012), restriction (Panchuk and others, 2006), early alteration (Melim and others, 2001; Knauth and Kennedy, 2009), and burial diagenesis (Derry, 2010). In the Taishir Fm, the $\delta^{13}C$ profiles can be correlated for >100 km across the margin (figs. 3 and 8). The fidelity of the carbonate $\delta^{13}C$ signal is further supported by the tight covariance with organic $\delta^{13}C$ values (Shields and others, 2002; Johnston and others, 2012).

The Cryogenian Trezona $\delta^{13}C$ excursion (Halverson and others, 2005; Swanson-Hysell and others, 2010; Rose and others, 2012), on the other hand, is not well developed in Mongolia. Trend in $\delta^{13}C$ values especially in the Taishir negative $\delta^{13}C$ excursion is comparable with the Trezona, which is further complicated by nonvariable values in $^{87}Sr/^{86}Sr$ (fig. 8 and Halverson and others, 2007). However, the removal of T4 in all localities except the Khongor Range, Zuun-Arts, and Ikh Goliin Tsakhir is suggestive of glacial erosion (Macdonald and others, 2009a) that may be responsible for an absence of Trezona excursion. This is further supported by limestone clasts in the Khongor diamictite that yield comparatively depleted $\delta^{13}C$ values (fig. 8) distinct from those of the underlying T3.

One of the distinct features of the Cryogenian carbonate record of the Zavkhan Terrane is the prevalence of limestone (fig. 8) compared to comparable carbonate dominated records in Namibia (Halverson and others, 2005) and Arctic Alaska (Macdonald and others, 2010). Parallel sections of unaltered and dolomitized successions provide an opportunity to document the $\delta^{13}C$ effects of dolomitization, which reveals variations of up to 8 permil between undolomitized and dolomitized sections (fig. 8).

In the Ediacaran strata, the early-Ediacaran Maieberg $\delta^{13}C$ excursion (Halverson and others, 2002; Hoffman and Schrag, 2002) is preserved in the TST and HST of the Ol Fm wherever the underlying Taishir Fm carbonates are preserved as limestone. However, the excursion is absent in localities where the underlying Taishir Fm and upper portion of the Ol Fm are dolomitized (fig. 12).

Carbon isotope signatures of Sh1 TST through Sh3 are comparable to other stratigraphically equivalent early Ediacaran strata globally (Misi and Veizer, 1998; Calver, 2000; Fike and others, 2006; Macdonald and others, 2013; Zhu and others, 2013). The return of $\delta^{13}C$ values in Sh4 from +6 to +8 permil back to +2 to +0.5 permil is also recognized from stratigraphically equivalent successions preserved in South China (Zhu and others, 2013), Namibia (Halverson and others, 2005) and NW Canada (Macdonald and others, 2013).

In our correlation framework, there is an up to 5 permil difference between limestone dominated Sh3 and Sh4 preserved in outer-mid-ramp and dolostone dominated Sh3 and Sh4 present in mid-inner-ramp depositional environment. Although $\delta^{13}C$ values can vary by as much as 2 permil between coexisting dolomite-calcite pairs (Degens and Epstein, 1964), the data presented here suggest that evolution of dolomitizing fluid has the potential to drive $\delta^{13}C$ variability within limestone and its dolomitized equivalent as demonstrated in the upper Taishir (T3), Ol, and Shuurgat (Sh3 and Sh4) fms. Due to the correspondence of lateral $\delta^{13}C$ variability with dolomitization fronts, we propose that the replacement and recrystallization of the primary carbonates from dolomitizing fluids played a crucial role in modifying $\delta^{13}C$

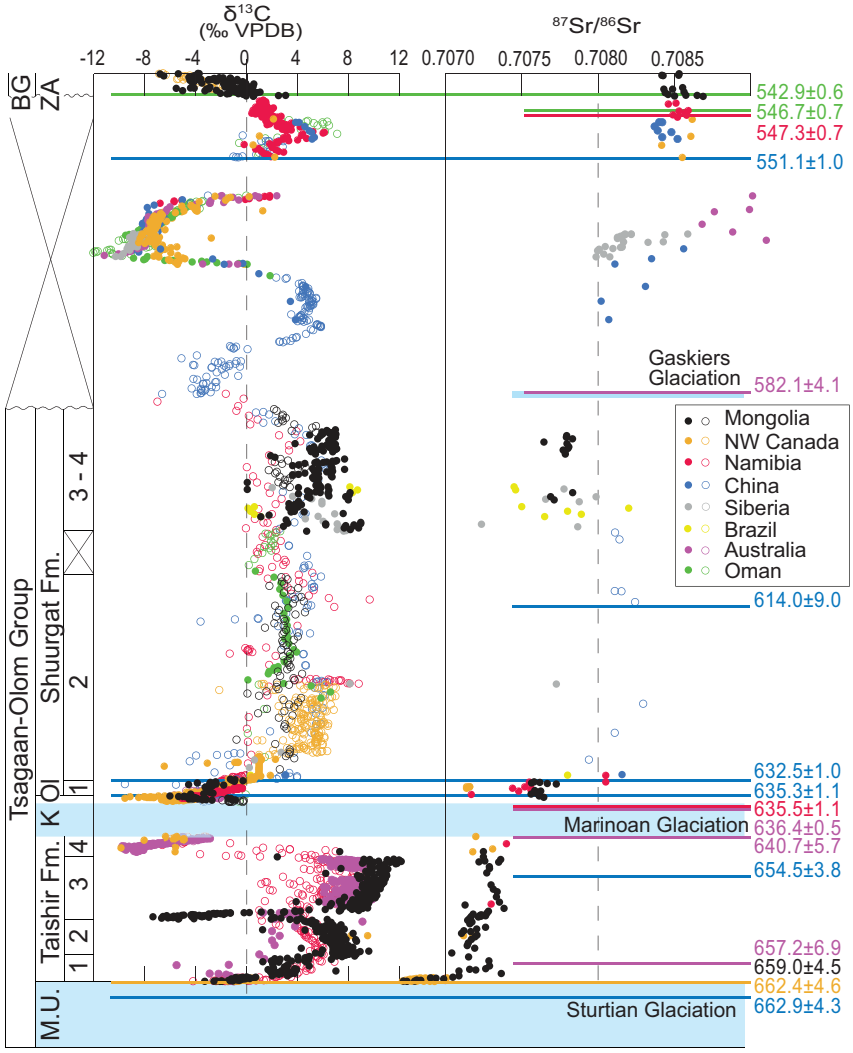

Fig. 17. Global correlations of Cryogenian strata from key locations with associated isotopic and geochronologic data. All of the data are color coded for geographic location: Black = Mongolia, Purple = Australia, Red = Namibia, Blue = China, Green = Oman, Yellow = Brazil, and Orange = NW Canada. The approximate depositional span of each formation from which the chemostratigraphic data were utilized is shown on right-hand side. Each of these stratigraphic successions contains multiple unconformities of unknown extent, so there are certainly additional intervals in which strata are not present, and this figure is purely meant as an exercise to summarize our current age model for the Cryogenian and Ediacaran. Data from non-dolomitized carbonates are shown by filled and dolomitized by open circles. The $\delta^{13}C$ data is from Mongolia (this paper, Macdonald and others, 2009a), northwestern Canada (Johnston and others, 2012; Macdonald and others, 2013; Rooney and others, 2014), Namibia (Halverson and others, 2005), Australia (McKirdy and others, 2001; Swanson-Hysell and others, 2010; Rose and others, 2012), Oman (Fike and others, 2006), China (Sawaki and others, 2010b; Zhu and others, 2013), Brazil (Misi and Veizer, 1998), and Siberia (Pokrovskii and others, 2006; Melezhik and others, 2009). Strontium isotope data is from Mongolia (this study, Brasier and others, 1996; Shields and others, 2002), northwestern Canada (Kaufman and others, 1993; Narbonne and others, 1994; Rooney and others, 2014), Namibia (Kaufman and others, 1993; Yoshioka and others, 2003; Halverson and others, 2007), Australia (Calver, 2000), China (Sawaki and others, 2010b; Cui and others, 2015), Brazil (Misi and Veizer, 1998), and Siberia (Pokrovskii and others, 2006; Melezhik and others, 2009). Geochronological constraints are from Mongolia (Rooney and others, 2015), Australia (Calver and others, 2004; Calver and others, 2013; Rooney and others, 2014) and others (Schmitz and others, 2012 with references therein). All uncertainties for reported dates include the internal, tracer solution, (where applicable), and decay constant uncertainties for the U-Pb and Re-Os geochronometers.

profiles. In general, it appears that dolomitization dampens $\delta^{13}C$ variability and shifts the mean values. This phenomenon is not unique to Mongolia. Large lateral $\delta^{13}C$ gradients have also been documented between Ediacaran carbonates deposited in foreslope and platform settings in Namibia (Halverson and others, 2005; Hoffman and others, 2007; Hoffman, 2011). We suggest that these lateral gradients are most easily attributable to differences in the water-rock ratio or the isotopic composition of the fluid during dolomitization rather than seawater isotopic gradients.

Strontium isotopes.—Because of the long (2.4 Ma, Jones and Jenkyns, 2001) residence time in the ocean, Sr isotopes also provide a correlation tool for Precambrian carbonates that complement $\delta^{13}C$ correlations (DePaulo and Ingram, 1985; Banner, 2004). A cutoff value of Sr concentration of <500 ppm was used as a screening method for diagenetic alteration for the selection of $^{87}Sr/^{86}Sr$ values to compare our data with those from NW Canada (Narbonne, 1994; Halverson and others, 2007; Rooney and others, 2014), Namibia (Kaufman and others, 1993; Yoshioka and others, 2003; Halverson and others, 2007), China (Sawaki and others, 2010b), Siberia (Pokrovskii and others, 2006; Melezhik and others, 2009), Brazil (Misi and Veizer, 1998), Australia (Calver, 2000) and Oman [(table A4 (http://earth.geology.yale.edu/~ajs/SupplementaryData/2016/Bold), figs. 17 and A1).

The rise in $^{87}Sr/^{86}Sr$ from 0.70673 to 0.70737 in Member T1 of the Taishir Fm is in agreement with values measured previously between 0.70675 to 0.70694 (Brasier and others, 1996; Shields and others, 2002), which is mirrored in the Rasthof Fm of Namibia (Yoshioka and others, 2003) and the Twitya Fm of NW Canada (Rooney and others, 2014). The carbon isotope chemostratigraphy from these three areas is also very similar, as discussed above. After this dramatic rise in the Sturtian cap carbonate, Sr isotope values are relatively steady through the rest of the Taishir Fm, with a slight rise near the base of T3.

A comparatively elevated $^{87}Sr/^{86}Sr$ value of 0.7091 ± 0.0001 (average value from Liu and others, 2014) was measured in the Ol Fm cap dolostone, which is similar to what Liu and others (2013) reported in Group-II of the Nuccaleena Fm cap dolostone in South Australia and in Member 1 of the Doushantuo Fm from China (Sawaki and others, 2010b). Although these values may be attributed to diagenetic alteration that lowers Sr concentration, elevated $^{87}Sr/^{86}Sr$ values are still persistent in step-leaching treatments, which have been used as evidence for a glacial meltwater plume with a radiogenic $^{87}Sr/^{86}Sr$ composition (Liu and others, 2014). Our single leach $^{87}Sr/^{86}Sr$ measurements of the Ol Fm are from the TST limestone succession, and the values of 0.70756 and 0.70765 (figs. 12 and 17) agree with what Liu and others (2014) reported in the same interval, becoming less radiogenic up-section.

Overall, $^{87}Sr/^{86}Sr$ values increase from the basal Taishir Fm to the top of the Shuurgat Fm, from 0.70673 to 0.70795, excluding the values measured in the Ol cap dolostone (Liu and others, 2014) and are significantly less radiogenic compared to the values of >0.7083 reported (Brasier and others, 1996) in the latest Ediacaran-Cambrian Zuun-Arts Fm. Globally, the most reliable $^{87}Sr/^{86}Sr$ values from early to middle Ediacaran sections deposited prior to the Shuram excursions range from 0.7073 to 0.7083 (fig. 17) (Narbonne and others, 1994; Misi and Veizer, 1998; McKirdy and others, 2001; Yoshioka and others, 2003; Pokrovskii and others, 2006; Halverson and others, 2007; Melezhik and others, 2009; Sawaki and others, 2010a; Sawaki and others, 2010b; Rooney and others, 2014). In contrast, limestone strata deposited after the Shuram excursion, in the late Ediacaran between ~552 and 541 Ma, have $^{87}Sr/^{86}Sr$ values between 0.7083 and 0.7090 (Narbonne and others, 1994; Brasier and others, 1996; McKirdy and others, 2001; Halverson and others, 2007; Melezhik and others, 2009; Pokrovsky and others, 2011). Hence, $^{87}Sr/^{86}Sr$ data from the Shuurgat Fm suggest that this unit was likely deposited during the early to middle Ediacaran, prior to

the Shuram excursion, and confirm previous suggestions that the karst surface between the Shuurgat and Zuun-Arts Fm represents a major hiatus (fig. 17).

Together, our new Cryogenian and Ediacaran $^{87}Sr/^{86}Sr$ compilation (fig. 17) suggests that, rather than a gradual rise to more radiogenic values from an increase of continental margins during the rifting of Rodinia (Halverson and others, 2007), the Cryogenian to Ediacaran rise is stepwise, likely reflecting extreme weathering in the aftermath of the Cryogenian Snowball Earth events, and an additional extreme weathering event associated with the Shuram $\delta^{13}C$ excursion.

Construction of an Age Model

The carbon and strontium isotope profiles of the Taishir Fm and a Re-Os age of 659.0 ± (3.9/4.5) (Rooney and others, 2015) obtained from T1 are very similar to the 662.4 ± (3.9/4.6) Ma Twitya Fm in northwest Canada, and consequently, in our age model the base of the Taishir Fm is pinned at 660 Ma. The T1 cap carbonate was previously dated using $^{207}Pb/^{204}Pb$ on carbonate yielding a $^{207}Pb/^{206}Pb$ isochron date of 632 ± 47 Ma (MSWD = 7.3) (Ovchinnikova and others, 2012). Although this method is neither very precise nor reliable because of the mobility of U and Pb in carbonate (Sumner and Bowring, 1996), this date is within error estimates based on global correlations.

The age of the Taishir Fm is further constrained by correlations of the overlying Khongor Fm diamictite with the Marinoan glaciation and basal Ol Fm with the Marinoan cap carbonate (Macdonald and others, 2009a). This suggests that the underlying Khongor Fm diamictite is an end-Cryogenian glacial deposit, with the termination bracketed by $^{206}Pb/^{238}U$ CA-ID-TIMS dates of 635.5 ± 0.6 Ma and 635.2 ± 0.6 Ma from zircon from China (Condon and others, 2005), 635.5 ± 1.2 Ma from zircon from Namibia (Hoffmann and others, 2004), and 636.4 ± 0.5 Ma from zircon from Australia (Calver and others, 2013). By correlation, these data constrain the age of the Taishir Fm and the Khongor Fm to between 659 and 635 Ma. Assuming that the start of the Marinoan glaciation was ~640 Ma and taking into account the absence and erosion of the Trezona excursion in the Zavkhan Terrane, in our age model, the top of the Taishir Fm carbonate is given with a geochemically interpolated age of 643 Ma (fig. 17). However, we acknowledge that the Marinoan glaciation may have started earlier and the top of the Taishir Fm is as old as *ca.* 650 Ma.

There are no absolute ages on the Ol or Shuurgat fms, and thus our age model relies on chemostratigraphic correlation to other Ediacaran successions globally, particularly Namibia (Halverson and others, 2005) and South China (Condon and others, 2005; Zhu and others, 2013) (fig. 17). Using $\delta^{13}C$ correlations with South China, the entire Ol Fm and Sh1 of the Shuurgat Fm are bracketed by $^{206}Pb/^{238}U$ CA-ID-TIMS dates of 635.2 ± 0.6 and 632.5 ± 0.5 Ma at the base. The uncomformity at the top of the Sh4 could explain why the Gaskiers glaciation and Shuram $\delta^{13}C$ excursion are not preserved in the Zavkhan Terrane (see fig. 18, Halverson and others, 2010) and hence a 584 Ma age (Hoffman and Li, 2009) is assigned to the top of the Shuurgat Fm (fig. 17). The age of the Shuram $\delta^{13}C$ excursion is constrained between *ca.* 582 Ma and 551 Ma with the correlation of the Gaskiers glaciation with dropstones in the Bunyeroo Fm (Gostin and others, 2010) and the placement of the 551 Ma ash in South China in the Miaohe member of the Denying Fm (An and others, 2015), and the duration of the excursion remains poorly constrained.

The Cryogenian and Ediacaran Carbon Cycle

Although $\delta^{13}C$ trends are reproducible in limestone sections across the Zavkhan Terrane, dolomitized sections show large lateral isotopic variability. It is generally accepted that dolomite records a primary seawater signal with minor variations from the equivalent limestone (Degens and Epstein, 1964) due to amount of concentration

of carbon in aqueous fluids (Knoll and others, 1986; Kaufman and others, 1997). However, as discussed previously, this assumption does not hold true for much of the Cryogenian strata in southwest Mongolia, in which ≤8 permil variability is present between limestone and coeval dolomitized strata (figs. 8 and 12). Globally, both Cryogenian and Ediacaran carbonate are dominated by dolostone (Halverson and others, 2002; Macdonald and others, 2010) and consequently, most Neoproterozoic $\delta^{13}C$ compilations are based on them (Halverson and others, 2010). The data presented herein underscore the need to use caution when using $\delta^{13}C$ data from dolomites for correlations and compilations. By using data obtained from dolomite, the truly extreme variability of Neoproterozoic $\delta^{13}C$ values preserved in limestone may have been dampened.

In limestone-dominated sections, our correlations suggest that the Taishir $\delta^{13}C$ excursion is preserved, but the Trezona $\delta^{13}C$ excursion is largely removed under the sub-Khongor erosional surface, and the Shuram $\delta^{13}C$ excursion is missing below the karstic surface at the base of the Zuun-Arts Fm (fig. 17). The Taishir and Trezona $\delta^{13}C$ excursions present two of the largest perturbations to the carbon cycle in the geological record (Johnston and others, 2012), comparable with the Ediacaran Shuram excursion (Grotzinger and others, 2011). Although the nadir of the Shuram excursion is more negative (-12‰), the Shuram departs from a less enriched background (+2 to +4‰), compared to the Taishir and Trezona excursions that start from a ~+8 to +10 permil background and plummet to −7 permil. Thus, many of the arguments and models for the origin and nature of the Shuram $\delta^{13}C$ excursion (for example Derry, 2010; Grotzinger and others, 2011) are applicable to the Cryogenian $\delta^{13}C$ excursions.

Through comparisons with Pliocene-Pleistocene $\delta^{13}C$ anomalies associated with glacio-eustatic sea level fall and subaerial exposure, and by the covariance between $\delta^{13}C$–$\delta^{18}O$, multiple authors have proposed that the Trezona excursion was driven by meteoric diagenesis and remineralization of a terrestrial biosphere (Knauth and Kennedy, 2009; Swart and Kennedy, 2012). However, it is unlikely that there was a significant terrestrial biosphere during the Cryogenian (Sanderson, 2003; Zimmer and others, 2007; Genzel, 2008) and consequently extensive organic matter remineralization in the uppermost portion of the sediments near these purported exposure surfaces is unlikely. Although exposure surfaces related to the Marinoan glaciation are present directly above the Trezona excursion at all of the locations in which it has been described, in Mongolia the Trezona excursion is largely absent beneath a sub-glacial erosion surface. However, the Taishir excursion is in a broad TST to HST, and the nearest exposure surface is >100 m above the excursion. Therefore, meteoric alteration, if it was driving the Taishir excursion, must have occurred in the lower vadose, phreatic, or mixing zone wedges (Melim and others, 2001) associated with the sub-Khongor Fm exposure surfaces at the top of the Taishir Fm. Moreover, there is no petrographic evidence for large-scale replacement and meteoric cements directly associated with the excursion. Lastly, $\delta^{13}C$ and $\delta^{18}O$ do not covary while $\delta^{13}C_{carb}$ and $\delta^{13}C_{org}$ do covary in the Taishir excursion [table A3 (http://earth.geology.yale.edu/~ajs/SupplementaryData/2016/Bold), Johnston and others, 2012]. Thus, although meteoric diagenesis may be consistent with some features of the Trezona excursion, it is completely inconsistent with the sequence stratigraphic architecture and geochemistry of the Taishir excursion in Mongolia.

Another feature of the Trezona excursion in Australia (Swanson-Hysell and others, 2010) and Namibia (Johnston and others, 2012) is that $\delta^{13}C_{carb}$ and $\delta^{13}C_{org}$ do not covary. This lack of covariance between $\delta^{13}C_{carb}$ and $\delta^{13}C_{org}$ inspired Rothman and others (2003) to propose the existence of a large Neoproterozoic dissolved organic carbon pool (DOC) that was periodically remineralized, driving dynamic behavior in the isotopic composition of the dissolved inorganic carbon pool (DIC). Moreover, the

existence of a large DOC reservoir in Neoproterozoic oceans is inconsistent with $\delta^{13}C$ records from NW Canada and Mongolia that show covariance throughout the Cryogenian period (Johnston and others, 2012). Johnston and others (2012) instead suggested that the lack of covariance in $\delta^{13}C_{carb}$ and $\delta^{13}C_{org}$ in Australia and Namibia could be explained by bulk organic carbon in TOC-lean samples being more prone to masking by detrital and migrated organic matter. Thus, the $\delta^{13}C$ data from Mongolia is inconsistent with driving mechanisms that evoke the remineralization of a large DOC reservoir. Johnston and others (2012) suggested that the Taishir excursion was due to the addition of isotopically light carbon to the ocean/atmosphere through either oxidation of organic matter associated with the uplift and erosion of previously deposited strata (compare Higgins and Schrag, 2006) or the release of methane (Schrag and others, 2002). These models predict a timescale consistent with the mixing time of the ocean. That is, the excursion should not last more than 100 ka. The average thickness of the Taishir excursion is ~30 m. The maximum average sedimentation rate calculated above suggests a duration of the Taishir excursion of 100 ka to 1 Ma, broadly consistent with these models and perhaps suggestive of increased sedimentation rates. However, these models do not directly address the positive background $\delta^{13}C$ values of the Cryogenian.

Schrag and others (2013) proposed an alternative model whereby both the positive background $\delta^{13}C$ values and the negative excursions are related to changes in a large, isotopically depleted sink of carbon in authigenic carbonate. The precipitation of authigenic carbonate is inhibited by the amount of O_2 in seawater due to the acidity generated via oxidation of reduced compounds (C_{org}, H_2S, Fe^{2+}) (Higgins and others, 2009). During the Taishir excursion, the addition of carbon to the ocean/atmosphere would lead to an increased global production of authigenic carbon, thereby producing a negative feedback on changes to the carbon isotopic composition of the ocean, whereas the addition of oxidants to the ocean, either as free oxygen or other electron acceptors (Fe(III), SO_4^{2-}) could have led to a greater importance of aerobic respiration over anaerobic respiration, further limiting the amount of organic matter delivered to the sediment for anaerobic respiration. Although the ultimate origin of large shifts in the Cryogenian $\delta^{13}C$ composition of the oceans remains enigmatic, our data reinforce the reproducibility and fidelity of these signals (fig. 8).

CONCLUSIONS

With detailed mapping, stratigraphy, sedimentology, geochemistry, the Tsagaan-Olom Group is now confidently correlated with Cryogenian and early-Ediacaran successions around the globe. Moreover, detrital age spectra of the lower Zavkhan, Maikhan-Uul, Taishir and Shuurgat fms provide the first strong evidence for the presence of Proterozoic basement on the Zavkhan Terrane. The age spectra reveal dominant age peaks at 1950 to 2100 and 2400 to 2600 Ma. These data have some similarities and some differences from previously reported basement ages from Tarim, North China, Siberia and NE Gondwana and highlight uncertainties related to the origin and travels of the Proterozoic continental fragments that form the core of the CAOB.

The Zavkhan Terrane is mantled with the Zavkhan Fm, dated at 802.11 ± 0.45/0.56/1.0, 797.22 ± 0.56 and 787.45 ± 0.47/0.58/1.0 Ma, and rift-related rocks of the Khasagt Fm. After 729.8 ± 1.4 Ma, the Zavkhan Terrane was covered with ice sheets and lodgement tills of the lower Maikhan-Uul Fm. During this glaciation, the ice-grounding line retreated and readvanced, and coarse siliciclastic turbidite beds were deposited in the middle Maikhan-Uul Fm. Although these strata have previously been interpreted to mark a transgression (Lindsay and others, 1996), they were not necessarily deposited in open water and could have formed below an ice shelf or in a glacio-lacustrine setting. Deposition of rain-out diamictites in the upper member of the Maikhan-Uul Fm culminated with a local regression and exposure, followed by a

laterally extensive transgression and carbonate deposition of Member T1 of the Taishir Fm. This local regression was likely either the product of glacio-isostatic rebound or ice gravity. Carbon and strontium isotope values, along with Re-Os geochronology confirm previous suggestions that at least the upper Maikhan-Uul Fm is correlative with the 717 to 660 Ma Sturtian glaciation.

The Taishir Fm was deposited on an isolated, passively subsiding homoclinal carbonate ramp in four large-scale sequences. The Taishir $\delta^{13}C$ excursion occurs in the TST of the third sequence. These data are consistent with the input of isotopically light carbon to the ocean, either from the mantle, methane, or organic carbon, or from an oxidation event that lead to the crash of the authigenic carbonate sink—these scenarios are not mutually exclusive. Above the Taishir excursion, $\delta^{13}C$ values become extremely enriched before dropping again prior to deposition of the Khongor Fm diamictite. This downward trend in $\delta^{13}C$ is correlated to the onset of the Trezona excursion. By distinguishing between these excursions, these geochemical records can now be globally integrated together into composite records. The data from Mongolia provide the backbone for understanding the great geochemical, climatic and biological changes that characterize the Cryogenian glacial interlude.

The Khongor Fm, the Marinoan glacial diamictite, is absent at most exposures on the Zavkhan Terrane. Nonetheless, the presence of isolated, thick diamictites on the Khunkher block with striated clasts and soft-sedimentary folding suggest that the Khongor Fm was deposited during deglaciation as a glacial moraine. These glacial deposits are overlain by a cap dolostone of the Ol Fm, which contains sedimentary features including tubestone stromatolites, giant wave ripples, and both aragonite and barite fans, that are characteristic of the *ca.* 635 Ma basal Ediacaran cap dolostone. In addition, $^{87}Sr/^{86}Sr$ values obtained from limestone of the upper Ol Fm match values preserved in limestone that overlies the Marinoan cap dolostone in Australia. Furthermore, the absence of the Shuram excursion in Mongolia, and $^{87}Sr/^{86}Sr$ values of <0.70795 in the Shuurgat Fm suggest that much of the mid- to late Ediacaran is missing at a karst surface between the Shuurgat and Zuun-Arts fms.

In both Ediacaran and Cryogenian strata, large lateral $\delta^{13}C$ gradients are apparent in dolomitized strata. These data emphasize the importance of building composite $\delta^{13}C$ curves and assessing the nature of the carbon cycle with the least-altered samples, preferably limestones. The $\delta^{13}C$ variability of the Neoproterozoic is dampened in dolomitized strata, and the least-altered samples indicate that both the positive and negative $\delta^{13}C$ excursions in our Cryogenian and Ediacaran composite curve are even greater than what have been depicted in previous compilations. That is, in the most pristinely preserved sections, large carbon isotope excursions are a robust and reproducible feature of Neoproterozoic records.

ACKNOWLEDGMENTS

We thank: NASA MIT Astrobiology node and NASA Geobiology grant # NNH10ZDA001N-EXO for support; the NSF GRF (to EFS) for support; J.C. Creveling and David Jones for help in the field; Claire Bucholz for discussions and help drafting figure 1; our field assistants Bataa, Erdenebayar Oyun, Tsolmon Adiya, Javkhlan Otgonkhuu, Gerelt Sarantuya, Javzandulam Chuluunbaatar, Munkh-Erdene Delger, Munkh Jugder, Ariunsanaa Dorj, Odbayar Erdenebat, Dan Bradley, Tanya Petach and Sarah Moon; Bayasgalan Amgalan, Altantsetseg Baldandorj, Oyungerel Sambuu, D. Oyun and Lkhagva-Ochir Said for help with logistics; Chuluun Minjin, and D. Dorjnamjaa for valuable scientific input; Greg Eischeid and Sarah Manley for use of and assistance in the Harvard University Laboratory for Paleoceanography; our three external reviewers, Ashleigh Hood, Alfred Kröner, and Huiming Bao, for their insightful comments and suggestions for improvement of the manuscript.

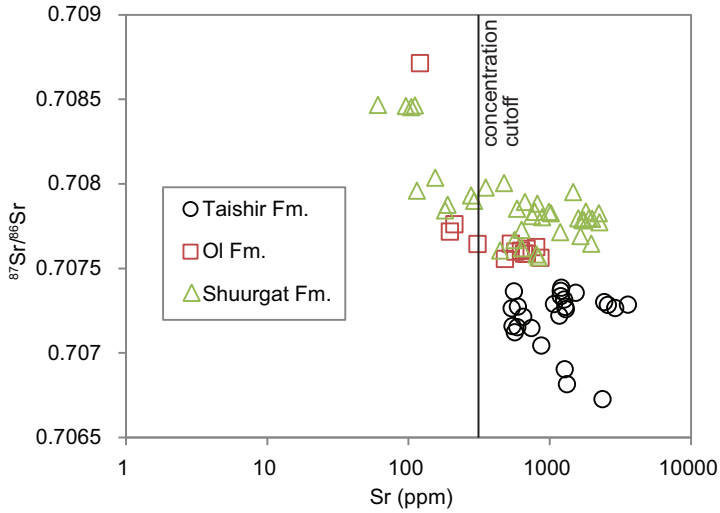

Fig. A1. Sr isotope values of the Tsagaan-Olom Group carbonates plotted against Sr concentration with concentration cut-off shown. Screening method follows Halverson and others (2007).

APPENDIX

LA-ICPMS Method

Zircon grains were separated from rocks using standard techniques, including crushing, pulverizing, washing, magnetic separation, heavy liquids, and hand picking, and annealed at 900 °C for 60 hours in a muffle furnace. Annealed zircon grains were directly poured into a petri dish, agitated, and divided into quarters. Depending on the number of zircons separated from each sample, all of the zircons from one quarter were selected. Grains that suit the requirements for analysis were analyzed. These randomly selected grains were mounted in epoxy and polished until their centers were exposed. Cathodoluminescence (CL) images were obtained with a JEOL JSM-1300 scanning electron microscope and Gatan MiniCL. Zircon was analyzed by laser ablation inductively coupled plasma mass spectrometry (LA-ICPMS) using a ThermoElectron X-Series II quadrupole ICPMS and New Wave Research UP-213 Nd:YAG UV (213 nm) laser ablation system at the Boise State University. In-house analytical protocols, standard materials, and data reduction software were used for acquisition and calibration of U-Pb dates and a suite of high field strength elements (HFSE) and rare earth elements (REE) (Paces and Miller, 1993; Norman and others, 1996; Black and others, 2003; Sláma and others, 2008). Zircon was ablated with a laser spot of 25 or 30 μm wide using fluence and pulse rates of 5 J/cm2 and 10 Hz, respectively, during a 45 second analysis (15 sec gas blank, 30 sec ablation) that excavated a pit ~25 μm deep. Ablated material was carried by a 1.2 L/min He gas stream to the nebulizer flow of the plasma. Quadrupole dwell times were 5 ms for Si and Zr, 200 ms for ^{49}Ti and ^{207}Pb, 80 ms for ^{206}Pb, 40 ms for ^{202}Hg, ^{204}Pb, ^{208}Pb, ^{232}Th, and ^{238}U and 10 ms for all other HFSE and REE; total sweep duration is 950 ms. Background count rates for each analyte were obtained prior to each spot analysis and subtracted from the raw count rate for each analyte. For concentration calculations, background-subtracted count rates for each analyte were internally normalized to ^{29}Si and calibrated with respect to NIST SRM-610 and -612 glasses as the primary standards. Ablation pits that appear to have intersected glass or mineral inclusions were identified based on Ti and P signal excursions, and associated sweeps were discarded. U-Pb dates from these analyses are considered valid if the U-Pb ratios appear to have been unaffected by the inclusions. Signals at mass 204 were normally indistinguishable from zero following subtraction of mercury backgrounds measured during the gas blank (<1000 cps 202Hg), and thus dates are reported without common Pb correction. Rare analyses that appear contaminated by common Pb were rejected based on mass 204 greater than baseline.

Data were collected in seven experiments in December 2012, May 2013, and December 2014. For U-Pb and ^{207}Pb/^{206}Pb dates, instrumental fractionation of the background-subtracted ratios was corrected and dates were calibrated with respect to interspersed measurements of zircon standards and reference materials. The primary standard Plešovice zircon (Sláma and others, 2008) was used to monitor time-

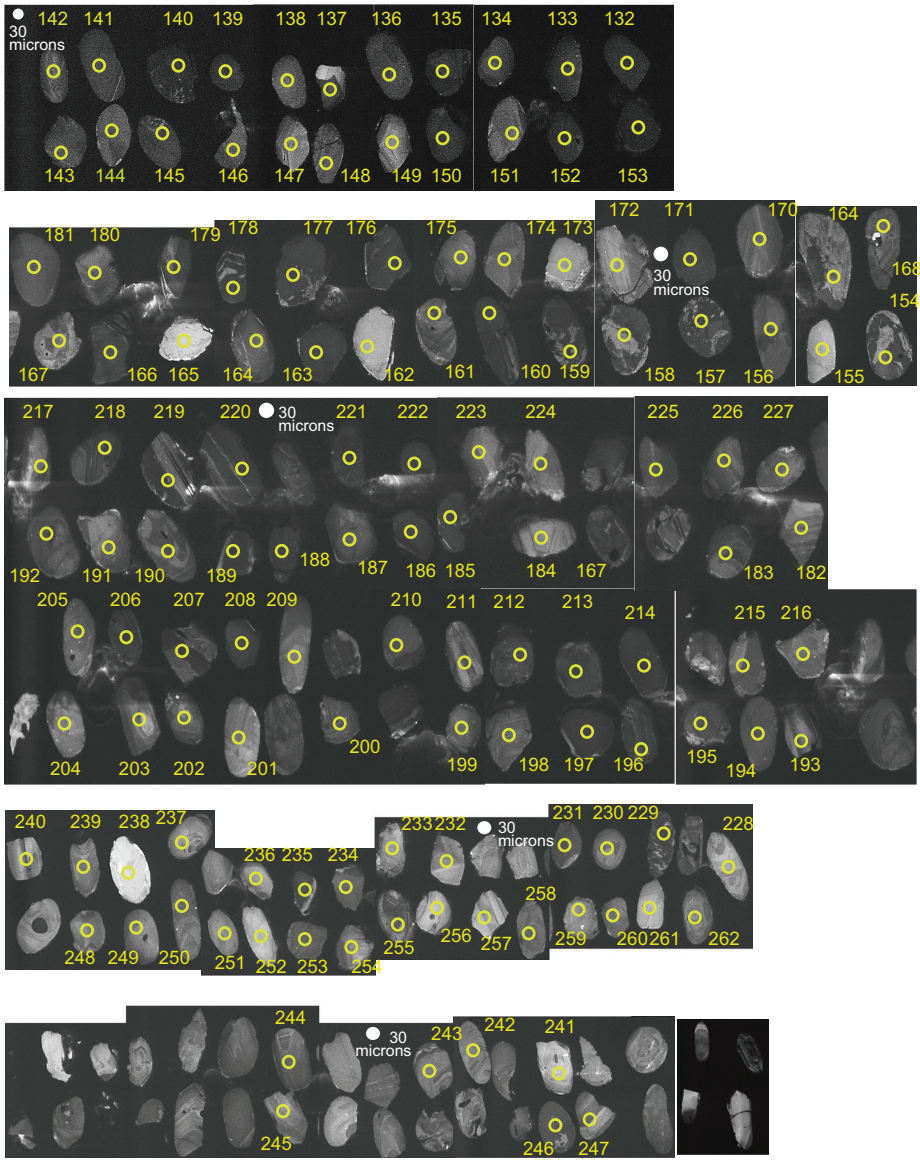

Fig. A2. Cathodoluminescence images of zircon grains dated by U-Pb LA-ICPMS from sample U1333.

dependent instrumental fractionation based on two analyses for every 10 analyses of unknown zircon. A polynomial fit to the standard analyses yields each sample-specific fractionation factor. A secondary correction to $^{206}Pb/^{238}U$ of 1.3–3.3% (dependent upon experiment) was made based upon the bias indicated by weighted mean dates from the zircon standards Temora (418 Ma) and FC1 (1098 Ma), which were treated as unknowns and measured once for every 10 analyses of unknown zircon. The secondary correction is thought to mitigate matrix-dependent variations due to contrasting compositions and ablation characteristics between the Plešovice zircon and other standards (and unknowns); because all primary and secondary standards are chemically abraded, bias between standards is not considered to be due to Pb loss.

Radiogenic isotope ratio and age error propagation for all analyses includes uncertainty contributions from counting statistics and background subtraction. Because the detrital zircon analyses are interpreted

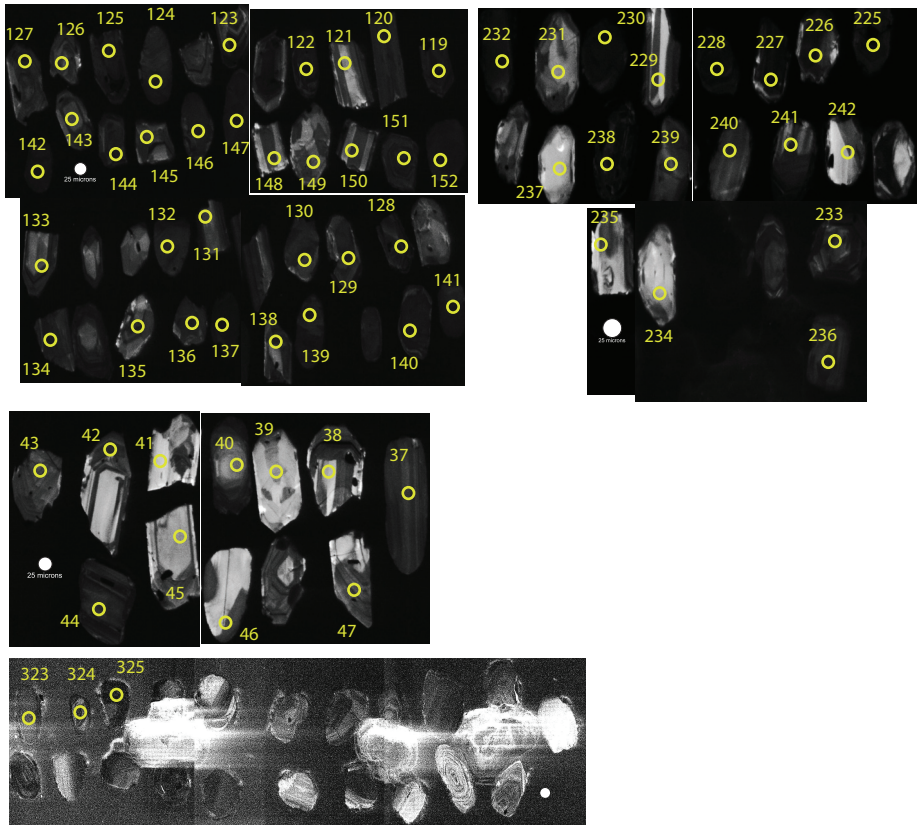

Fig. A3. Cathodoluminescence images of zircon grains dated by U-Pb LA-ICPMS from sample U1214.

individually, uncertainties from the standard calibrations are propagated into the errors on each date. These uncertainties are the local standard deviations of the polynomial fits to the interspersed primary standard measurements versus time for the time-dependent, relatively larger U-Pb fractionation factor, and the standard errors of the means of the consistently time-invariant and smaller $^{207}Pb/^{206}Pb$ fractionation factor. These uncertainties are 1.1–1.6% (2σ) for $^{206}Pb/^{23}8U$ and 0.5–0.9% (2σ) for $^{207}Pb/^{206}Pb$.

Age interpretations are based on $^{207}Pb/^{206}Pb$ dates for analyses with $^{207}Pb/^{206}Pb$ dates >1000 Ma. Analyses with >20% positive discordance and >10% negative discordance are not considered. The $^{206}Pb/^{238}U$ dates are used for analyses with $^{207}Pb/^{206}Pb$ dates <1000 Ma. Errors on the dates from individual analyses are given at 2σ.

CA-ID-TIMS U-Pb Geochronology Method

Zircons were separated from all samples using standard crushing, magnetic, and high-density liquid separations. Individually selected zircon grains were analyzed by the U-Pb isotope dilution thermal-ionization mass spectrometry (ID-TIMS) technique following the detailed procedures described in Ramezani and others (2011). All zircons were pre-treated by a chemical abrasion (CA-TIMS) method modified after Mattinson (2005) to mitigate the effects of radiation-induced Pb loss, and spiked with the EARTHTIME ET535 mixed ^{205}Pb-^{233}U-^{235}U tracer prior to dissolution and chemical separation of U and Pb. All isotopic measurements were made on a Sector 54 mass spectrometer instrument at the Massachusetts Institute of Technology. Uranium and lead isotopic data reduction, date calculation and propagation of uncertainties were carried out using computer applications and algorithms of Bowring and others (2011) and McLean and others (2011).

Sample dates representing the best estimate for the zircon crystallization age – and interpreted as the volcanic eruption and/or maximum depositional age – are derived from weighted mean $^{206}Pb/^{238}U$ date of

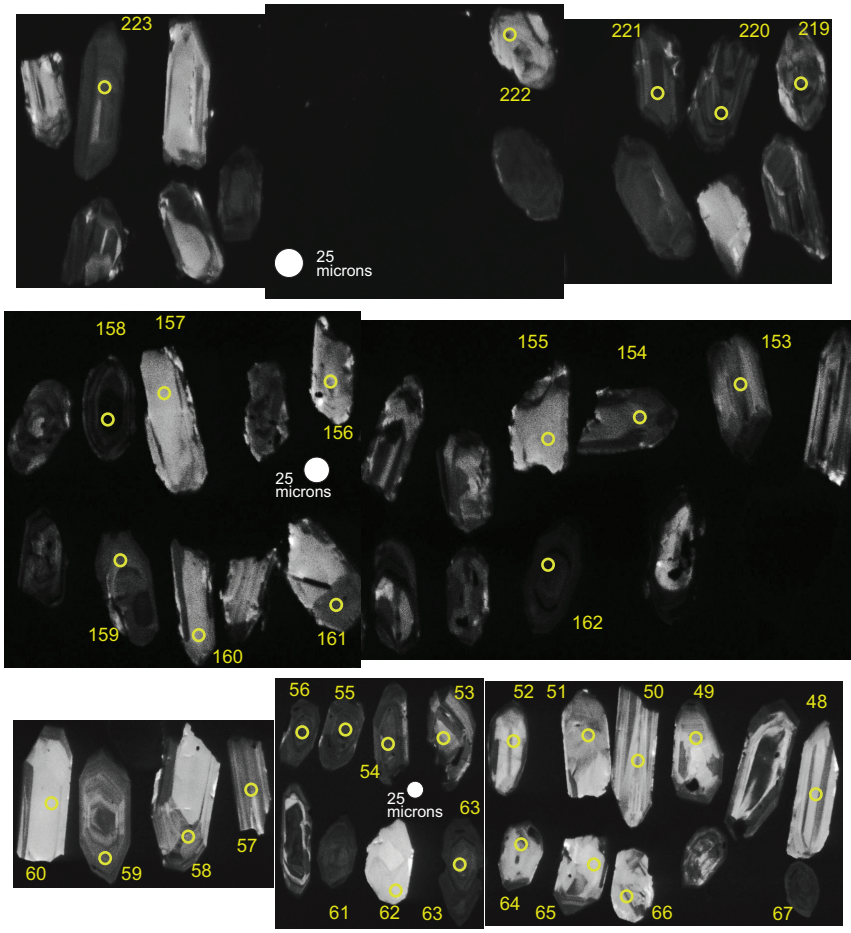

Fig. A4. Cathodoluminescence images of zircon grains dated by U-Pb LA-ICPMS from sample F1203-272.1.

a statistically coherent cluster of the youngest zircon analyses from each sample, provided that there are at least three precise analyses to form a cluster. Uncertainties on weighted mean dates are reported at 95% confidence level and follow the notation ±X/Y/Z Ma, where X is the internal (analytical) uncertainty in the absence of all external errors, Y incorporates the U-Pb tracer calibration error and Z includes the latter as well as the decay constant errors of Jaffey and others (1971). Total uncertainties (Z) are necessary for comparison of dates from different isotopic chronometers (for example U-Pb versus $^{40}Ar/^{39}Ar$ or Re-Os).

Carbonate Carbon and Oxygen Isotope Methods

All carbonate samples were cut perpendicular to bedding, revealing internal textures. Between 5–60 mg of powder were microdrilled from the matrix, avoiding veining, fractures, and siliciclastic components. Carbonate $\delta^{13}C$ and $\delta^{18}O$ isotopic data were acquired simultaneously on a VG Optima dual inlet mass spectrometer attached to a VG Isocarb preparation device (Micromass, Milford, MA) in the Harvard University Laboratory for Geochemical Oceanography. ~1-mg micro-drilled samples were reacted in a common, purified H_3PO_4 bath at 90 °C. Evolved CO_2 was collected cryogenically and analyzed using an in-house reference gas. External error (1σ) from standards was better than ± 0.1‰ for both $\delta^{13}C$ and $\delta^{18}O$. Samples were calibrated to VPDB (Value of the Pee-Dee Belemnite) using the Cararra marble standard. Potential memory effect resulting from the common acid-bath system was minimized by increasing the reaction time to ten minutes for dolostone samples. Memory effect is estimated at <0.1‰ based on

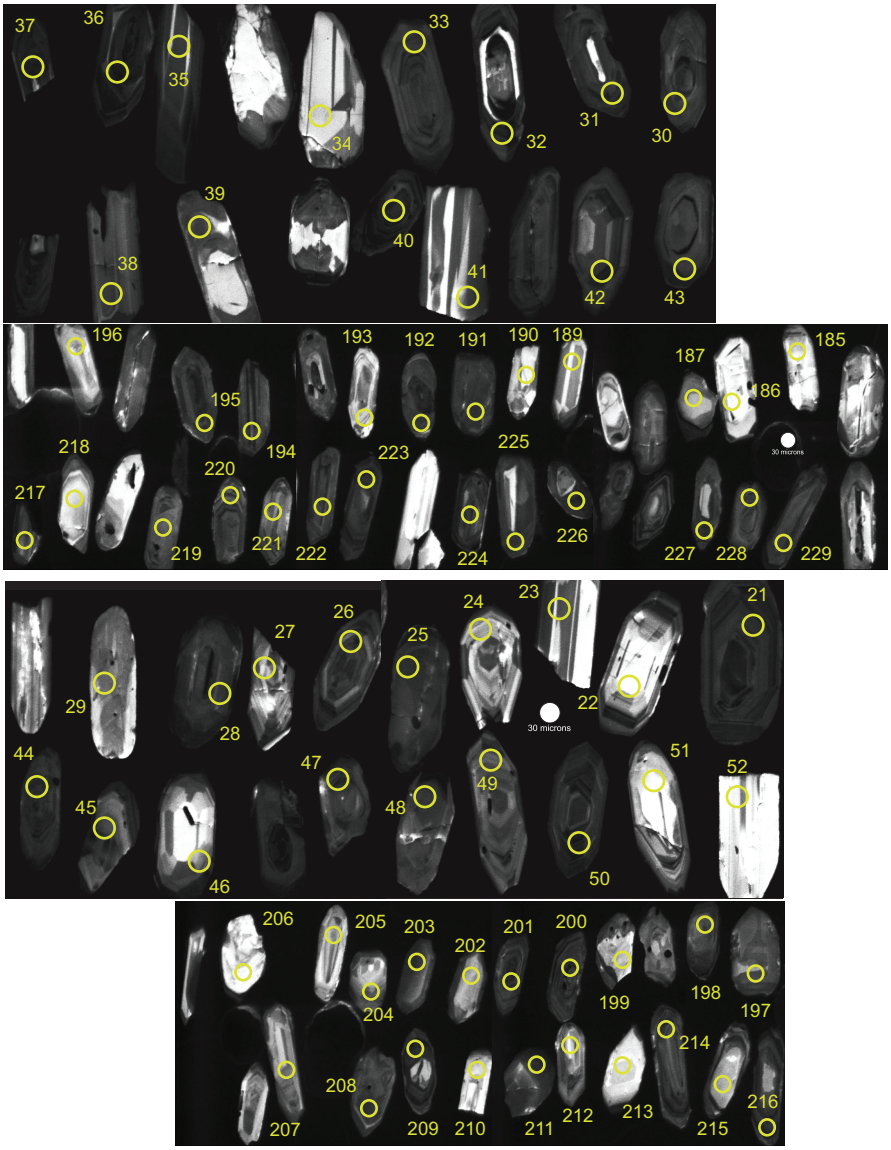

Fig. A5. Cathodoluminescence images of zircon grains dated by U-Pb LA-ICPMS from sample F1206-146.1.

variability of standards run after dolostone samples. Carbon ($\delta^{13}C$) and oxygen ($\delta^{18}O$) isotopic results are reported in permil notation of $^{13}C/^{12}C$ and $^{18}O/^{16}O$, respectively, relative to the standard VPDB.

Strontium Isotope Methods

Strontium isotopic analyses were performed on the same aliquots of powders used for carbon and oxygen isotopic analyses. Here we report $^{87}Sr/^{86}Sr$ measurements of 14 samples of the Ol Fm, 11 samples of Sh1 of the Shuurgat Fm, 16 samples of the basal Sh3a and 15 samples of the Sh3b of the Shuurgat Fm analyzed using a ThermoScientific Neptune multicollector inductively-coupled-plasma mass spectrometer (MC-ICP-MS) at Woods Hole Oceanographic Institute (WHOI) (table A4, http://earth.geology.yale.edu/~ajs/SupplementaryData/2016/Bold). Forty-four samples of the Taishir Fm were analyzed using an

Isotopix 396 IsoProbe T™ in the MIT Radiogenic Isotope Laboratory. In order to test the fidelity of the $^{87}Sr/^{86}Sr$ measurements by ICP-MS, three, Sr-rich (>500 ppm) lime-micrite horizons (F949 – 148, 164, and 184) of the T1 cap carbonate of the Taishir Fm were analyzed with a minimum of 5 duplicates each. On average, these "standards" yielded values of 0.70726, 0.70732, and 0.70741, respectively, displaying variation only in the 4th and 5th decimal place compared to data obtained using TIMS [0.70722, 0.707273, and 0.70739, respectively; table A4 (http://earth.geology.yale.edu/~ajs/SupplementaryData/2016/Bold)].

MC-ICP-MS Sr analyses: For all analyses, 50 ± 2 mg of powder was dissolved in 15 ml Falcon tubes with an initial washing step using 2 ml of a 1:1 methanol water solution (all steps had 3 cycles interspersed with ~15 min sonication). The second step involved adding 1 ml 0.2 N ammonium acetate and the final washing is with deionized water prior to final digestion using 5 ml of 0.5 N acetic acid. Duplicates were created for a subset of samples and 3 ml of the 5 ml acetic acid solution was transferred to a clean tube for major and minor element concentrations, and 1 ml to another clean tube for Sr column chemistry.

Strontium column chemistry was performed on 1 ml of sample to isolate Sr from coexisting matrix elements. The samples, previously dissolved in acetic acid, were dried and redissolved in 3N HNO_3. This step was repeated three times to ensure that all the acetic acid was evaporated. The solution was then loaded onto a preconditioned Sr Spec column. After three consecutive loadings of 0.25 ml 3N HNO_3, to ensure that other elements had been removed, Sr was eluted by 1 reservoir loading (~1 ml) of ultrapure water. $^{87}Sr/^{86}Sr$ values were generated using ThermoScientific Neptune MC-ICP-MS. The measurements were performed with typical ^{88}Sr beam intensities from 30 to 50 volts. $^{87}Sr/^{86}Sr$ ratios were corrected for Kr and Rb, and normalized using the exponential law. The standard NBS 987 was analyzed frequently between samples to monitor the consistency of the measured values and on average, yielded a value of 0.7102719 compared to data reported using TIMS (Smalley and others, 1994).

TIMS Sr analyses: For all analyses, 15 mg of sample powder was used. Initial washing step was 1:1 methanol rinse to remove suspended clays, which is followed by leaching and dissolution steps. Samples were leached three times in 0.2N ammonium acetate and then rinsed three times with MQH_2O. Calcite fraction of each sample was dissolved in 0.5N acetic acid, separated from the insoluble fraction in 3N HNO_3. Sr was separated from the matrix following standard Sr chromatography procedures and measured on an Isotopix IsoProbe T™ in dynamic mode, with target intensity of 3V ^{88}Sr. All data were corrected to $^{86}Sr/^{88}Sr = 0.1194$ for internal mass bias. Each analysis represents a minimum of 60 ratio measurements, with internal precision of better than 0.001% (1-σ). Analyses were referenced against NBS SRM 987 (0.71025), with a long-term average of 0.71024 and 2-σ external precision of 0.000014; no bias correction was made.

REFERENCES

Abbot, D. S., Voigt, A., and Koll, D., 2011, The Jormungand global climate state and implications for Neoproterozoic glaciations: Journal of Geophysical Research-Atmospheres, v. 116, n. D18103, http://dx.doi.org/10.1029/2011JD015927

Aharon, P., 1988, Oxygen, carbon and U-series isotopes of aragonites from Vestfold Hills, Antarctica: Clues to geochemical processes in subglacial environments: Geochimica et Cosmochimica Acta, v. 52, n. 9, p. 2231–2331, http://dx.doi.org/10.1016/0016-7037(88)90134-2

Ahr, W. M., 1973, The carbonate ramp: An alternative to the shelf model: Gulf Coast Association of Geological Societies Transactions, v. 23, p. 221–225.

Aitken, J. D., 1991, The Ice Brook Formation and Post-Rapitan, Late Proterozoic glaciation, Mackenzie Mountains, Northwest Territories: Geological Survey of Canada Bulletin, v. 404, p. 1–43, http://dx.doi.org/10.4095/132664

Allen, P. A., and Etienne, J. L., 2008, Sedimentary challenge to Snowball Earth: Nature Geoscience, v. 1, p. 817–926, http://dx.doi.org/10.1038/ngeo355

An, Z., Jiang, G., Tong, J., Tian, L., Ye, Q., Song, H., and Song, H., 2015, Stratigraphic position of the Ediacaran Miaohe biota and its constrains on the age of the upper Doushantuo $\delta^{13}C$ anomaly in the Yangtze Gorges area, South China: Precambrian Research, v. 271, p. 243–253, http://dx.doi.org/10.1016/j.precamres.2015.10.007

Badarch, G., Byamba, J., Mahbadar, Ts., Minjin, Ch., Orolmaa, D., Tomurtogoo, O., and Khosbayar, Ts, 1998, Geological map of Mongolia: Ulaanbaatar, Mongolia, Mongolian Academy of Sciences, Mineral Resources Authority of Mongolia.

Badarch, G., Cunningham, W. D., and Windley, B., 2002, A new terrane subdivision for Mongolia: implications for the Phanerozoic crustal growth of Central Asia: Journal of Asian Earth Sciences, v. 21, p. 87–110, http://dx.doi.org/10.1016/S1367-9120(02)00017-2

Banner, J. L., 2004, Radiogenic isotopes: systematics and applications to earth surface processes and chemical stratigraphy: Earth-Science Reviews, v. 65, n. 3–4, p. 141–194, http://dx.doi.org/10.1016/S0012-8252(03)00086-2

Benn, D. I., Le Hir, G., Bao, H., Donnadieu, Y., Dumas, C., Fleming, E. J., Hambrey, M. J., McMillan, E. A., Petronis, M. S., Ramstein, G., Stevenson, C. T. E., Wynn, P. M., and Fairchild, I. J., 2015, Orbitally forced ice sheet fluctuations during the Marinoan Snowball Earth glaciation: Nature Geoscience, v. 8, p. 704–707, http://dx.doi.org/10.1038/ngeo2502

Bezzubetsev, V. V., 1963, On the Precambrian-Cambrian stratigraphy of the Dzabkhan River Basin: Gostoptekhizdat, Materials on the Geology of MPR, v. 1963, p. 29–42.
Black, L. P., Kamo, S. L., Allen, C. M., Aleinikoff, J. N., Davis, D. W., Korsch, R. J., and Foudoulis, C., 2003, TEMORA 1: a new zircon standard for Phanerozoic U–Pb geochronology: Chemical Geology, v. 200, n. 1–2, p. 155–170, http://dx.doi.org/10.1016/S0009-2541(03)00165-7
Bold, U., Macdonald, F. A., Smith, E. F., Crowly, J. C., Minjin, C., and Dorjnamjaa, D., 2013, Elevating the Neoproterozoic Tsagaan-Olom Formation to a Group: Mongolian Geoscientist, v. 39, n. 5, p. 89–94.
Bosak, T., Lahr, D. J. G., Pruss, S. B., Macdonald, F. A., Dalton, L., and Matys, E., 2011a, Agglutinated tests in post-Sturtian cap carbonates of Namibia and Mongolia: Earth and Planetary Science Letters, v. 308, n. 1–2, p. 29–40, http://dx.doi.org/10.1016/j.epsl.2011.05.030
Bosak, T., Macdonald, F., Lahr, D., and Matys, E., 2011b, Putative Cryogenian ciliates from Mongolia: Geology, v. 39, n. 12, p. 1123–1126, http://dx.doi.org/10.1130/G32384.1
Bosak, T., Lahr, D. J. G., Pruss, S. B., Macdonald, F. A., Gooday, A. J., Dalton, L., and Matys, E. D., 2012, Possible early foraminiferans in post-Sturtian (716–635 Ma) cap carbonates: Geology, v. 40, p. 67–70, http://dx.doi.org/10.1130/G32535.1
Boulton, G. S., 1978, Boulder shapes and grain-size distributions of debris as indicators of transport paths through a glacier and till genesis: Sedimentology, v. 25, n. 6, p. 773–799, http://dx.doi.org/10.1111/j.1365-3091.1978.tb00329.x
Boulton, G. S., Dobbie, K. E., and Zatsepin, S., 2001, Sediment deformation beneath glaciers and its coupling to the sublacial hydraulic system: Quaternary International, v. 86, n. 1, p. 3–28, http://dx.doi.org/10.1016/S1040-6182(01)00048-9
Bowring, S. A., Grotzinger, J. P., Condon, D. J., Ramezani, J., Newall, M., and Allen, P. A., 2007, Geochronologic constraints on the chronostratigraphic framework of the Neoproterozoic Huqf Supergroup, Sultanate of Oman: American Journal of Science, v. 307, n. 10, p. 1097–1145, http://dx.doi.org/10.2475/10.2007.01
Bowring, J. F., McLean, N. M., and Bowring, S. A., 2011, Engineering cyber infrastructure for U-Pb geochronology: Tripoli and U-Pb_Redux: Geochemistry, Geophysics, Geosystems, v. 12, http://dx.doi.org/10.1029/2010GC003479
Brasier, M. D., Magaritz, M., Corfield, R., Luo, H., Wu, X., Lin, O., Jiang, Z., Hamdi, B., He, T., and Fraser, A. G., 1990, The carbon- and oxygen-isotope record of the Precambrian-Cambrian boundary interval in China and Iran and their correlation: Geological Magazine, v. 127, n. 4, p. 319–332, http://dx.doi.org/10.1017/S0016756800014886
Brasier, M. D., Dorjnamjaa, D., and Lindsay, J. F., 1996a, The Neoproterozoic to early Cambrian in southwest Mongolia: an introduction: Geological Magazine, v. 133, n. 4, p. 365–369, http://dx.doi.org/10.1017/S0016756800007548
Brasier, M. D., Shields, G., Kuleshov, V. N., and Zhegallo, E. A., 1996b, Integrated chemo- and biostratigraphic calibration of early animal evolution: Neoproterozoic -early Cambrian of southwest Mongolia: Geological Magazine, v. 133, n. 4, p. 445–485, http://dx.doi.org/10.1017/S0016756800007603
Bucholz, C. E., Jagoutz, O., Schmidt, M. W., and Sambuu, O., 2014, Phlogopite-and clinopyroxene-dominated fractional crystallization of an alkaline primitive melt: petrology and mineral chemistry of the Dariv Igneous Complex, Western Mongolia: Contributions to Mineralogy and Petrology, v. 167, article 994, p. 1–28, http://dx.doi.org/10.1007/s00410-014-0994-6
Burashnikov, V. V., 1990, Tectonics of the Urgamal zone, Early Calidonides of western Mongolia: Moscow, Russian Academy of Sciences, 25 p.
Burchette, T. P., and Wright, V. P., 1992, Carbonate ramp depositional systems: Sedimentary Geology, v. 79, n. 1–4, p. 3–57, http://dx.doi.org/10.1016/0037-0738(92)90003-A
Calver, C. R., 2000, Isotope stratigraphy of the Ediacaran (Neoproterozoic III) of the Adelaide Rift Complex, Australia, and the overprint of water column stratification: Precambrian Research, v. 100, n. 1–3, p. 121–150, http://dx.doi.org/10.1016/S0301-9268(99)00072-8
Calver, C. R., Black, L. P., Everard, J. L., and Seymour, D. B., 2004, U-Pb zircon age constraints on late Neoproterozoic glaciation in Tasmania: Geology, v. 32, n. 10, p. 893–896, http://dx.doi.org/10.1130/G20713.1
Calver, C., Crowley, J. L., Wingate, M. T. D., Evans, D. A. D., Raub, T. D., and Schmitz, M. D., 2013, Globally synchronous Marinoan deglaciation indicated by U-Pb geochronology of the Cottons Breccia, Tasmania, Australia: Geology, v. 41, n. 10, p. 1127–1130, http://dx.doi.org/10.1130/G34568.1
Cohen, P. A., Macdonald, F. A., Pruss, S., Matys, E., and Bosak, T., 2015, Fossils of putative marine algae from the Cryogenian glacial interlude of Mongolia: Palaios, v. 30, n. 3, p. 238–247, http://dx.doi.org/10.2110/palo.2014.069
Condon, D. J., and Bowring, S. A., 2011, A user's guide to Neoproterozoic geochronology, *in* Arnaud, E., Halverson, G. P., and Shields-Zhou, G., editors, The Geological Record of Neoproterozoic Glaciations: Geological Society, London, Memoirs, v. 36, p. 135–149, http://dx.doi.org/10.1144/M36.9
Condon, D. J., Zhu, M., Bowring, S., Wang, W., Yang, A., and Jin, Y., 2005, U-Pb ages from the Neoproterozoic Doushanto Formation, China: Science, v. 308, n. 5718, p. 95–98, http://dx.doi.org/10.1126/science.1107765
Creveling, J. R., Mitrovica, J. X., Chan, N.-H., Latychev, K., and Matsuyama, I., 2012, Mechanisms for oscillatory true polar wander: Nature, v. 491, p. 244–248, http://dx.doi.org/10.1038/nature11571
Cui, H., Kaufman, A. J., Xiao, S., Zhu, M., Zhou, C., and Liu, X.-M., 2015, Redox architecture of an Ediacaran ocean margin: Integrated chemostratigraphic ($\delta^{13}C$–$\delta^{34}S$–$^{87}Sr/^{86}Sr$–Ce/Ce*) correlation of the Doushantuo Formation, South China: Chemical Geology, v. 405, p. 48–62, http://dx.doi.org/10.1016/j.chemgeo.2015.04.009
Davis, P. T., Briner, J. P., Coulthard, R. D., Finkel, R. W., and Miller, G. H., 2006, Preservation of Arctic

landscapes overridden by cold-based ice sheets: Quaternary Research, v. 65, n. 1, p. 156–163, http://dx.doi.org/10.1016/j.yqres.2005.08.019
Degens, E. T., and Epstein, S., 1964, Oxygen and carbon isotope ratios in coexisting calcites and dolomites from recent and ancient sediments: Geochimica et Cosmochimica Acta, v. 28, n. 1, p. 23–44, http://dx.doi.org/10.1016/0016-7037(64)90053-5
DePaulo, D. J., and Ingram, B. L., 1985, High-Resolution Stratigraphy with Strontium Isotopes: Science, v. 227, n. 4689, p. 938–941, http://dx.doi.org/10.1126/science.227.4689.938
Derry, L. A., 2010, A burial diagenesis origin for the Ediacaran Shuram-Wonoka carbon isotope anomaly: Earth and Planetary Science Letters, v. 294, n. 1–2, p. 152–162, http://dx.doi.org/10.1016/j.epsl.2010.03.022
Deynoux, M., 1985, Terrestrial or waterlain glacial diamictites? Three case studies from the Late Precambrian and Late Ordovician glacial drifts in West Africa: Palaeogeography, Palaeoclimatology, Palaeoecology, v. 51, n. 1–4, p. 97–141, http://dx.doi.org/10.1016/0031-0182(85)90082-3
Domack, E., O'Brien, P., Harris, P., Taylor, F., Quilty, P. G., Santis, L. D., and Raker, B., 1998, Late Quaternary sediment facies in Prydz Bay, East Antarctica and their relationship to glacial advance onto the continental shelf: Antarctic Science, v. 10, p. 236–246, http://dx.doi.org/10.1017/S0954102098000339
Domack, E. W., and Hoffman, P. F., 2011, An ice grounding-line wedge from the Ghaub glaciation (635 Ma) on the distal foreslope of the Otavi carbonate platform, Namibia, and its bearing on the snowball Earth hypothesis: Geological Society of America Bulletin, v. 123, n. 7–8, p. 1448–1477, http://dx.doi.org/10.1130/B30217.1
Domack, E. W., Jacobson, E. A., Shipp, S., and Anderson, J. B., 1999, Late Pleistocene–Holocene retreat of the West Antarctic Ice-Sheet system in the Ross Sea: Part 2–Sedimentologic and stratigraphic signature: Geological Society of America Bulletin, v. 111, n. 10, p. 1517–1536, http://dx.doi.org/10.1130/0016-7606(1999)111<1517:LPHROT>2.3.CO;2
Dorjnamjaa, D., and Enkhbaatar, B., 2011, Classification of flora of the Precambrian and Cambrian periods and their stratigraphic importance, Mongolian Geology and Mineral Resources: Ulaanbaatar, Mongolia, Soyombo Printing, p. 12–26.
Dunham, J. B., and Olson, E. R., 1980, Shallow Subsurface Dolomitization of Subtidally Deposited Carbonate Sediments in the Hanson Creek Formation (Ordovician—Silurian) of Central Nevada, *in* Zenger, D. H., Dunham, J. B., and Ethington, R. L., editors, Concepts and Models of Dolomitization: SEPM Special Publication, v. 28, p. 139–161, http://dx.doi.org/10.2110/pec.80.28.0139
Edel, J. B., Schulmann, K., Hanžl, P., and Lexa, O., 2014, Palaeomagnetic and structural constraints on 90° anticlockwise rotation in SW Mongolia during the Permo–Triassic: Implications for Altaid oroclinal bending. Preliminary palaeomagnetic results: Journal of Asian Earth Sciences, v. 94, p. 157–171, http://dx.doi.org/10.1016/j.jseaes.2014.07.039
Erwin, D. H., Laflamme, M., Tweedt, S. M., Sperling, E. A., Pisani, D., and Peterson, K. J., 2011, The Cambrian Conundrum: Early Divergence and Later Ecological Success in the Early History of Animals: Science, v. 334, n. 6059, p. 1091–1097, http://dx.doi.org/10.1126/science.1206375
Fairchild, I. J., and Spiro, B., 1990, Carbonate minerals in glacial sediments: geochemical clues to palaeoenvironment: Geological Society, London, Special Publications, v. 53, p. 201–216, http://dx.doi.org/10.1144/GSL.SP.1990.053.01.11
Fanning, C. M., and Link, P. K., 2008, Age constraints for the Sturtian glaciation: data from the Adelaide Geosyncline, South Australia and Pocatello Formation Idaho, USA: Melbourne, Australia, Geological Society of Australia Abstracts, No. 91, Selwyn Symposium 2008, p. 57–62.
Fike, D. A., Grotzinger, J. P., Pratt, L. M., and Summons, R. E., 2006, Oxidation of the Ediacaran Ocean: Nature, v. 444, p. 744–747, http://dx.doi.org/10.1038/nature05345
Gensel, P. G., 2008, The earliest land plants: Annual Review of Ecology, Evolution and Systematics, v. 39, p. 459–477, http://dx.doi.org/10.1146/annurev.ecolsys.39.110707.173526
Gibson, T. M., Myrow, P. M., Macdonald, F. A., Minjin, C., and Gehrels, G. F., 2013, Depositional history, tectonics, and detrital zircon geochronology of Ordovician and Devonian strata in southwestern Mongolia: Geological Society of America Bulletin, v. 125, n. 5–6, p. 877–893, http://dx.doi.org/10.1130/B30746.1
Goldring, R., and Jensen, S., 1996, Trace fossils and biofabrics at the Precambrian-Cambrian boundary interval in western Mongolia: Geological Magazine, v. 133, n. 4, p. 403–415, http://dx.doi.org/10.1017/S0016756800007573
Gostin, V. A., McKirdy, D. M., Webster, L. J., and Williams, G. E., 2010, Ediacaran ice-rafting and coeval asteroid impact, South Australia: insights into the terminal Proterozoic environment: Australian Journal of Earth Sciences, v. 57, n. 7, p. 859–869, http://dx.doi.org/10.1080/08120099.2010.509408
Grotzinger, J. P., Fike, D. A., and Fischer, W. W., 2011, Enigmatic origin of the largest-known carbon isotope excursion in Earth's history: Nature Geoscience, v. 4, p. 285–292, http://dx.doi.org/10.1038/ngeo1138
Halverson, G. P., Hoffman, P. F., Schrag, D. P., and Kaufman, A. J., 2002, A major perturbation of the carbon cycle before the Ghaub glaciation (Neoproterozoic) in Namibia: Prelude to snowball Earth?: Geochemistry, Geophysics, Geosystems, v. 3, n. 6, p. 1–24, http://dx.doi.org/10.1029/2001GC000244
Halverson, G. P., Hoffman, P. F., Schrag, D. P., Maloof, A. C., and Rice, A. H. N., 2005, Toward a Neoproterozoic composite carbon-isotope record: Geological Society of America Bulletin, v. 117, n. 9–10, p. 1181–1207, http://dx.doi.org/10.1130/B25630.1
Halverson, G. P., Dudás, F. Ö., Maloof, A. C., and Bowring, S. A., 2007, Evolution of the $^{87}Sr/^{86}Sr$ composition of Neoproterozoic Seawater: Palaeogeography, Palaeoclimatology, Palaeoecology, v. 256, n. 2–3, p. 103–129, http://dx.doi.org/10.1016/j.palaeo.2007.02.028

Halverson, G. P., Wade, B. P., Hurtgen, M. T., and Barovich, K. M., 2010, Neoproterozoic Chemostratigraphy: Precambrian Research, v. 182, n. 4, p. 337–350, http://dx.doi.org/10.1016/j.precamres.2010.04.007

Higgins, J. A., and Schrag, D. P., 2006, Beyond methane: Towards a theory for the Paleocene–Eocene thermal maximum: Earth and Planetary Science Letters, v. 245, n. 3–4, p. 523–537, http://dx.doi.org/10.1016/j.epsl.2006.03.009

Higgins, J. A., Fischer, W. W., and Schrag, D. P., 2009, Oxygenation of the ocean and sediments: Consequences for the seafloor carbonate factory: Earth and Planetary Science Letters, v. 284, n. 1–2, p. 25–33, http://dx.doi.org/10.1016/j.epsl.2009.03.039

Hoffman, P. F., 1991, Did the breakout of Laurentia turn Gondwanaland inside-out?: Science, v. 252, n. 5011, p. 1409–1412, http://dx.doi.org10.1126/science.252.5011.1409

——— 2011, Strange bedfellows: glacial diamictite and cap carbonate from the Marinoan (635 Ma) glaciation in Namibia: Sedimentology, v. 58, n. 1, p. 57–119, http://dx.doi.org/10.1111/j.1365-3091.2010.01206.x

Hoffman, P. F., and Halverson, G. P., 2008, Otavi Group of the western Northern Platform, the Eastern Kaoko Zone and the western Northern Margin Zone, *in* Miller, R. M., editor, The Geology of Namibia, v. 2. Handbook of the Geological Survey of Namibia: Windhoek, p. 13.69–13.136.

Hoffman, P. F., and Li, Z.-X., 2009, A palaeogeographic context for Neoproterozoic glaciations: Palaeogeography, Palaeoclimatology, Palaeoecology, v. 277, n. 3–4, p. 158–172, http://dx.doi.org/10.1016/j.palaeo.2009.03.013

Hoffman, P. F., and Schrag, D. P., 2002, The snowball Earth hypothesis; testing the limits of global change: Terra Nova, v. 14, n. 3, p. 129–155, http://dx.doi.org/10.1046/j.1365-3121.2002.00408.x

Hoffman, P. F., Kaufman, A. J., Halverson, G. P., and Schrag, D. P., 1998, A Neoproterozoic Snowball Earth: Science, v. 281, n. 5381, p. 1342–1346, http://dx.doi.org/10.1126/science.281.5381.1342

Hoffman, P. F., Halverson, G. P., Domack, E. W., Husson, J. M., Higgins, J. A., and Schrag, D. P., 2007, Are basal Ediacaran (635 Ma) post-glacial "cap dolostones" diachronous?: Earth and Planetary Science Letters, v. 258, n. 1–2, p. 114–131, http://dx.doi.org/10.1016/j.epsl.2007.03.032

Hoffman, P. F., Macdonald, F. A., and Halverson, G. P., 2011, Chemical sediments associated with Neoproterozoic glaciation: iron formation, cap carbonate, barite and phosphorite, *in* Arnaud, E., Halverson, G. P., and Shields, G., editors, The Geologic Record of Neoproterozoic Glaciations: Geological Society, London, Memoirs, v. 36, p. 67–80, http://dx.doi.org/10.1144/m36.5

Hoffmann, K. H., Condon, D. J., Bowring, S. A., and Crowley, J. L., 2004, U-Pb zircon date from the Neoproterozoic Ghaub Formation, Namibia: Constraints on Marinoan glaciation: Geology, v. 32, n. 9, p. 817–820, http://dx.doi.org/10.1130/G20519.1

Ilyin, A. V., 1990, Proterozoic supercontinent, its latest Precambrian rifting, breakup, dispersal into smaller continents, and subsidence of their margins: Evidence from Asia: Geology, v. 18, n. 12, p. 1231–1234, http://dx.doi.org/10.1130/0091-7613(1990)018<1231:psilpr>2.3.co;2

Jaffey, A. H., Flynn, K. F., Glendenin, L. E., Bentley, W. C., and Essling, A., 1971, Precision measurement of half-lives and specific activities of ^{235}U and ^{238}U: Physical Review C, v. 4, n. 5, p. 1889, http://dx.doi.org/10.1103/PhysRevC.4.1889

Jahn, B. M., Litvinovsky, B. A., Zanvilevich, A. N., and Reichow, M., 2009, Peralkaline granitoid magmatism in the Mongolian-Transbaikalian Belt: Evolution, petrogenesis and tectonic significance: Lithos, v. 113, n. 3–4, p. 521–539, http://dx.doi.org/10.1016/j.lithos.2009.06.015

Jian, P., Kröner, A., Jahn, B.-m., Windley, B. F., Shi, Y., Zhang, W., Zhang, F., Miao, L., Tomurhuu, D., and Liu, D., 2014, Zircon dating of Neoproterozoic and Cambrian ophiolites in West Mongolia and implications for the timing of orogenic processes in the central part of the Central Asian Orogenic Belt: Earth-Science Reviews, v. 133, p. 62–93, http://dx.doi.org/10.1016/j.earscirev.2014.02.006

Johnston, D. T., Macdonald, F. A., Gill, B. C., Hoffman, P. F., and Schrag, D. P., 2012, Uncovering the Neoproterozoic carbon cycle: Nature, v. 483, p. 320–324, http://dx.doi.org/10.1038/nature10854

Jones, C. E., and Jenkyns, H. C., 2001, Seawater strontium isotopes, oceanic anoxic events, and seafloor hydrothermal activity in the Jurassic and Cretaceous: American Journal of Science, v. 301, n. 2, p. 112–149, http://dx.doi.org/10.2475/ajs.301.2.112

Kaufman, A. J., Jacobsen, S. B., and Knoll, A. H., 1993, The Vendian record of Sr and C isotopic variations in seawater: implications for tectonics and paleoclimate: Earth and Planetary Science Letters, v. 120, n. 3–4, p. 409–430, http://dx.doi.org/10.1016/0012-821X(93)90254-7

Kaufman, A. J., Knoll, A. H., and Narbonne, G. M., 1997, Isotopes, ice ages, and terminal Proterozoic Earth history: Proceedings of the National Academy of Sciences of the United States of America, v. 95, n. 13, p. 6600–6605, http://dx.doi.org/10.1073/pnas.94.13.6600

Keeley, J. A., Link, P. K., Fanning, C. M., and Schmitz, M. D., 2013, Pre- to synglacial rift-related volcanism in the Neoproterozoic (Cryogenian) Pocatello Formation, SE Idaho: New SHRIMP and CA-ID-TIMS constraints: Lithosphere, v. 5, n. 1, p. 128–150, http://dx.doi.org/10.1130/L226.1

Kennedy, M., Mrofka, D., and von der Borch, C., 2008, Snowball Earth termination by destabilization of equatorial permafrost methane clathrate: Nature, v. 453, p. 642–645, http://dx.doi.org/10.1038/nature06961

Khomentovsky, V. V., and Gibsher, A. S., 1996, The Neoproterozoic-Lower Cambrian in northern Govi-Altai, western Mongolia: Regional setting, lithostratigraphy and biostratigraphy: Geological Magazine, v. 133, n. 4, p. 371–390, http://dx.doi.org/10.1017/S001675680000755X

Kirschvink, J. L., 1992, Late Proterozoic low-latitude global glaciation: The Snowball Earth, *in* Schopf, J. W., and Klein, C., editors, The Proterozoic Biosphere: Cambridge, Cambridge University Press, p. 51–52.

Knauth, P. L., and Kennedy, M. J., 2009, The late Precambrian greening of the Earth: Nature, v. 460, p. 728–732, http://dx.doi.org/10.1038/nature08213

Knoll, A. H., Hayes, J. M., Kaufman, A. J., Swett, K., and Lambert, I. B., 1986, Secular variation in carbon isotope ratios from Upper Proterozoic successions of Svalbard and East Greenland: Nature, v. 321, p. 832–838, http://dx.doi.org/10.1038/321832a0

Knoll, A. H., Javaux, E. J., Hewitt, D., and Cohen, P. A., 2006, Eukaryotic organisms in Proterozoic oceans: Philosophical Transactions of the Royal Society of London B: Biological Sciences, v. 361, n. 1470, p. 1023–1038, http://dx.doi.org/10.1098/rstb.2006.1843

Kozakov, I. K., Yarmolyuk, V. V., Kovach, V. P., Bibikova, E. V., Kirnozova, T. I., Kozlovskii, A. M., Plotkina, Y. V., Fugzan, M. M., Lebedev, V. I., and Erdenezhargal, C., 2012, The early Baikalian crystalline complex in the basement of the Dzabkhan Microcontinent of the Early Caledonian orogenic area, Central Asia: Stratigraphy and Geological Correlation, v. 20, n. 3, p. 231–239, http://dx.doi.org/10.1134/S0869593812030057

Kröner, A., Lehmann, J., Schulmann, K., Demoux, A., Lexa, O., Tomurhuu, D., Štípská, P., Liu, D., and Wingate, M. T., 2010, Lithostratigraphic and geochronological constraints on the evolution of the Central Asian Orogenic Belt in SW Mongolia: Early Paleozoic rifting followed by late Paleozoic accretion: American Journal of Science, v. 310, n. 7, p. 523–574, http://dx.doi.org/10.2475/07.2010.01

Kuzmichev, A. B., and Larionov, A. N., 2011, The Sarkhoi Group in East Sayan: Neoproterozoic (~ 770–800 Ma) volcanic belt of the Andean type: Russian Geology and Geophysics, v. 52, n. 7, p. 685–700, http://dx.doi.org/10.1016/j.rgg.2011.06.001

Kuzmichev, A. B., Bibikova, E. V., and Zhuravlev, D. Z., 2001, Neoproterozoic (~800 Ma) orogeny in the Tuva-Mongolia Massif (Siberia): island arc-continent collision at the northeast Rodinia margin: Precambrian Research, v. 110, n. 1–4, p. 109–126, http://dx.doi.org/10.1016/S0301-9268(01)00183-8

Lan, Z., Li, X., Zhu, M., Chen, Z., Zhang, Q., Li, Q., Lu, D., Liu, Y., and Tang, G., 2014, A rapid and synchronous initiation of the wide spread Cryogenian glaciations: Precambrian Research, v. 255, Part 1, p. 401–411, http://dx.doi.org/10.1016/j.precamres.2014.10.015

Le Heron, D. P., 2012, The Cryogenian record of glaciation and deglaciation in South Australia: Sedimentary Geology, v. 243–244, p. 57–69, http://dx.doi.org/10.1016/j.sedgeo.2011.09.013

Le Heron, D. P., and Busfield, M. E., 2015, Pulsed iceberg delivery driven by Sturtian ice sheet dynamics: An example from Death Valley, California: Sedimentology, http://dx.doi.org/10.1111/sed.12225

Le Heron, D. P., Cox, G. M., Trundley, A. E., and Collins, A. S., 2011, Sea ice-free conditions during the early Sturtian glaciation (early Cryogenian) glaciation, South Australia: Geology, v. 39, n. 1, p. 31–34, http://dx.doi.org/10.1130/G31547.1

Le Heron, D. P., Busfield, M. E., and Kamona, F., 2013, An interglacial on snowball Earth? Dynamic ice behaviour revealed in the Chuos Formation, Namibia: Sedimentology, v. 60, n. 2, p. 411–427, http://dx.doi.org/10.1111/j.1365-3091.2012.01346.x

Le Heron, D. P., Busfield, M. E., and Prave, A. R., 2014, Neoproterozoic ice sheets and olistoliths: multiple glacial cycles in the Kingston Peak Formation, California: Journal of the Geological Society, v. 171, n. 4, p. 528–538, http://dx.doi.org/10.1144/jgs2013-130

Lehmann, J., Schulmann, K., Lexa, O., Corsini, M., Kröner, A., Štípská, P., Tomurhuu, D., and Otgonbator, D., 2010, Structural constraints on the evolution of the Central Asian Orogenic Belt in SW Mongolia: American Journal of Science, v. 310, n. 7, p. 575–628, http://dx.doi.org/10.2475/07.2010.02

Levashova, N. M., Kalugin, V. M., Gibsher, A. S., Yff, J., Ryabinin, A. B., Meert, J. G., and Malone, S. J., 2010, The origin of the Baydaric microcontinent, Mongolia: Constraints from paleomagnetism and geochronology: Tectonophysics, v. 485, n. 1–4, p. 306–320, http://dx.doi.org/10.1016/j.tecto.2010.01.012

Li, Z. X., Bogdanova, S. V., Collins, A. S., Davidson, A., De Waele, B., Ernst, R. E., Fitzsimons, I. C. W., Fuck, R. A., Gladkochub, D. P., Jacobs, J., Karlstrom, K. E., Lu, S., Natapov, L. M., Pease, V., Pisarevsky, S. A., Thrane, K., and Vernikovsky, V., 2008, Assembly, configuration, and break-up history of Rodinia: A synthesis: Precambrian Research, v. 160, n. 1–2, p. 179–210, http://dx.doi.org/10.1016/j.precamres.2007.04.021

Lindsay, J. F., 1989, Depositional controls on glacial facies associations in a basinal setting, Late Proterozoic, Amadeus Basin, central Australia: Palaeogeography, Palaeoclimatology, Palaeoecology, v. 73, n. 3–4, p. 205–232, http://dx.doi.org/10.1016/0031-0182(89)90005-9

Lindsay, J. F., Brasier, M. D., Shields, G., Khomentovsky, V. V., and Bat-Ireedui, Y. A., 1996, Glacial facies associations in a Neoproterozoic back-arc setting, Zavkhan Basin, western Mongolia: Geological Magazine, v. 133, n. 4, p. 391–402, http://dx.doi.org/10.1017/S0016756800007561

Liu, C., Wang, Z., and Raub, T. D., 2013, Geochemical constraints on the origin of Marinoan cap dolostones from Nuccaleena Formation, South Australia: Chemical Geology, v. 351, p. 95–104, http://dx.doi.org/10.1016/j.chemgeo.2013.05.012

Liu, C., Wang, Z., Raub, T. D., Macdonald, F. A., and Evans, D. A. D., 2014, Neoproterozoic cap-dolostone deposition in stratified glacial meltwater plume: Earth and Planetary Science Letters, v. 404, p. 22–32, http://dx.doi.org/10.1016/j.epsl.2014.06.039

Macdonald, F. A., 2011, The Tsagaan Oloom Formation, southwestern Mongolia, *in* Arnaud, E., Halverson, G. P., and Shields-Zhou, G., editors, The geological record of Neoproterozoic glaciations: Geological Society, London, Memoirs, v. 36, p. 331–337, http://dx.doi.org/0.1144/M36.29

Macdonald, F. A., Jones, D. S., and Schrag, D. P., 2009a, Stratigraphic and tectonic implications of a newly discovered glacial diamictite-cap carbonate couplet in southwestern Mongolia: Geology, v. 37, n. 2, p. 123–126, http://dx.doi.org/10.1130/G24797A.1

Macdonald, F. A., McClelland, W. C., Schrag, D. P., and Macdonald, W. P., 2009b, Neoproterozoic glaciation on a carbonate platform margin in Arctic Alaska and the origin of the North Slope subterrane: Geological Society of America Bulletin, v. 121, n. 3–4, p. 448–473, http://dx.doi.org/10.1130/B26401.1

Macdonald, F. A., Schmitz, M. D., Crowley, J. L., Roots, C. F., Jones, D. S., Maloof, A. C., Strauss, J. V., Cohen, P. A., Johnston, D. T., and Schrag, D. P., 2010, Calibrating the Cryogenian: Science, v. 327, n. 5970, p. 1241–1243, http://dx.doi.org/10.1126/science.1183325

Macdonald, F. A., Strauss, J. V., Sperling, E. A., Halverson, G. P., Narbonne, G. M., Johnston, D. T., Kunzmann, M., Schrag, D. P., and Higgins, J. A., 2013, The stratigraphic relationship between the

Shuram carbon isotope excursion, the oxygenation of Neoproterozoic oceans, and the first appearance of the Ediacara biota and bilaterian trace fossils in northwestern Canada: Chemical Geology, v. 362, p. 250–272, http://dx.doi.org/10.1016/j.chemgeo.2013.05.032

Mattinson, J. M., 2005, Zircon U-Pb chemical abrasion ("CA-TIMS") method: Combined annealing and multi-step partial dissolution analysis for improved precision and accuracy of zircon ages: Chemical Geology, v. 220, n. 1–2, p. 47–66, http://dx.doi.org/10.1016/j.chemgeo.2005.03.011

McKirdy, D. M., Burgess, J. M., Lemon, N. M., Yu, X., Cooper, A. M., Gostin, V. A., Jenkins, R. J. F., and Both, R. A., 2001, A chemostratigraphic overview of the late Cryogenian interglacial sequence in the Adelaide fold-thrust belt, South Australia: Precambrian Research, v. 106, n. 1–2, p. 149–186, http://dx.doi.org/10.1016/S0301-9268(00)00130-3

McLean, N. M., Bowring, J. F., and Bowring, S. A., 2011, An algorithm for U-Pb isotope dilution data reduction and uncertainty propagation: Geochemistry, Geophysics, Geosystems, v. 12, http://dx.doi.org/10.1029/2010GC003478

Melezhik, V. A., Pokrovskii, B. G., Fallick, A. E., Kuznetsov, A. B., and Bujakaite, M. I., 2009, Constraints on $^{87}Sr/^{86}Sr$ of Late Ediacaran seawater: insight from Siberian high-Sr limestones: Journal of the Geological Society, London, v. 166, n. 1, p. 183–191, http://dx.doi.org/10.1144/0016-76492007-171

Melim, L. A., Swart, P. K., and Maliva, R. G., 2001, Meteoric and marine burial diagenesis in the subsurface of Great Bahama Bank, *in* Ginsberg, R. N., editor, Subsurface Geology of a Prograding Carbonate Platform Margin, Great Bahama Bank: Results of the Bahamas Drilling Project: SEPM Special Publication, v. 70, p. 137–161, http://dx.doi.org/10.2110/pec.01.70.0137

Misi, A., and Veizer, J., 1998, Neoproterozoic carbonate sequences of the Una Group, Irecê Basin, Brazil: chemostratigraphy, age and correlations: Precambrian Research, v. 89, n. 1–2, p. 87–100, http://dx.doi.org/10.1016/S0301-9268(97)00073-9

Narbonne, G. M., 1994, New Ediacaran fossils from the Mackenzie Mountains, Northwestern Canada: Journal of Paleontology, v. 68, n. 3, p. 411–416, http://www.jstor.org/stable/1306192

Narbonne, G. M., Kaufman, A. J., and Knoll, A. H., 1994, Integrated chemostratigraphy and biostratigraphy of the Windermere Supergroup, northwestern Canada: Implications for Neoproterozoic correlations and the early evolution of animals: Geological Society of America Bulletin, v. 106, n. 10, p. 1281–1291, http://dx.doi.org/10.1130/0016-7606(1994)106<1281:ICABOT>2.3.CO;2

Norman, M. D., Pearson, N. J., Sharma, A., and Griffin, W. L., 1996, Quantitative analysis of trace elements in geological materials by laser ablation ICPMS: instrumental operating conditions and calibration values of NIST glasses: Geostandards Newsletter, v. 20, n. 2, p. 247–261, http://dx.doi.org/10.1111/j.1751-908X.1996.tb00186.x

Och, L. M., and Shields-Zhou, G., 2012, The Neoproterozoic oxygenation event: Environmental perturbations and biogeochemical cycling: Earth-Science Reviews, v. 110, p. 26–57.

Ovchinnikova, G. V., Kuznetsov, A. B., Vasil'eva, I. M., Gorokhov, I. M., Letnikova, E. F., and Gorokhovskii, B. M., 2012, U-Pb age and Sr isotope signature of cap limestone from the Neoproterozoic Tsagaan Oloom Formation, Dzabkhan River Basin, Western Mongolia: Stratigraphy and Geological Correlation, v. 20, n. 6, p. 516–527, http://dx.doi.org/10.1134/S0869593812060056

Paces, J. B., and Miller, J. D., Jr., 1993, Precise U-Pb ages of Duluth complex and related mafic intrusions, northeastern Minnesota: Geochronological insights to physical, petrogenetic, paleomagnetic, and tectonomagmatic processes associated with the 1.1 Ga midcontinent rift system: Journal of Geophysical Research–Solid Earth, v. 98, n. B8, p. 13997–14013, http://dx.doi.org/10.1029/93JB01159

Panchuk, K. M., Holmden, C. E., and Leslie, S. A., 2006, Local controls on carbon cycling in the Ordovician midcontienent region of North America, with implications for carbon isotope secular curves: Journal of Sedimentary Research, v. 76, n. 2, p. 200–211, http://dx.doi.org/10.2110/jsr.2006.017

Pearce, J. A., and Peate, D. W., 1995, Tectonic implications of the composition of volcanic arc magmas: Annual Review of Earth and Planetary Sciences, v. 23, p. 251–286, http://dx.doi.org/10.1146/annurev.ea.23.050195.001343

Planavsky, N. J., Rouxel, O. J., Bekker, A., Lalonde, S. V., Konhauser, K. O., Reinhard, C. T., and Lyons, T. W., 2010, The evolution of the marine phosphate reservoir: Nature, v. 467, p. 1088–1090, http://dx.doi.org/10.1038/nature09485

Pokrovskii, B. G., Melezhik, V. A., and Bujakaite, M. I., 2006, Carbon, Oxygen, Strontium, and Sulfur Isotopic Compositions in Late Precambrian Rocks of the Patom Complex, Central Siberia: Communication 1. Results, Isotope Stratigraphy, and Dating Problems: Lithology and Mineral Resources, v. 41, n. 1, p. 450–474, http://dx.doi.org/10.1134/S0024490206050063

Pokrovsky, B. G., Mavromatis, V., and Pokrovsky, O. S., 2011, Co-variation of Mg and C isotopes in late Precambrian carbonates of the Siberian Platform: A new tool for tracing the change in weathering regime?: Chemical Geology, v. 290, n. 1–2, p. 67–74, http://dx.doi.org/10.1016/j.chemgeo.2011.08.015

Powell, R. D., 1990, Glacimarine processes at grounding-line fans and their growth to ice-contact deltas, *in* Dowdeswell, J. A., and Scourse, J. D., editors, Glacimarine Environments-Processes and Sediments: Geological Society, London, Special Publications, p. 53–73, http://dx.doi.org/10.1144/gsl.sp.1990.053.01.03

Pruss, S. B., Bosak, T., Macdonald, F. A., McLane, M., and Hoffman, P. F., 2010, Microbial facies in a Sturtian cap carbonate, the Rasthof Formation, Otavi Group, northern Namibia: Precambrian Research, v. 181, n. 1–4, p. 187–198, http://dx.doi.org/10.1016/j.precamres.2010.06.006

Ramezani, J., Hoke, G. D., Fastovsky, D. E., Bowring, S. A., Therrien, F., Dworkin, S. I., Atchley, S. C., and Nordt, L. C., 2011, High-precision U-Pb zircon geochronology of the Late Triassic Chinle Formation, Petrified Forest National Park (Arizona, USA): Temporal constraints on the early evolution of dinosaurs: Geological Society of America Bulletin, v. 123, n. 11–12, p. 2142–2159, http://dx.doi.org/10.1130/B30433.1

Read, J. F., 1982, Carbonate platforms of passive (extensional) continental margins: Types, characteristics

and evolution: Tectonophysics, v. 81, n. 3–4, p. 195–212, http://dx.doi.org/10.1016/0040-1951(82)90129-9

Ridge, J. C., Balco, G., Bayless, R. L., Beck, C. C., Carter, L. B., Dean, J. L., Voytek, E. B., and Wei, J. H., 2012, The new North American Varve Chronology: A precise record of southeastern Laurentide Ice Sheet deglaciation and climate, 18.2–12.5 kyr BP, and correlations with Greenland ice core records: American Journal of Science, v. 312, n. 7, p. 685–722, http://dx.doi.org/10.2475/07.2012.01

Rojas-Agramonte, Y., Kröner, A., Demoux, A., Xia, X., Wang, W., Donskaya, T., Liu, D., and Sun, M., 2011, Detrital and xenocrystic zircon ages from Neoproterozoic to Palaeozoic arc terranes of Mongolia: Significance for the origin of crustal fragments in the Central Asian Orogenic Belt: Gondwana Research, v. 19, n. 3, p. 751–763, http://dx.doi.org/10.1016/j.gr.2010.10.004

Rooney, A. D., Macdonald, F. A., Strauss, J. V., Dudás, F. Ö., Hallmann, C., and Selby, D., 2014, Re-Os geochronology and coupled Os-Sr isotope constraints on the Sturtian snowball Earth: Proceedings of the National Academy of Sciences of the United States of America, v. 111, n. 1, p. 51–56, http://dx.doi.org/10.1073/pnas.1317266110

Rooney, A. D., Strauss, J. V., Brandon, A. D., and Macdonald, F. A., 2015, A Cryogenian chronology: Two long-lasting synchronous Neoproterozoic glaciations: Geology, v. 43, n. 5, p. 459–462, http://dx.doi.org/10.1130/G36511.1

Rose, C. V., Swanson-Hysell, N. L., Husson, J. M., Poppick, L. N., Cottle, J. M., Schoene, B., and Maloof, A. C., 2012, Constraints on the origin and relative timing of the Trezona δ^{13} C anomaly below the end-Cryogenian glaciation: Earth and Planetary Science Letters, v. 319, p. 241–250, http://dx.doi.org/10.1016/j.epsl.2011.12.027

Rothman, D. H., Hayes, J. M., and Summons, R. E., 2003, Dynamics of the Neoproterozoic carbon cycle: Proceedings of the National Academy of Sciences of the United States of America, v. 100, n. 14, p. 8124–8129, http://dx.doi.org/10.1073/pnas.0832439100

Ruzhentsev, S. V., and Burashnikov, V. V., 1995, Tectonics of the western Mongolian Salairides: Geotectonics, v. 29, n. 5, p. 379–394, http://eos.wdcb.ru/transl/geot/9505/pap00.htm

Ruzhentsev, S. V., and Pospelov, I. I., 1992, The south Mongolian Variscan fold system: Geotectonics, v. 26, p. 383–395.

Sanderson, M. J., 2003, Molecular data from 27 proteins do not support a Precambrian origin of land plants: American Journal of Botany, v. 90, n. 6, p. 954–956, http://dx.doi.org/10.3732/ajb.90.6.954

Sarg, J., 1988, Carbonate sequence stratigraphy, *in* Wilgus, C. K., Hastings, B. S., Kendall, C. G. S. C., Posamentier, H. W., Ross, C. A., van Wagoner, J. C., editors, Sea-Level Changes: An Integrated Approach: SEPM Special Publications, n. 42, p. 155–182.

Sawaki, Y., Kawai, T., Shibuya, T., Tahata, M., Omori, S., Komiya, T., Yoshida, N., Hirata, T., Ohno, T., Windley, B. F., and Maruyama, S., 2010a, $^{87}Sr/^{86}Sr$ chemostratigraphy of Neoproterozoic Dalradian carbonates below the Port Askaig Glaciogenic Formation, Scotland: Precambrian Research, v. 179, n. 1–4, p. 150–164, http://dx.doi.org/10.1016/j.precamres.2010.02.021

Sawaki, Y., Ohno, T., Tahata, T., Komiya, T., Hirata, T., Maruyama, S., Windley, B. F., Han, J., Shu, D., and Li, Y., 2010b, The Ediacaran radiogenic Sr isotope excursion in the Doushantuo Formation in the Three Gorges area, South China: Precambrian Research, v. 176, n. 1–4, p. 46–64, http://dx.doi.org/10.1016/j.precamres.2009.10.006

Schmitz, M., Gradstein, F., Ogg, J., and Ogg, G., 2012, Appendix 2—Radiometric ages used in GTS2012: The Geologic Time Scale, p. 1045–1082.

Schrag, D. P., Berner, R. A., Hoffman, P. F., and Halverson, G. P., 2002, On the initiation of snowball Earth: Geochemistry, Geophysics, Geosystems, v. 3, http://dx.doi.org/10.1029/2001GC000219

Schrag, D. P., Higgins, J. A., Macdonald, F. A., and Johnston, D. T., 2013, Authigenic carbonate and the history of the global carbon cycle: Science, v. 339, n. 6119, p. 540–543, http://dx.doi.org/10.1126/science.1229578

Sengör, A. M. C., Natal'In, B. A., and Burtman, V. S., 1993, Evolution of the Altaid tectonic collage and Palaeozoic crustal growth in Eurasia: Nature, v. 364, p. 299–307, http://dx.doi.org/10.1038/364299a0

Shields, G., Stille, P., Brasier, M. D., and Atudorei, N.-V., 1997, Stratified oceans and oxygenation of the late Precambrian environment: a post glacial geochemical record from the Neoproterozoic of W. Mongolia: Terra Nova, v. 9, n. 5–6, p. 218–222, http://dx.doi.org/10.1111/j.1365-3121.1997.tb00016.x

Shields, G. A., Braiser, M. D., Stille, P., and Dorjnamjaa, D., 2002, Factors contributing to high $\delta^{13}C$ values in Cryogenian limestones of western Mongolia: Earth and Planetary Science Letters, v. 196, n. 3–4, p. 99–111, http://dx.doi.org/10.1016/S0012-821X(02)00461-2

Sláma, J., Košler, J., Condon, D. J., Crowley, J. L., Gerdes, A., Hanchar, J. M., Horstwood, M. S. A., Morris, G. A., Nasdala, L., Norberg, N., Schaltegger, U., Schoene, B., Tubrett, M. N., and Whitehouse, M., 2008, Plešovice zircon—A new natural reference material for U–Pb and Hf isotopic microanalysis: Chemical Geology, v. 249, n. 1–2, p. 1–35, http://dx.doi.org/10.1016/j.chemgeo.2007.11.005

Smalley, P. C., Higgins, A. C., Howarth, R. J., Nicholson, H., Jones, C. E., Swinburne, N. H. M., and Bessa, J., 1994, Seawater Sr isotope variations through time: A procedure for constructing a reference curve to date and correlate marine sedimentary rocks: Geology, v. 22, n. 5, p. 431–434, http://dx.doi.org/10.1130/0091-7613(1994)022<0431:SSIVTT>2.3.CO;2

Smith, E. F., Macdonald, F. A., Petach, T. A., Bold, U., and Schrag, D. P., 2015, Integrated stratigraphic, geochemical, and paleontological late Ediacaran to early Cambrian records from southwestern Mongolia: Geological Society of America Bulletin, http://dx.doi.org/10.1130/B31248.1

Stampfli, G. M., and Borel, G. D., 2002, A plate tectonic model for the Paleozoic and Mesozoic constrained by dynamic plate boundaries and restored synthetic oceanic isochrons: Earth and Planetary Science Letters, v. 196, n. 1–2, p. 17–33, http://dx.doi.org/10.1016/S0012-821X(01)00588-X

Sumner, D. Y., and Bowring, S. A., 1996, U-Pb geochronologic constraints on deposition of the Campbell-

rand Subgroup, Transvaal Supergroup, South Africa: Precambrian Research, v. 79, n. 1–2, p. 25–35, http://dx.doi.org/10.1016/0301-9268(95)00086-0

Sun, J.-F., Yang, J.-H., Wu, F.-Y., and Wilde, S. A., 2012, Precambrian crustal evolution of the eastern North China Craton as revealed by U–Pb ages and Hf isotopes of detrital zircons from the Proterozoic Jing'eryu Formation: Precambrian Research, v. 200, p. 184–208, http://dx.doi.org/10.1016/j.precamres.2012.01.018

Swanson-Hysell, N. L., Rose, C. V., Calmet, C. C., Halverson, G. P., Hurtgen, M. T., and Maloof, A. C., 2010, Cryogenian glaciation and the onset of carbon-isotope decoupling: Science, v. 328, n. 5978, p. 608–611, http://dx.doi.org/10.1126/science.1184508

Swart, P. K., 2008, Global synchronous changes in the carbon isotopic composition of carbonate sediments unrelated to changes in the global carbon cycle: Proceedings of the National Academy of Sciences of the United States of America, v. 105, n. 37, p. 13741–13745, http://dx.doi.org/10.1073/pnas.0802841105

Swart, P. K., and Kennedy, M. J., 2012, Does the global stratigraphic reproducibility of $\delta^{13}C$ in Neoproterozoic carbonates require a marine origin? A Pliocene-Pleistocene comparison: Geology, v. 40, n. 1, p. 87–90, http://dx.doi.org/10.1130/G32538.1

Togtokh, D., Baatarkhuyag, A., and Bayardalai, S., 1995, The report of result of the geological grouppedmapping at scale 1:200000: Ulaanbaatar, Mongolia, p. 1575.

Vandeginste, V., Sweenen, R., Gleeson, S. A., Ellam, R. M., Osadetz, K., and Roure, F., 2005, Zebra dolomitization as a result of focused fluid flow in the Rocky Mountains Fold and Thrust Belt, Canada: Sedimentology, v. 52, n. 5, p. 1067–1095, http://dx.doi.org/10.1111/j.1365-3091.2005.00724.x

Wilhem, C., Windley, B. F., and Stampfli, G. M., 2012, The Altaids of Central Asia: A tectonic and evolutionary innovative review: Earth-Science Reviews, v. 113, n. 3–4, p. 303–341, http://dx.doi.org/10.1016/j.earscirev.2012.04.001

Yang, J., Cawood, P. A., Du, Y., Huang, H., Huang, H., and Tao, P., 2012, Large Igneous Province and magmatic arc sourced Permian–Triassic volcanogenic sediments in China: Sedimentary Geology, v. 261–262, p. 120–131, http://dx.doi.org/10.1016/j.sedgeo.2012.03.018

Yarmolyuk, V. V., Kovalenko, V. I., Anisimova, I. V., Sal'nikova, E. B., Kovach, V. P., Kozakov, I. K., Kozlovsky, A. M., Kudryashova, E. A., Kotov, A. B., Plotkina, Y. V., Terent'eva, L. B., and Yakovleva, S. Z., 2008, Late Riphean alkali granites of the Zabhan Microcontinent: Evidence for the timing of Rodinia breakup and formation of microcontinents in the Central Asian Fold Belt: Doklady Earth Sciences, v. 420, n. 1, p. 583–588, http://dx.doi.org/10.1134/S1028334X08040132

Yoshioka, H., Asahara, Y., Tojo, B., and Kawakami, S., 2003, Systematic variations in C, O, and Sr isotopes and elemental concentrations in Neoproterozoic carbonates in Namibia: implications for a glacial to interglacial transition: Precambrian Research, v. 124, n. 1, p. 69–85, http://dx.doi.org/10.1016/S0301-9268(03)00079-2

Zhang, C.-L., Zou, H.-B., Li, H.-K., and Wang, H.-Y., 2013, Tectonic framework and evolution of the Tarim Block in NW China: Gondwana Research, v. 23, n. 4, p. 1306–1315, http://dx.doi.org/10.1016/j.gr.2012.05.009

Zhou, C., Tucker, R., Xiao, S., Peng, Z., Yuan, X., and Chen, Z., 2004, New constraints on the ages of Neoproterozoic glaciations in south China: Geology, v. 32, n. 5, p. 437–440, http://dx.doi.org/10.1130/G20286.1

Zhu, M., Lu, M., Zhang, J., Zhao, F., Li, G., Aihua, Y., Zhao, X., and Zhao, M., 2013, Carbon isotope chemostratigraphy and sedimentary facies evolution of the Ediacaran Doushantuo Formation in western Hubei, South China: Precambrian Research, v. 225, p. 7–28, http://dx.doi.org/10.1016/j.precamres.2011.07.019

Zimmer, A., Lang, D., Richardt, S., Frank, W., Reski, R., and Rensing, S. A., 2007, Dating the early evolution of plants: detection and molecular clock analyses of orthologs: Molecular genetics and genomics, v. 278, n. 4, p. 393–402, http://dx.doi.org/10.1007/s00438-007-0257-6

Zonenshain, L. P., 1973, The evolution of Central Asiatic geosynclines through sea-floor spreading: Tectonophysics, v. 19, n. 3, p. 213–232, http://dx.doi.org/10.1016/0040-1951(73)90020-6